ABSTRACT

Title of Dissertation: STRATOSPHERIC OZONE TRENDS
AS DETERMINED BY REGIME ANALYSIS:
THE SOUTHERN HEMISPHERE

Marcos Froilán Andrade Flores, Doctor of Philosophy, 2004

Dissertation directed by: Professor Robert D. Hudson
Department of Meteorology

Recent studies in the Northern Hemisphere have shown that the total ozone field can be classified by meteorological regimes, whose boundaries are the tropospheric upper-level jets. A similar approach has been followed to classify the Southern Hemisphere. Total ozone data from the TOMS instruments have been used to locate the upper-level jets and therefore, the regimes' boundaries. Here however, I use vertically integrated potential vorticity from the reanalysis data from NCEP/NCAR and ECMWF to estimate the first guess in an iterative procedure that calculates the ozone regime boundary values. The classification of the total ozone field using these boundary values was validated using daily rawinsonde temperature profiles, SAGE II ozone profiles, and TOMS total ozone data. Rawinsondes showed that, on any given day, the tropopause heights within a regime were relatively constant despite the large latitudinal extent of the regime itself. Data from SAGE II also showed that the classification produces distinct

ozone profiles for each regime, which is consistent with the fact that total ozone is nearly constant within each regime, as shown by TOMS data.

The temporal behavior of total ozone within each regime between 1979 and 2004 was analyzed for the 25º-60ºS latitude band. Total ozone trend analysis showed that statistically significant decadal trends within each regime were smaller than the overall trend in this band with no classification. In addition, the areas of the meteorological regimes within the 25º-60ºS latitude band also showed statistically significant trends. During the period of study, the area of the tropical regime has increased at the expense of the areas of the midlatitude and polar regimes. Both processes, changes in total ozone within each regime as well as changes in their contribution to the 25º-60ºS band, are responsible for the overall trend in that region. The analysis also showed that the QBO and the solar flux have an important influence on the temporal behavior of both the total ozone within each regime and their corresponding areas. The results indicate, as is the case of the Northern Hemisphere, that the total ozone regime boundaries have migrated poleward between 1979 and 2004.

STRATOSPHERIC OZONE TRENDS AS DETERMINED BY REGIME ANALYSIS: THE SOUTHERN HEMISPHERE

by

Marcos Froilán Andrade Flores

Dissertation submitted to the Faculty of the Graduate School of the
University of Maryland, College Park in partial fulfillment
of the requirements for the degree of
Doctor of Philosophy
2004

Advisory Committee:

Professor Robert Hudson, Chair
Dr. Hugo Berbery
Professor Ruth DeFries
Professor Russell Dickerson
D. U. Professor Eugenia Kalnay
Professor Owen Thompson

DEDICATION

A mi esposa Valeria, por su fortaleza, aliento y amor en todo momento.

A mi hijo Mateo, la luz de mi vida.

A mis padres Luisa y Carmelo, y mi abuelita Cristina, quienes me han guiado y enseñado el valor de lo justo y bueno en la vida.

To my wife Valeria, for her strength, support, and love at all times.

To my son Mateo, the light of my life.

To my parents Luisa and Carmelo, and to my beloved grandmother Cristina, who have guided and taught me the value of justice and good in life.

ACNOWLEDGMENTS

My appreciation to Prof. Robert Hudson, for his wise guidance, patience, and understanding, and to Melanie Follette, for her support, help, and most important of all, her friendship during these five years.

I would also like to thank to the Fulbright Program for giving me the opportunity to continue my graduate studies in the United States; to the Department of Physics at the Universidad Mayor de San Andrés (Bolivia) for its financial support; and to The South American Climate Change (SACC) Consortium for their help through the SAAC Fellowship 2003 Grant.

Table of Contents

1. INTRODUCTION

Traditionally, temporal trends of atmospheric elements have been studied by examining the vertical and horizontal structure of the atmosphere. Vertically, the tropopause has typically been used to spatially separate the troposphere from the stratosphere, in addition to separating their respective processes. On the contrary, there is no commonly accepted method to separate the atmosphere horizontally, other than latitudinal criteria. In this sense, bands of constant latitude have usually been employed to compute trends. However, it is clear that the atmosphere is a fluid with highly non-linear behavior, and therefore there is no physical reason to restrict its analysis by latitude unless only mean temporal and spatial quantities are studied. Even in these cases, the average could smooth out many features that might be important on small or short scales.

Using observational analyses, meteorologists have identified large regions in the atmosphere that have similar physical and chemical characteristics. For instance, temperature and moisture have been used to classify some air masses. The problem is, however, the difficulty in defining the boundaries of these "air masses" both spatially and temporally. Recently, Hudson et al. (2003) have proposed the use of the total ozone column to locate the boundaries of three regions in the atmosphere. Their approach shows some important characteristics of these "regimes":

a) They are permanent features of the atmosphere.
b) They exist on a global scale.
c) The variability of any physical or chemical quantity associated with a regime is considerably smaller than the variability of the same quantity in the atmosphere without any classification by regime.

This reduction of variability within each regime leads to a more precise and accurate analysis of trends, and maybe more importantly, to a better understanding of the mechanisms underlying any long-term change. Hudson et al. (to be submitted) have analyzed the ozone trends within each regime in the Northern Hemisphere. Their findings suggest a dynamical origin as well as chemical of the observed trends in the extra-tropics. It is clear, however, that analyses of both hemispheres are required in order to have a global picture of what is happening.

The present study intends to complete the analysis carried out for the Northern Hemisphere by Hudson et al. (2003). Although the basis of the method has been established in the cited paper, there are clear and obvious differences between Northern and Southern Hemispheres (Schoeberl and Krueger, 1983):

i) Less land, and therefore fewer disturbances, produce less contrast between regimes, making the identification of the upper level fronts more difficult (Karoly et al., 1998).

ii) Less land also means fewer ground-based stations and therefore larger uncertainties in satellite retrievals as well as in the reanalysis information (Kistler et al., 2001).

iii) The presence of a stronger polar vortex and larger Antarctic "ozone hole" distorts the dynamics of the upper-level jets, complicating the determination of the regime boundaries.

As a result, new or additional tools must be used in order to delineate the regime boundaries, and to check their robustness and reliability. Many ideas were tested in the Northern Hemisphere (where there are many more ground stations and satellite information is more reliable) and then applied to the Southern Hemisphere.

The main goals of this thesis are:

a) Classify the Southern Hemisphere total ozone field by meteorological regimes in the band 25º-60ºS.

b) Analyze total ozone trends within each regime, as well as their contributions to the mentioned latitude band.

This thesis is divided into 6 chapters. Chapter 2 gives a basic description of the atmosphere and a "theoretical" background based on observational evidence. Chapter 3 explains the method employed to classify the Southern Hemisphere total ozone field, and Chapter 4 describes the validation of this classification. Chapter 5 discusses the long-term behavior of ozone within each regime. Finally, the conclusions and discussion are presented in Chapter 6.

2. BACKGROUND

2.1 Basic Concepts

The atmosphere can be defined as a mixture of gases that surround the Earth. Due to gravitational forces, its mean density drops exponentially with altitude. Approximately 90% of the atmosphere's mass lies in the lower 10 to 16 km.

2.1.1 Vertical structure of the atmosphere

The atmosphere is typically divided into four layers based on its thermal structure: the *troposphere*, the *stratosphere*, the *mesosphere*, and the *thermosphere*. The upper limits of the three first layers are called: the *tropopause*, the *stratopause*, and the *mesopause,* respectively. These regions are relatively narrow transition zones.

Troposphere

Troposphere means "region of mixing" and is so named because of the vigorous convective air currents within the layer. It is the atmospheric layer closest to the planet and contains the largest percentage of atmospheric mass. In this region, the atmospheric average vertical temperature decreases by about 6 degrees Celsius per kilometer. Because water vapor content depends strongly on temperature, its concentration decreases rapidly with altitude. As a result, the troposphere contains 99 % of the water vapor in the atmosphere. Its concentration is greatest above the tropics, where it can be as high as 3 %, and decreases toward the polar regions. This species plays a major role in regulating air temperature because it absorbs both solar energy and thermal radiation from the planet's surface. Finally, it should be mentioned that all weather phenomena occur within the troposphere which is the most turbulent region of the atmosphere.

As it will be shown later, the upper limit of the troposphere, the tropopause, ranges in height from 8 km in polar regions, to 16 km at the equator. Its height also varies with season.

Stratosphere

The stratosphere is the second major layer of air in the atmosphere. It resides between 8 and 50 km above the planet's surface. Air temperature is relatively constant in the lowest part of the stratosphere and then increases with altitude to reach its maximum value around 50 km at the stratopause. This rise in temperature is related to absorption of ultraviolet radiation by the ozone layer. Incoming electromagnetic radiation from the Sun is converted to kinetic energy when the atmosphere's molecules absorb ultraviolet radiation, resulting in heating of the stratosphere. The resulting temperature profile produces a very stable atmosphere that inhibits vertical convection. As a result, the stratosphere is much more stratified than the troposphere, hence its name. For the same reason, mixing between tropospheric and stratospheric air requires special conditions to be possible.

Volume mixing ratios of oxygen and nitrogen in the stratosphere are basically the same as in the troposphere but concentrations of trace gases vary markedly. Water vapor content, for instance, is very low (about 4 ppmv) as opposed to ozone concentration which reaches a maximum in this layer.

Mesosphere

The mesosphere extends from approximately 50 km to 80 km. It is characterized by decreasing temperatures (as in the troposphere), which reach 190-180 K at an altitude of 80 km. In this region, concentrations of ozone and water vapor are negligible. At these

altitudes, the residual gases begin to stratify according to molecular mass due to gravitational separation.

Thermosphere

The thermosphere is located above the mesosphere and is separated from it by a transition layer the called mesopause. The temperature in the thermosphere generally increases with altitude up to 1000-1500 K. This increase in temperature is due to the absorption of intense solar radiation by the limited amount of remaining molecular oxygen. At an altitude of 100-200 km, the major atmospheric components are still nitrogen and oxygen. At this extreme altitude gas molecules are widely separated.

2.1.2 The tropopause

The tropopause has been historically defined by the vertical structure of atmospheric temperature (Hoinka, 1997). However, observational and theoretical studies suggested the use of concentrations of trace gases (Bethan et al., 1996), or potential vorticity (Reed, 1955; Danielsen, 1968) as quantities that can also be used to mark the location of the tropopause. In particular, ozone concentration and potential vorticity have been extensively used to determine the origin of air parcels and tropopause height. These three methods, temperature profile, trace gas concentrations, and potential vorticity, are briefly described below.

Thermal tropopause

The World Meteorological Organization (WMO) defined the tropopause height as "the lowest level at which the lapse rate decreases to 2ºC/km or less, provided that the average lapse rate between this level and all higher levels within 2 km does not exceed 2ºC/km" (WMO, 1957). The tropopause evaluated using this lapse rate definition is called the

thermal tropopause. Further work (Reed and Danielsen, 1959; Danielsen, 1968), however, showed that this definition does not always produce an unambiguous designation of the tropopause. In fact, there are several regions in the atmosphere where the transition from a tropospheric to a stratospheric lapse rate can occur over a depth of several kilometers (Bethan et al., 1996), making it very difficult to define a narrow region as the transition zone, i.e. in the vicinity of the jet streams (Reichler et al., 1995). In these regions, several discontinuities can be observed (Hoinka, 1997), so the lapse rate changes from its tropospheric to its stratospheric value by successive steps. Despite of all these problems, the thermal definition is still widely used because of its simplicity, and because it is not subject to additional restrictions.

Dynamical tropopause

Another way to define the tropopause is using *Ertel's potential vorticity* as proposed by Reed (1955). This quantity can be understood as the product of the fluid vorticity multiplied by its static stability. For large-scale atmospheric motions, where the processes can be considered adiabatic and frictionless, potential vorticity, q_θ, can be defined in isentropic coordinates as follows (Hoskins et al, 1985):

$$q_\theta = -g \frac{\zeta_\theta + f}{\frac{\partial p}{\partial \theta}} \tag{2.1}$$

where $f=2\Omega\sin\phi$ is the Coriolis parameter, g is gravity, ζ_θ is the isentropic relative vorticity, p is pressure, and θ is potential temperature. The tropopause defined using q_θ is called the "dynamical tropopause" and is understood to be a near-zero-order discontinuity

that separates low values in the troposphere from high values in stratosphere (Hoinka, 1997).

The WMO (1986) defines the dynamical tropopause by the value of 1.6 pvu, where pvu stands for "potential vorticity unit" (1 pvu = 10^{-6} K m^2 kg^{-1} s^{-1}). Other studies, however, suggest values between 1 pvu (Shapiro, 1980) and 3.5 pvu (Hoerling, 1991; Hoinka, 1996). In any case, the location of the dynamical tropopause is usually assigned to a surface with potential vorticity equal to some critical value. Hoerling et al. (1991) demonstrated that this approach provides good analyses of the tropopause at mid-latitude ridges, where the determined pressures were generally within 20 hPa of the observed values of the tropopause pressure. On the other hand, larger differences were found during periods of rapid development of an upper-level shortwave. Hoinka et al. (1996) compared rawinsonde observations over three locations between 55º and 65º with the dynamical tropopause derived from ECMWF data. They found that there were climatological differences in the tropopause pressure, some of them positive and some of them negative. This underlies the difficulty of choosing a particular value for q_θ to define the position of the tropopause at synoptic or larger scales.

In practice, the dynamical tropopause has been defined as the 2-pvu surface. Air with q_θ lower than 2 pvu is considered to be from tropospheric origin, while air having values higher than 2 pvu is assumed to be from stratospheric origin. Compared to the thermal definition, the dynamical tropopause is much more continuous, both spatially and temporally, than the lapse-rate-defined tropopause (Morgan and Nielsen-Gammon, 1998). This seems to be particularly important in the vicinity of developing baroclinic disturbances (Morgan and Nielsen-Gammon, 1998).

Chemical tropopause

Ozone concentration is not constant with altitude. Typically, ozone concentration is low in the troposphere (of the order of 50 ppbv), where the lack of shortwave electromagnetic radiation together with the presence of elements that act as a sink in the atmosphere make it difficult to sustain a stable concentration of this gas. Relatively large ozone concentrations[1] are observed only under particular meteorological situations in this layer. The presence of chemical precursors as well as intense solar radiation are basic ingredients to produce tropospheric ozone (Finlayson-Pitts and Pitts, 1999).

Air in the stratosphere is very dry and stratified. With fewer elements that can "clean" the atmosphere (mainly hydroxyls) and higher intensities of shortwave radiation, relative stable concentrations of ozone are possible. At altitudes around 25 km, the concentration is on the order of 10 ppmv (Steinbrecht et al., 1998).

Despite the fact that ozone concentration has been used to define the tropopause height for a long time, there is no equivalent thermal-WMO definition. Different criteria are employed for different researchers. However, ozone mixing ratio and its vertical gradient are typically used for that purpose. For instance, following Bethan et al. (1996), the "ozone tropopause" can be defined as the region where the following three criteria are met:

i) ozone mixing ratio is greater than 80 ppbv

ii) ozone mixing ratio immediately above exceeds 110 ppbv

iii) vertical gradient of ozone mixing ratio, evaluated over a depth of 200 m, exceeds 60 ppbv km^{-1}

[1] The Environmental Protection Agency (EPA) considers exposure to more than 85 ppbv of ozone for more than eight hours is dangerous for human health.

In this specific case, the first criterion was obtained from climatological values of the ratio ozone/PV reported by Beekmann et al. (1994). They found that this ratio typically is around 40-50 ppbv per pvu in the extratropics. The second criterion is used to assure that the stratosphere is the layer above the point chosen in i). The last criterion is also based on empirical evidence.

When data from ozonesondes were used to compare the chemical and thermal definitions, it was found that the ozone tropopause lay almost 1 km below the thermal tropopause in most of the cases. However, when the thermal tropopause was very well defined this difference was considerable smaller (Bethan et al., 1996).

In summary, it seems likely that the tropopause height will depend upon the method chosen to define it. Poor vertical resolution in models, instrumentation problems, or simply the way in which the tropopause is defined in each method, could contribute to these differences.

2.1.3 Atmospheric circulation and upper-level jets

The atmosphere behaves like a gigantic heat engine that is constantly fed by energy from the Sun. It is that energy that maintains the temperature difference between the equator and the poles, which in turn drives the planetary atmospheric circulation. The conversion of electromagnetic energy into heat energy, and ultimately into kinetic energy, requires not only horizontal but also vertical motion. In general, however, vertical speeds are much smaller than horizontal ones, making it possible to describe the atmosphere as a 2-dimensional fluid.

From a purely atmospheric point of view, there are two basic ways in which heat and momentum can be transported from the equator to the poles: direct meridional circulation, and eddy transport. The former mechanism is dominant in the tropics where air rises at the equator, with the maximum ascent in the summer hemisphere and strongest descent in the winter hemisphere at around 25º-30º latitude (James, 1994). This simple "model" of meridional atmospheric motion explains one of the most obvious responses of the atmospheric flow to the heating excess in the tropics and the deficit at high latitudes. The physical law that underlies this low-latitude circulation (also known as the Hadley cell) is the conservation of angular momentum. At higher latitudes, however, the conservation of angular momentum does not explain the observed mean zonal winds, i.e. the midlatitude westerlies. In those regions horizontal cells carry most of the heat and momentum polewards (Barry and Chorley, 1992).

A simplified and idealized model of the meridional circulation is shown in figure 2.1. In addition to the Hadley cell, two other cells are represented in this figure: the *Ferrel* and *Polar* cells. Like the Hadley cell, the Polar cell is also a *direct* circulation cell.

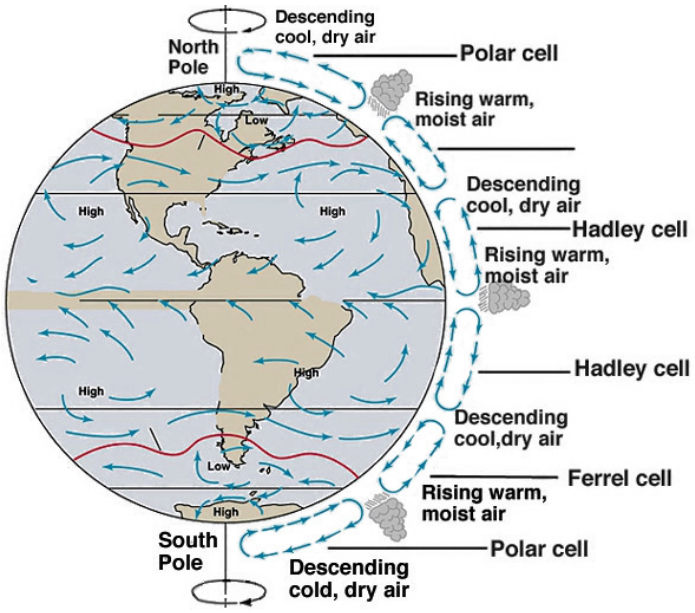

Figure 2.1 Three-cell model of the meridional circulation **(**from the University of Florida Global Change Tutorial Earth Systems Sciences Notes at http://ess.geology.ufl.edu/ess/Notes/ AtmosphericCirculation/atmoscell_big.jpeg).

On the contrary, the Ferrel cell is believed to be an *indirect* cell that is driven by the other two adjacent cells. Associated with these cells are two tropospheric upper-level *jet streams*: the *subtropical jet*, located in the vicinity of the descending branch of the Hadley circulation, about 30º latitude, and the *polar jet* located on average at a latitude of 60º in the vicinity of the polar cell. These four "rivers" of fast-flowing air (two in each hemisphere) are predominantly westerly winds.

Although simplistic, this model, called the *3-cell model*, captures many of the real features of the Earth's atmospheric circulation. The Intertropical Convergence Zone (ITCZ) and the Hadley cell are two of the most important characteristics described by it. However, the Polar and Ferrel cells are much more complex than what is described by this model. As a result, simple direct or indirect circulations are not enough to explain the observed features in those regions where horizontal mixing is dominant over momentum and heat transport. Figure 2.2 shows a more realistic (although still simplistic) schematic of the general meridional circulation.

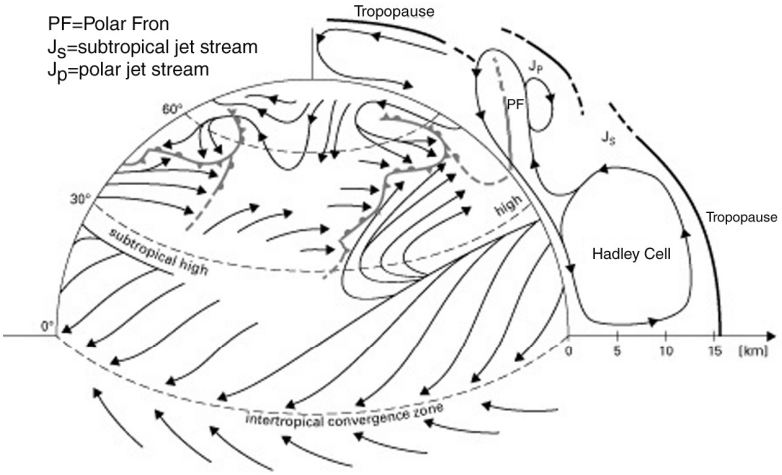

Figure 2.2 Idealized atmospheric circulation in the Northern Hemisphere. Three basic features can be distinguished: the (sub) tropical Hadley cell, a zone with relatively strong westerlies at mid-latitudes, and the polar anticyclone. Note that the tropopause extends to higher altitudes in the tropics. The polar front as well as the subtropical and polar jets is also depicted (from The Open University, http://www.ou.nl/open/dja/Klimaat/System/).

A few important attributes of the upper-level jets must be pointed out here:

a) Their mean position changes seasonally as the location of maximum energy input changes

b) The subtropical and polar jets can be typically found on the 200 mb and 300 mb isobaric surfaces respectively

c) These jets meander as they travel in the atmosphere (Rossby waves)

Figure 2.3 shows a schematic of the main structural parts of the atmosphere in an "instantaneous" (as opposed to an average) vertical-meridional cross section. Disturbances due to orography, atmospheric dynamics, or thermodynamics make the upper-level jets shift northward or southward (Fig 2.4). It is this variability in their position that makes them important for weather patterns. For instance, let us consider a town at mid-latitudes. Its weather will be strongly influenced by the relative position of the upper-level jets. If the location were equatorward of the subtropical jet, then the town would be "submerged" in tropical air, typically warm and humid. On the other hand, if

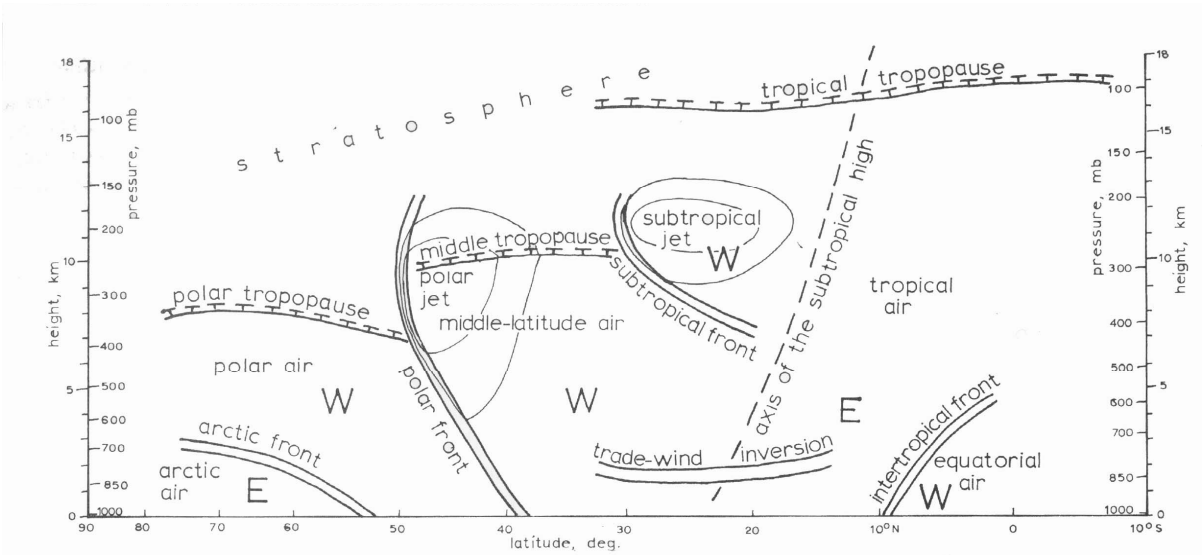

Figure 2.1 Main structural parts of the atmosphere in a vertical meridional section. Prevalent wind directions are indicated by W and E (from Djuric, 1994).

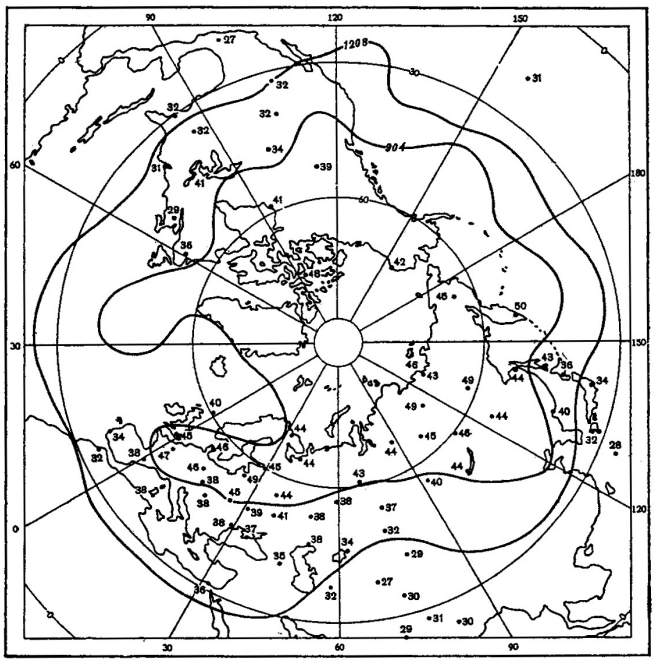

Figure 2.2 Isopleths of geopotential height at 200 mb and 300 mb used to define the location of the upper-level jets in the Northern Hemisphere on 23 April 1976. The numbers indicate total ozone (x10 DU). For a more complete explanation see section 3.5 (from Shalamyanskiy and Romanshkina, 1980).

the town were polarward of this jet, then cooler and drier air would be surrounding this town. Furthermore, the mean position of the upper-level jets is usually associated with storm tracks (Shapiro et al., 1999) and can therefore be linked directly to weather and climate variability.

2.1.4 The average atmosphere

Describing the atmosphere implies, at least in principle, the description of the global atmospheric circulation, which in turn requires specification of the evolving three-dimensional fields of meteorological variables (James, 1994). Due to practical and theoretical limitations however, some kind of averaging must be done in order to obtain understandable and reliable results.

There are a number of ways in which atmospheric data can be averaged. The earliest studies of the atmosphere were mainly concerned with zonal averages. The reason being, for any given station, that the temporal mean values depend more strongly

on latitude than on longitude. The latitude of an observing site on the Earth's surface is probably the most important single factor in determining its climate (James, 1994)[2].

The zonal average of any scalar quantity Q can be defined as:

$$[Q] = \frac{1}{2\pi}\int_0^{2\pi} Q\,\mathrm{d}\lambda \tag{2.2}$$

where λ is the longitude in radians. Note that, by definition, [*Q*] is independent of longitude. The local values of *Q* will be, in general, different from [*Q*]. These deviations are referred as the "zonal anomaly" of *Q*,

In the same way, data can be averaged in time as:

$$\bar{Q} = \frac{1}{\tau}\int_0^{\tau} Q\,\mathrm{d}t \tag{2.3}$$

where τ is some time long enough to make $\bar{Q}$ independent of time.

Since global circulation evolves in time as the seasons progress, a very popular averaging period is a "seasonal average" which typically is performed on three months of the year. For instance, a common way to do this uses December, January and February (DJF) to compute the time average for winter; March, April and May for spring, and so on.

[2] That is true if all the stations are at similar altitudes. I was born in a city located at 16.5ºS but at 3600 meters above sea level over the Andean mountains. In that region, topography is the most important factor that determines local climate.

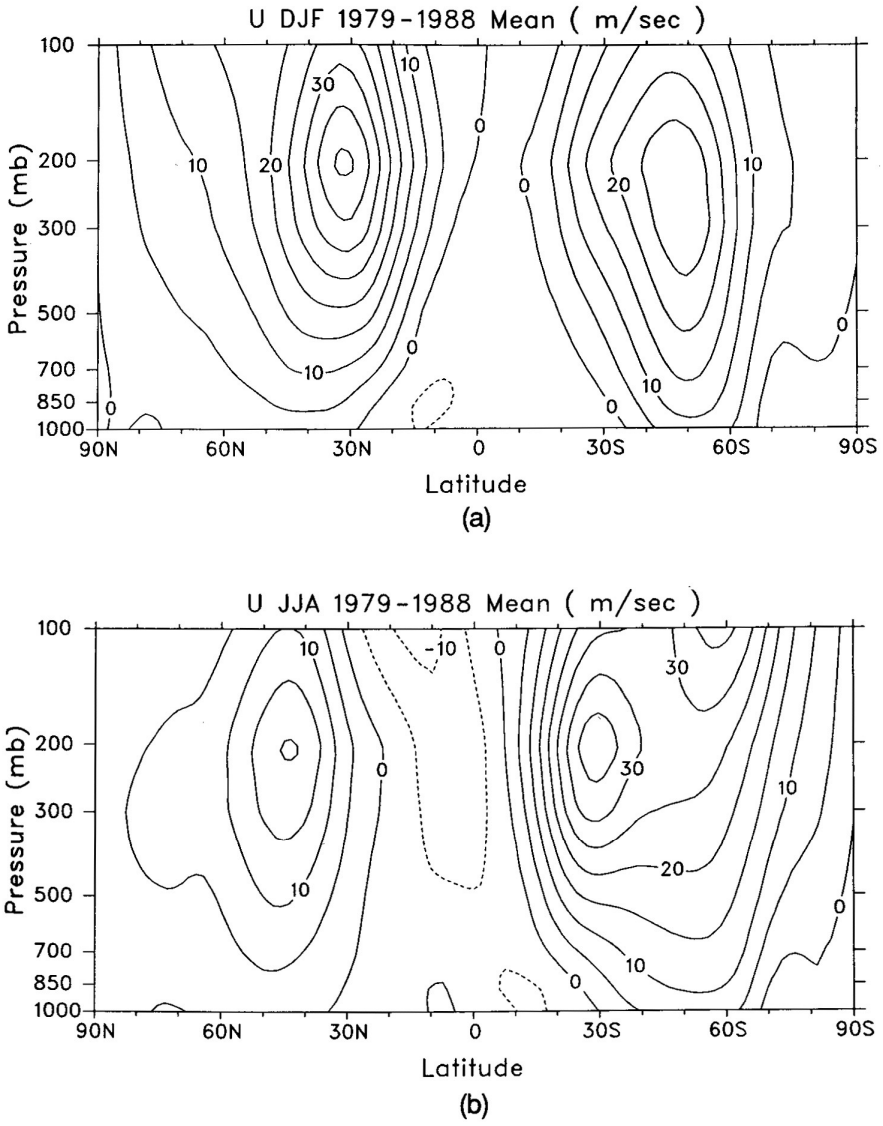

Figure 2.3 Vertical cross-section analysis of the average zonal component of the wind in m s-1 for a) the Southern Hemisphere summer months (Northern Hemisphere winter months) (December, January, and February) and b) the Southern Hemisphere winter months (Northern Hemisphere summer months) (June, July, and August)(from Bluestein, 1993).

Given our interest in upper level jets, potential vorticity, and the height of the tropopause, we will examine some figures where temporal and zonal averages have been performed for wind, potential temperature, and PV fields.

Figure 2.5 shows a vertical cross-section of the average zonal component of the wind for both hemispheres for December, January, and February (Southern Hemisphere

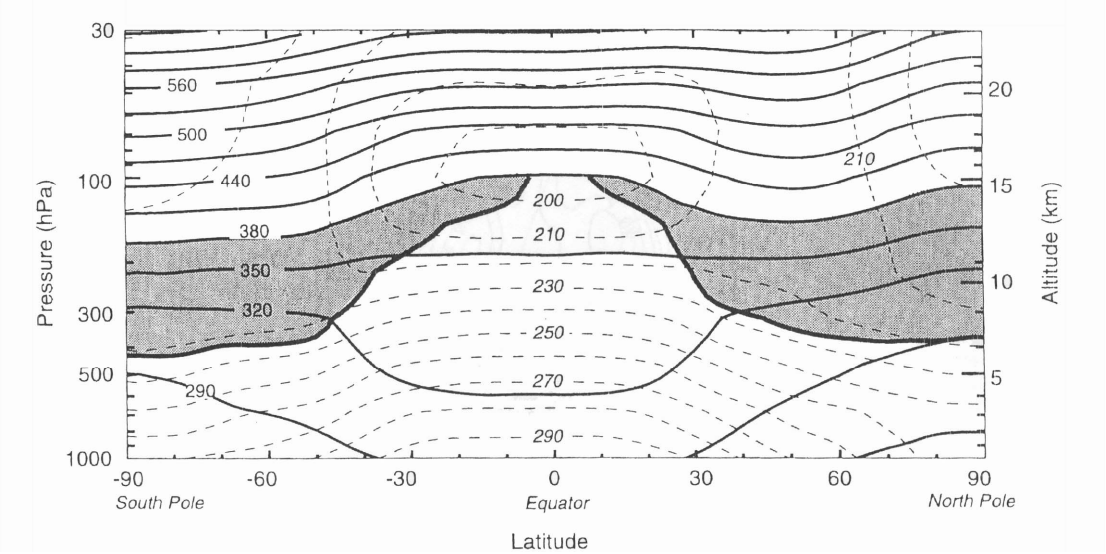

Figure 2.6 Latitude-altitude cross-section for January 1993 showing longitudinally averaged potential temperature (solid contours) and temperature (dashed contours). The heavy solid contour denotes the 2 pvu potential vorticity contour, which approximates the tropopause outside the tropics. Shaded areas denote the "lowermost stratosphere", whose isentropic or potential temperature surfaces span the tropopause (from Holton et al., 1995).

summer), and June, July, and August (Southern Hemisphere winter). These 3-month averages clearly show regions with maximum winds in the extra-tropical upper troposphere of both hemispheres. It can also be seen that the strongest winds occur on the winter hemisphere. These "cores" of high winds, some times referred to as *jet streams* (Bluestein, 1993), are closer to the equator in winter and further away in summer.

Figure 2.6 depicts a latitude-altitude cross section for January 1993 showing longitudinally averaged potential temperature (solid contours) and temperature (dashed contours). From this point of view, the atmosphere can be divided in three regions (Hoskins et al., 1991):

i) The "overworld", which consists of those isentropic surfaces that lie above the tropopause everywhere (approximately 380 K in figure 2.6)

ii) The “middleworld”, where the isentropic surfaces cross the tropopause (dashed regions in figure 2.6),

iii) The “underworld” where air parcels have a direct isentropic route to the surface

Figure 2.6 also shows the 2 pvu potential vorticity contour, which approximates the tropopause in the extratropics (Holton et al., 1995).

It should be noted that this time-longitude-average of the atmosphere shows only one jet stream and not two as described in section 2.1.3. In fact, this averaged atmosphere shows a smooth tropopause that descends towards the poles, in contrast with the “instantaneous” atmosphere (depicted in figure 2.3), which has a discontinuous and less inclined tropopause. Since the polar and subtropical jets meander with intrusions equator or poleward as large as 3000 km (Holton et al., 1995), either a temporal or longitudinal average (or both) will smooth the daily fields, “smearing out” any discontinuity that could exist (e.g. tropopause breaking). It is important, therefore, to keep in mind this difference between the daily and temporal-longitudinal averaged atmosphere.

2.2 Jets and Fronts

The term *jet stream* has been used to describe both regions of strong winds that are concentrated in a narrow and quasi-horizontal region, and the zonally time averaged maximum in the zonal component of the wind in the extratropical upper troposphere (see figure 2.5) (Bluestein, 1993). In this work we will use the first definition when we refer to a jet.

As mentioned in section 2.1.3, there are two permanent upper-level jets in each hemisphere: the subtropical and polar jets. Both jets are westerly flows that meander with

upper-air waves (Rossby waves).Structurally associated with these features are regions with large horizontal temperature gradients called *fronts* (Djuric, 1994).

One important feature of these fronts is that the height of the tropopause changes across them (Bluestein, 1993; Shapiro et al., 1980). Consider the thermal-wind relation

$$-\frac{\partial \vec{v}_g}{\partial \ln p} = \frac{R}{f}\hat{k} \times \nabla_p T \tag{2.4}$$

where R is the universal gas constant, f=2Ωsinϕ is the Coriolis parameter that represents the vertical component of planetary vorticity, v_g and u_g are the meridional and zonal components of the geostrophic wind, and $\hat{k}$ is the unitary vector in the vertical direction. If we now take the component of the geostrophic wind normal and left of the temperature gradient we have,

$$-\frac{\partial u_g}{\partial p} = -\frac{1}{f}\frac{\partial}{\partial y}\left(\frac{RT}{p}\right)_p \tag{2.5}$$

Therefore,

$$\frac{\partial^2 u_g}{\partial p^2} = \frac{R}{f}\left[\frac{1}{p}\frac{\partial}{\partial y}\left(\frac{\partial T}{\partial p}\right) - \frac{1}{p^2}\frac{\partial T}{\partial y}\right] \tag{2.6}$$

In terms of the potential temperature

$$\theta = T\left(\frac{p_0}{p}\right)^{R/C_p} \tag{2.7}$$

we have

$$\frac{\partial T}{\partial p} = \frac{T}{\theta}\frac{\partial \theta}{\partial p} + \frac{T}{p} \tag{2.8}$$

then,

$$\frac{\partial^2 u_g}{\partial p^2} = \frac{R}{f}\frac{\partial}{\partial y}\left(\frac{T}{p\theta}\frac{\partial \theta}{\partial p}\right) \tag{2.9}$$

Recalling that the static stability is defined as

$$\sigma = -\frac{RT}{p}\frac{\partial \ln \theta}{\partial p} \tag{2.10}$$

it follows that

$$\frac{\partial^2 u_g}{\partial p^2} = -\frac{1}{f}\frac{\partial \sigma}{\partial y} \tag{2.11}$$

At the region of maximum winds,

$$\frac{\partial^2 u_g}{\partial p^2} < 0 \tag{2.12}$$

The only way to satisfy eqs. (2.11) and (2.12) at the same time is to have $\frac{\partial \sigma}{\partial y} > 0$ in the Northern Hemisphere, and $\frac{\partial \sigma}{\partial y} < 0$ in the Southern Hemisphere (*f* is negative in the latter). These conditions imply that σ must increase toward the "cold" side of the jet (Bluestein, 1993).

2.2.1 The polar jet

The polar jet is usually found around 250-300 mb (Shapiro, 1987; Shalamyanskiy and Romanshkina, 1980; Bluestein, 1993). It is linked to strong quasihorizontal temperature gradients at low levels and strong vertical wind shear (Bluestein, 1993). The associated polar front usually has a slanting transition layer related to the baroclinic zone under the polar jet stream (Djuric, 1994). This layer can be anywhere between zero and several hundred kilometers wide (Djuric, 1994). Where the front is the narrowest, it transforms into a discontinuous surface with respect to meteorological variables such as temperature and humidity, changing abruptly from one side of the surface to the other. On the other hand, the polar front could be a weak shear line or a wider region with a small temperature contrast which may intensify later.

Precipitation often accompanies the polar front. It is common to find this front extending all the way to the surface (or close to it), and therefore it is more easily depicted in a surface weather chart than the subtropical front. The average polar jet position migrates north and south as the subsolar point does. In summer, the front is closer to the pole whereas in winter is closer to the equator. In the latter, migrations of the front deep into the tropics have been observed. According to Djuric (1994), the Northern Polar Front has been detected as far as 10ºN in Venezuela[3].

The polar-front jet is associated with the movement of major low-level air masses northward and southward as it meanders along its mean westerly direction. In this sense, identification of this jet and its future behavior often assist in predicting major changes in air masses, and therefore in temperature and weather over a region.

2.2.2 The subtropical jet

The *subtropical jet* is a fairly steady jet near 200 mb (Bluestein, 1993; Shalamyanskiy and Romanshkina, 1980) with a mean westerly direction. This jet is usually found at latitudes between 20º and 35º, but it can also migrate deep into high latitudes. As in the case of the polar jet, the subtropical jet is associated with a change in height of the tropopause (Bluestein, 1993).

The mean wind field shows that the subtropical jet appears to be almost a continuous feature around the globe (Bluestein, 1993). This jet is generally weaker, more persistent, and located at higher altitudes than its higher-latitude cousin. The zone of strong quasihorizontal temperature gradient under the subtropical jet is called the

[3] This is consistent with observations made at La Paz, Bolivia (16.5ºS, 67.8ºW) where a "surazo" (the passage of the Southern Hemisphere polar front) is often observed in winter.

subtropical front and is found in the upper troposphere and seldom observed below 500 mb (Djuric, 1994). That means that the meridional temperature gradient associated with the vertical shear under the subtropical jet is concentrated in a shallow layer, and not in a relatively deep layer as in the case of the polar front.

The distinction between the polar and the subtropical jet is often not clear on daily weather maps (Bluestein, 1993). Sometimes when the polar jet penetrates to subtropical latitudes, it seems to merge with the subtropical jet to form a single band of strong winds. However it is also possible that both jets align with each other in the vertical, producing extreme cyclonic events (Shapiro et al., 1999). In fact, it has been proposed that the interaction between the polar and subtropical jets contribute to the way that extratropical cyclones form. Shapiro and Donall-Grell (1994) suggested that different phasing and vertical and/or meridional alignments of the jets are accompanied by different

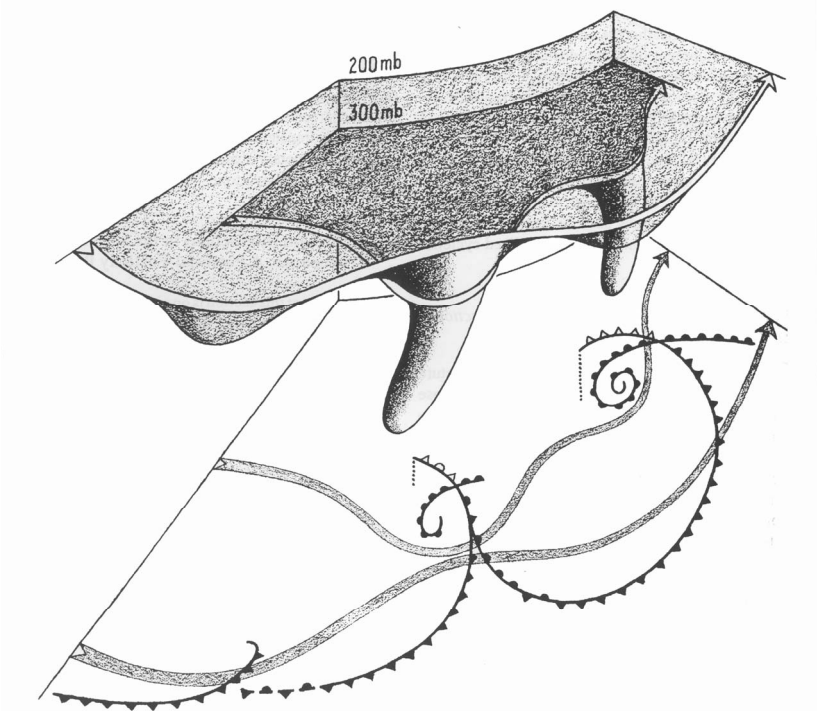

Figure 2.7 Schematic of upper level jets and fronts and different ways they can interact to produce different weather patterns (from Shapiro et al., 1999).

environmental shears that modulate the life (and type) of extratropical cyclones. Figure 2.7 illustrates the influence of upper-level jet streams and PV alignments on frontal structure within extratropical cyclones

2.2.3 The Arctic and Antarctic fronts

The boundaries between the polar vortex and the rest of the polar air are the *Arctic Front* in the Northern Hemisphere, and the *Antarctic Front* in the Southern Hemisphere. These fronts are usually present only in winter. For this reason, polar vortex air masses are sometimes associated with the polar night (Djuric, 1994). In winter in the polar regions, areas covered by snow produce a radiation inversion that does not disappear during the short day. Air beneath this inversion is known as arctic (antarctic) air when it covers large regions (more than 1000 km horizontally) of the poles. This arctic (antarctic) air can be brought far south (north) by large winter storms. It is relatively common for the arctic front to reach the polar front (Djuric, 1994) in which case both fronts coincide in a surface chart. It should be noted that despite ample literature about the existence of this front (Shapiro, 1985; Shapiro et al, 1987, Serreze et al., 2001), there is not a universal view about its permanent presence in the atmosphere or its association with an upper-level jet. In fact, many of the early studies suggested the existence of the arctic front in summertime only (Reed and Kunkel, 1960). However, these analyses were based on temporal-spatial averages of meteorological variables at high latitudes. This was very different than the direct experimental approach used to prove the existence of the winter polar front and its relationship to an upper-level jet (Shapiro, 1985; Shapiro et al., 1987).

2.3 Upper-level Jets and the Tropopause

It has been shown in the previous section that the static stability must increase toward the cold side of the upper-level jet. This basically implies that the tropopause height should also change across the upper-level jet. There is extensive observational and theoretical evidence that supports this fact (Reed, 1955; Danielsen, 1968; Danielsen et al., 1970; Shapiro, 1976, 1978, 1980, 1985; Keyser and Shapiro, 1986; Shapiro et al., 1987). In fact, the tropopause height not only changes across the upper-level jet but in the process it could be deformed (or even broken) to produce what is known as *tropopause folding*. This strong deformation occurs during large-scale cyclogenesis (Danielsen, 1985). The process was first proposed by Reed (1955), Reed and Danielsen (1959), and later experimentally verified by Danielsen (1968) by measuring radioactive tracers. Aircraft equipped to measure radioactive aerosols and products of nuclear bomb tests were flown in regions where the folded structure was predicted to exist. The observations (figure 2.8) clearly show not only the tropopause change from one side of the jet to the other but also that air of stratospheric origin is transported into the troposphere by the process of tropopause folding (Danielsen, 1968).

Additional insight into tropopause behavior in regions near the upper-levels jets was gained by analysis of numerous aircraft missions in the 1970's and 1980's. Shapiro (1974) showed data collected by two aircrafts during the passage of an upper-level front

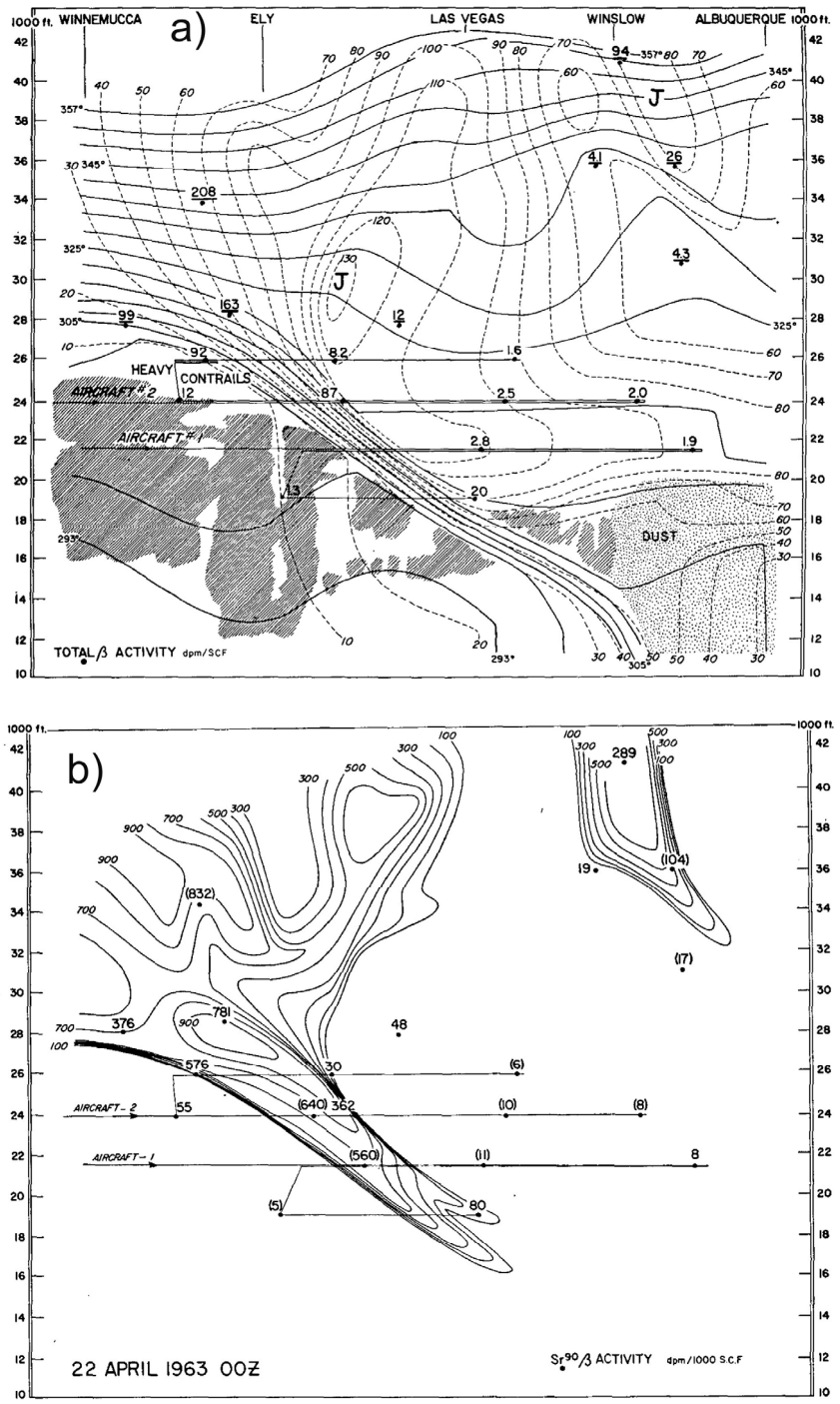

Figure 2.8 a) Vertical cross-section of potential temperature (solid lines), wind speed in knots (dashed lines), clouds (slanting lines) and dust (dots) for 0000 GMT 22 April 1963. Values at sampling sites are total β activity in disintegrations per minute/standard cubic feet (dpm/SCF). b) Potential vorticity (in 100 x 10^{-10} cm sec K gm^{-1}) computed from a) and β activity of strontium-90 (dpm/KSCF) (from Danielsen, 1968).

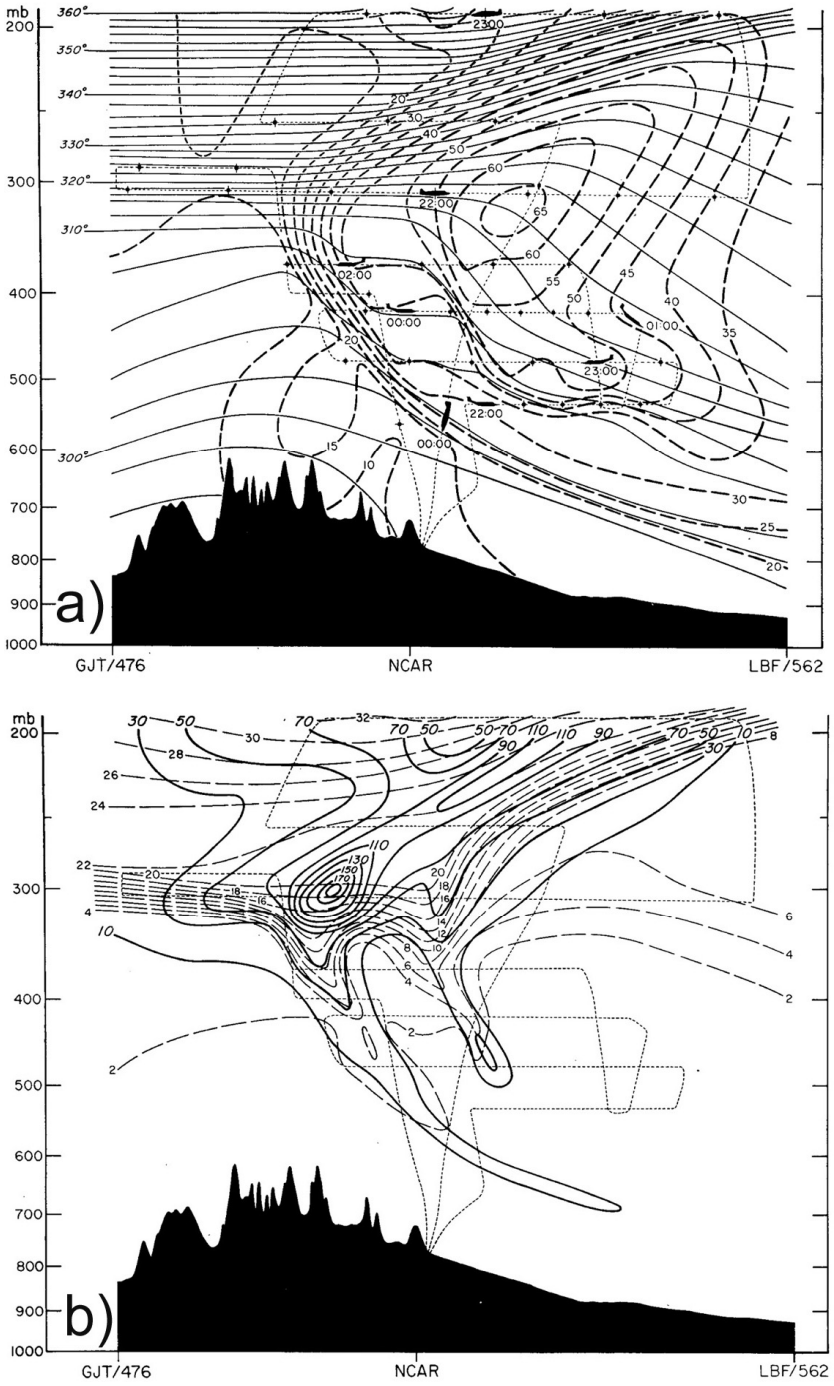

Figure 2.9 a) Cross-section of potential temperature and wind speed corresponding to flights performed across a jet stream for 1200 GMT 19 April 1971. Isentropes (K) are shown as solid lines; isotachs (m s^{-1}) as heavy dashed lines; and flight paths as light dashed lines with time (GMT) shown by the silhouetted aircraft and 10-min interval shown by time "hacks". Ground topography shaded. Positions of the Grand Junction, NCAR, and North Plate rawinsonde ascents marked along abscissa. b) Potential and ozone distribution for flight cross-section in b). Potential vorticity (10^{-6} s^{-1} K mb^{-1}) are shown as solid lines; ozone (parts per 10^8 per volume) as dashed lines) (from Shapiro et al., 1974).

over North America. Measurements typically included static and dynamic pressure, air temperature, wind speed, magnetic heading, and ozone partial pressure. Figure 2.9 presents results and analysis of the collected data. The cross-section shows packed isentropic surfaces in the stratosphere as expected, but also the core of highest winds, and higher static stability (lower tropopause) toward the cold side of the jet. In addition, a "tongue" of stratospheric air intruding into the troposphere is clearly depicted in that figure. Analysis of potential vorticity indicates that the tropopause, defined by a constant value of potential vorticity, is definitely lower on the cold side of the jet as expected from eq. 2.12.

In a later paper, Shapiro et al. (1987) examined other aircraft measurements carried out within the Arctic Gas and Aerosol Sampling Program. They showed a tropopause folding event associated with a very deep migration of the polar vortex into low latitudes for mid-January of 1985. Figures 2.10a and 2.10b show geopotential height, winds, and temperature for the 500 and 850 mb isobaric surfaces, respectively. The existence of narrow regions with strong winds is evident. In addition, projections of two cross sections are depicted in that figure (AA' and BB'). The cross section of potential temperature and wind along the line AA' (figure 2.11) shows the wind and temperature structure of a region within two frontal zones, each of them associated with a jet stream. The data depicts a strong upper-level jet at an approximate altitude of 370 mb, whereas a second weaker jet is almost on top of it at about 300 mb. Shapiro et al (1987) ascribed the former to the arctic jet and the latter with the polar jet stream. In both cases tropopause folding was evident although the more intense jet presented a stronger deformation of the tropopause with stratospheric air intruding even below 700 mb.

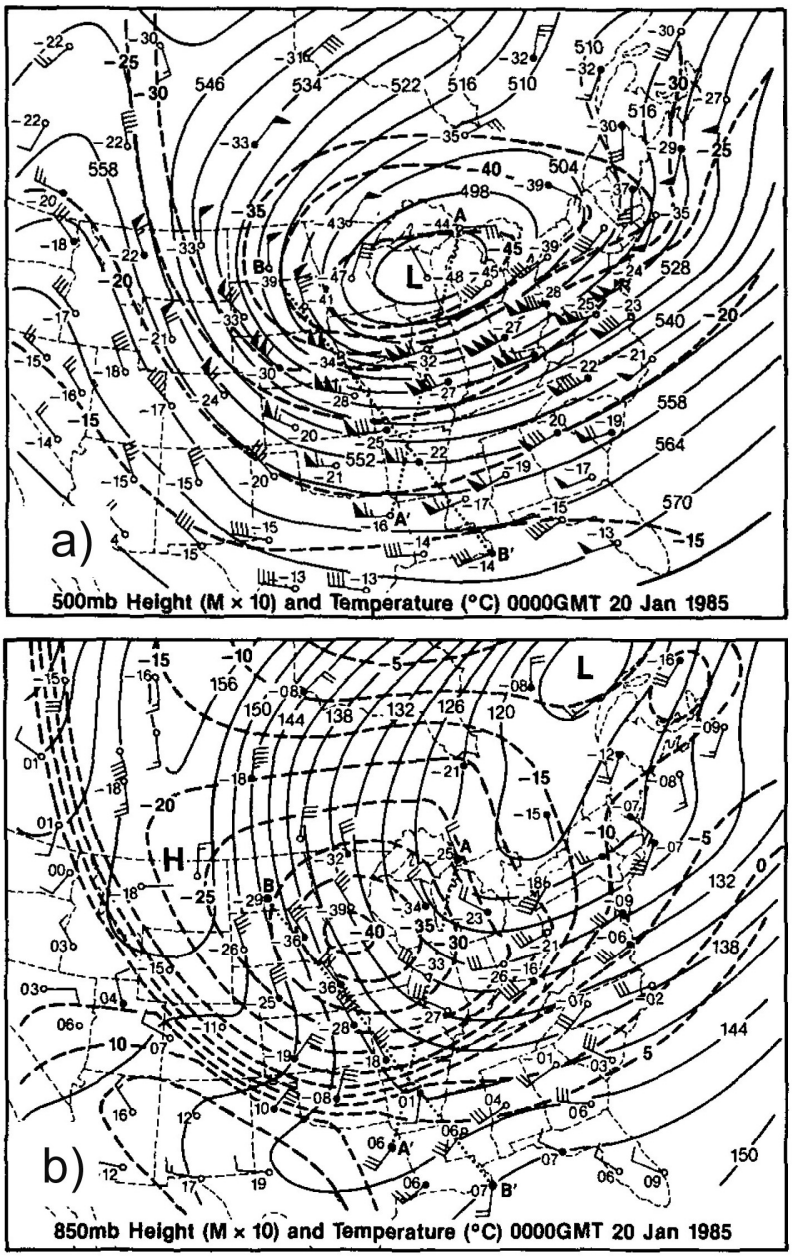

Figure 2.10 a) 500 mb geopotential height (decameters, solid lines) and temperature (ºC, dashed lines) at 0000 UTC 20 January 1985. Wind vector flags and barbs are as follow: flag=25 m s^{-1}, full barb = 10 m s^{-1}, half barb = 2.5 m s^{-1}. Projection lines for cross sections AA' (figure 3.5) are dotted lines. b) 850 mb geopotential height and temperature corresponding to a) (from Shapiro et al., 1987).

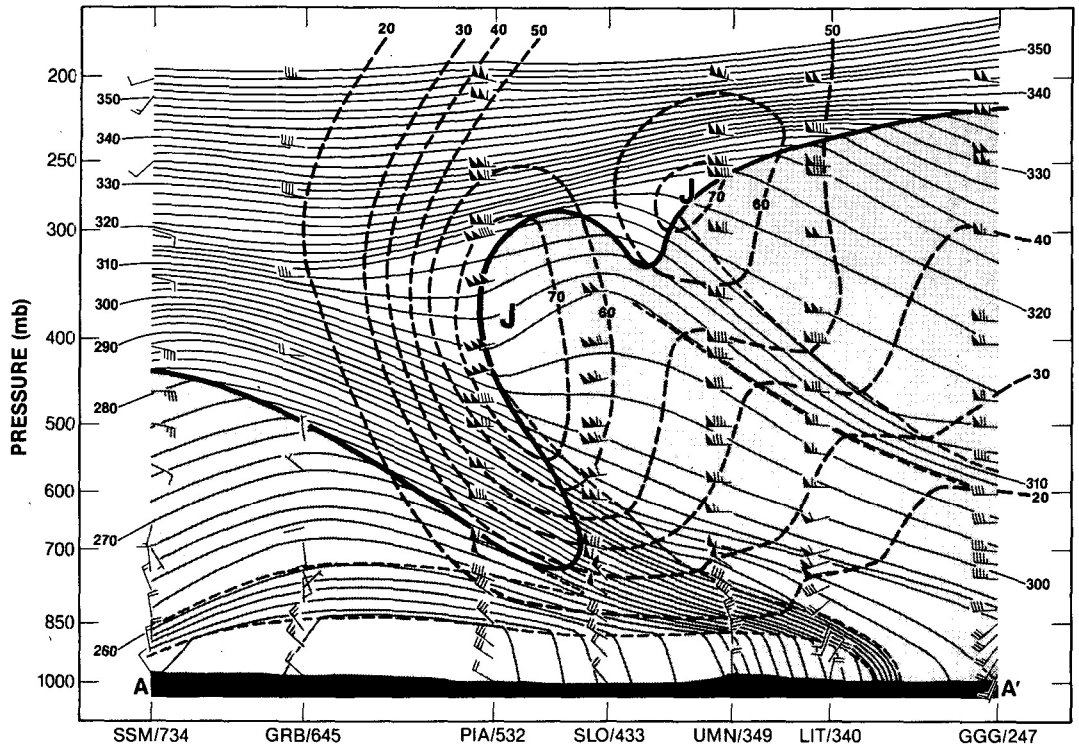

Figure 2.11 Cross-section analysis of potential temperature (K, thin solid lines) and wind speed (m s^{-1}, heavy dashed lines) between Sault Sainte Marie, Michigan (46.5ºN, 84.3ºW) and Longview, Texas (32.4ºN, 94.7ºW), along the projection line AA' of fig. 3.4. Heavy solid line marks the tropopause (10^{-7} K s^{-1} mb^{-1} isopleth of potential vorticity). Thin dashed lines indicate the tropospheric frontal and stable layer boundaries. Wind vectors are the same as in fig. 3.4 (from Shapiro et al., 1987).

Based on numerous cases studied with the aid of aircraft measurements and sondes released from ground stations, Shapiro et al. (1987) proposed a conceptual model of the meridional structure of the tropopause and principle jet streams. In that model (figure 2.12) the tropopause is always at higher altitude on the warm side of the jets. A realization of that model is given in figure 2.13 where a cross section analysis between 30º and 75ºN for 6 March 1979 shows good agreement with it.

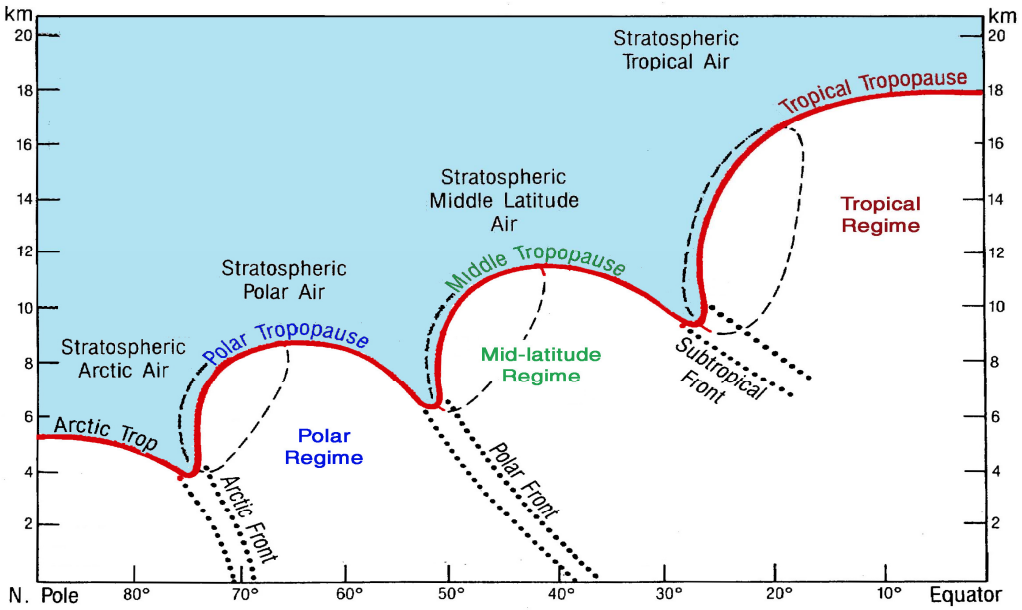

Figure 2.12 The "threefold" structure of the tropopause. Potential vorticity discontinuity tropopause shown as heavy solid line, with the stratosphere region stippled. The 40 m s^{-1} isotach (thin dashed line) encircles the cores of the three primary jet streams; the Arctic, Ja; the polar, Jp; and the subtropical, Js. Individual cross sections may exhibit spatial and temporal variations from that presented in this idealized meridional model (from Shapiro et al., 1987).

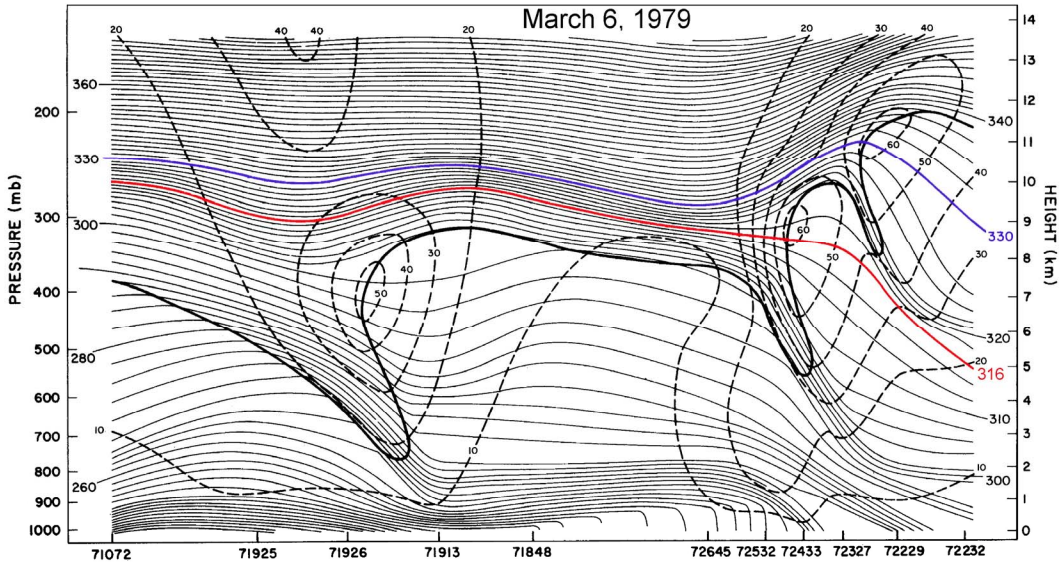

Figure 2.13 Cross-section of potential temperature (K, thin solid lines), wind speed (m s^{-1}, heavy dashed lines), and potential vorticity tropopause (10^{-7} K s^{-1} mb^{-1} isopleth, heavy solid line) at 1200 UTC 6 March 1979 along the projection line between Resolute, Canada (74.4ºN, 133.3ºW) and Boothsville, Lousiana (29.5ºN, 89.7ºW) (from Shapiro et al., 1987).

2.4 Total Ozone and Tropopause Height

The total ozone column (or simply *total ozone*) is defined as the vertically integrated ozone in a column from the surface to the top of the atmosphere. Except for events where tropospheric pollution is important, only about 10% of the total ozone resides in the troposphere (Staehelin et al., 2001). From the remaining 90%, only a small fraction resides above 35 km (Dessler, 2000). In addition, above 30 km ozone is in photochemical equilibrium (Dobson, 1968b).

From the beginning of ozone observations, measurements showed a large daily variability of total ozone in mid and high latitudes (Dobson, 1927). Given the small amount of ozone in the troposphere, these day-to-day fluctuations in the ozone column are expected to arise from variations in the concentration of ozone in the air between the regions where photochemistry takes place, the upper stratosphere, and the tropopause (Dobson, 1968b). Dobson (1927) observed a marked connection between total ozone and the "general type of atmospheric pressure distribution" (i.e. low or high pressure)[4]. In fact, as he mentioned later, there is a close connection between total ozone and meteorological variables (Dobson, 1968b; Petzoldt et al., 1994). Therefore, it is natural to expect the tropopause height to be highly correlated with the ozone column, as shown in figure 2.14, and for tropopause dynamics to play an important role in total ozone behavior (Morgan and Nielsen Gammon, 1998).

[4] It is interesting to note that once Dobson had enough ozone measurements, he compared them with surface pressures and found a clear negative correlation. However, when measurements of pressure in the middle troposphere were obtained, it was clear that the anticorrelation between pressure at 9km and total ozone was even stronger. Since at that time it was believed that the average height of ozone was around 40 km, the close connection between the upper troposphere-lower stratosphere and the upper stratosphere was surprising (for more historical details see Dobson, 1968a).

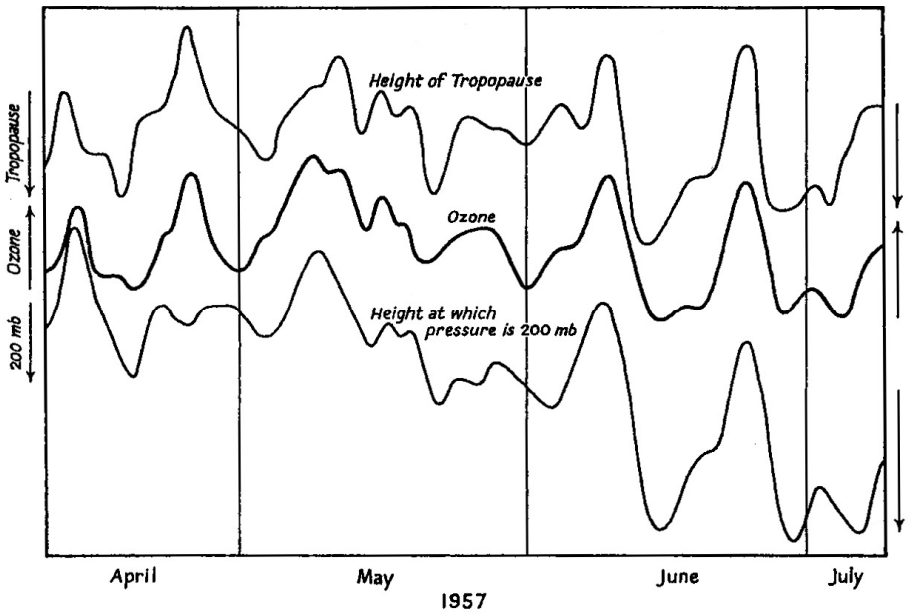

Figure 2.14 Three-day running average total ozone at Oxford, and tropopause height and 200 mb surface height at Crawley (110 km SE of Oxford) for 1957. Note that the top and bottom curves are plotted with heights increasing downwards (from Dobson, 1968).

Studies on the correlation between the tropopause height and total ozone at particular locations indicate a temporal correlation of approximately 0.5 for variations with periods shorter than a year (Steinbrecht et al., 1998) and ~0.75 when the annual cycle is included in the computations (Hoinka et al., 1996). These studies used long records (> 15 years) of almost simultaneous measurements from ozonesondes and total ozone ground-based instruments as well as rawinsondes and satellite-derived ozone measurements. Alternatively, Schubert and Munteanu (1988) and Dameris et al. (1995) used total ozone from satellite instruments and data from global analyses to estimate the correlation between tropopause height and total ozone. Schubert and Muntenau (1988), using data for 1979, found the highest correlation (>0.6) in the midlatitudes (approximately between 30º and 60º of latitude for both hemispheres), with a rapid decrease towards the equator and slower decrease towards the poles. Their analysis

suggests a stronger correlation in summer than in winter. Dameris et al. (1995) analyzed data for the winter of 91/92 in a region between 30º-80º N and 30ºW to 120ºE. They found a temporal correlation between tropopause height and total ozone as high as 0.6 in some of the analyzed regions during that winter. These studies indicate that a large portion of total ozone day-to-day variability can be ascribed to changes in tropopause height. This is consistent with results obtained by Reed (1950), Schoeberl and Krueger (1983), Salby and Callaghan (1993). A. Galliani et al. (1996), and others that show that both horizontal and vertical advection contribute to changes in the ozone column on short time scales (i.e. a few days).

2.5 Ozone and Potential Vorticity

Ertel's Potential Vorticity, or PV for short, is defined as

$$q = \rho^{-1}\vec{\zeta}_a \bullet \nabla\theta \tag{2.13}$$

where ρ is the air density, $\vec{\zeta}_a$ is the absolute vorticity and θ is potential temperature. Under the hydrostatic approximation and using isentropic coordinates, PV can be written in its isentropic form as (eq. 2.1)

$$q_\theta = -g\frac{f+\zeta_\theta}{\partial p/\partial\theta} \tag{2.1}$$

with ζ_θ being the vertical component of the relative 'isentropic vorticity' defined as

$$\zeta_\theta = \hat{k} \bullet \nabla_\theta \times \vec{V}_h = \left(\frac{\partial v}{\partial x}\right)_\theta - \left(\frac{\partial u}{\partial y}\right)_\theta \tag{2.14}$$

where *u* and *v* are the meridional and zonal components of the horizontal velocity $\vec{V}_h$ respectively. Equation (2.1) shows that PV is basically the product of a term that measures static stability ($\partial\theta/\partial p$) and a term that measures inertial stability (f+ζ_θ)

(Danielsen, 1985). The latter includes vorticity due to the Earth's rotation and vorticity due to motions relative to the Earth, respectively.

One of the most important features of potential vorticity is its conservative nature under frictionless motions (Hoskins et al., 1985). It can be shown that if θ is a function of the state variables p and ρ alone, then for isentropic motion of a parcel,

$$q = \rho^{-1}\vec{\zeta}_a \bullet \nabla\theta = \text{constant} \tag{2.15}$$

that is, PV is conserved following an air parcel. It is interesting to note that PV is conserved even for fully 3-dimensional non-hydrostatic motions (Hoskins et al., 1985).

Reed (1955) was one of the first to use PV to analyze upper-level fronts and their structure. His paper suggested that stratospheric air could be advected down following sloping "stratospheric" isentropes that penetrate deep into the troposphere. Reed and Danielsen (1959) proposed this process known as *tropopause folding*, and later, Danielsen (1968) confirmed experimentally the existence of these processes and the high spatial correlation between PV and ozone. Based on his results, he suggested that both PV and ozone could be used to determine whether or not a parcel of air was of stratospheric or tropospheric origin. Stratospheric air has high ozone mixing ratios and large values of PV (Danielsen, 1985), as opposed to tropospheric air which has low ozone mixing ratios and low PV values. In actual fact, PV and ozone (more exactly its mixing ratio, χ_{O_3}) are positively correlated, as are their gradients ∇q and $\nabla\chi_{O_3}$ (Danielsen, 1985). Figure (2.15) shows profiles obtained from measurements carried on two stations in the USA. Despite the coarse resolution of the PV data, the profiles are very similar to each other.

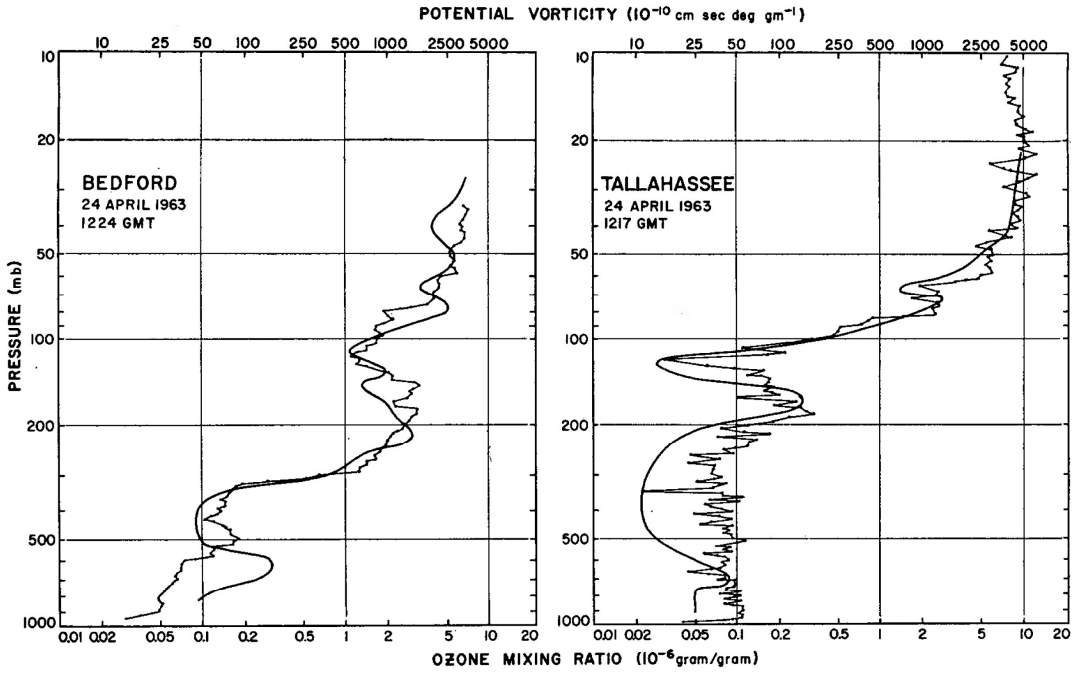

Figure 2.15 Vertical profiles of ozone mixing ratio (thin line) and potential vorticity (heavy line) derived from analysis of rawinsondes for Bedford, Mass., and Tallahassee, Fla., 1200 GMT 24 April 1963 (from Danielsen, 1968).

Mixing, which is adiabatic and irreversible, produces this positive correlation in the lower stratosphere (Danielsen, 1985). As a result, even in the case when stratospheric air penetrates into the troposphere, mixing will contribute to the "dilution" of both quantities keeping the correlation between them relative unchanged (Danielsen, 1985). However, if non-conservative processes are involved, this correlation can be changed or even broken completely (Danielsen, 1985). For instance, a gradient in diabatic heating can change PV but not ozone mixing ratio. By the same token, photochemical processes can change ozone mixing ratio without changing PV. Therefore, in the lower stratosphere and upper troposphere, where transport is the dominant mechanism to redistribute ozone and PV, change in the correlation between ozone mixing ratio and PV is expected to happen when non-conservative processes take place.

Following the pioneering work of Danielsen (1968), an extensive number of studies have confirmed the good correlation between ozone mixing ratio and PV in the lower stratosphere/upper troposphere both synoptically (Danielsen et al., 1970 ; Shapiro, 1980 and references therein; Danielsen, 1987) and statistically (Danielsen, 1985; Beekman et al., 1994, Rao et al., 2003). Danielsen (1985) compared two-dimensional (zonal-annual means) ozone mixing ratio and PV[5] distributions in order to analyze the correlation between them. He found that the area-weighted correlation between the deviations of the mean values of χ_{O_3} and PV are very high (> 0.9) in the upper troposphere and lower stratosphere (around 8 and 22 km of altitude). However, at about 24 km this positive correlation changes abruptly to a negative correlation. Danielsen (1985) attributed the former to dominance of transport whereas the latter was ascribed to photochemical dominance.

Beekman et al. (1994) on the other hand, compared ozonesonde and ECMWF analysis data. They used ozone mixing ratio from stations located between 41º and 52º N and computed the correlations for 225 mb and 500 mb isobaric surfaces. They found high correlation for the 225 mb surface (~0.8) and much lower correlation for the 500 mb surface (~0.4) when all seasons were included in the analysis. Interestingly, when the 500 mb data was analyzed by season, the highest correlation occurred between March and July (~0.5), and the lowest took place between August and October (~0.2). Rao et al. (2003) carried out a similar analysis for seven high latitude stations (60º-80ºN) between 1994 and 2001. Again the highest correlation between ozone mixing ratio and PV occurred for isobaric surfaces at 250 mb (~0.85) as compared to the correlation at 500 mb

[5] The deviations were defined as the difference between the zonal-temporal average and the horizontal (meridional and zonal)-temporal average.

(~0.3). In this case, however, the correlation at 250 mb was almost constant throughout the year.

The high (positive or negative) correlation between ozone and PV is not restricted to ozone mixing ratio but extends also to the ozone column. Good correlation between total ozone and PV at different isentropic and isobaric surfaces has also been found (Vaughan and Begum, 1989; Vaughan and Price, 1991; Riishøjgaard and E. Källén, 1997). Vaughan and Begun (1989) studied a region confined to south-east Asia and found that isentropic PV (IPV) correlated well with total ozone (< 0.7), especially at isentropic surfaces near the tropopause. The correlation was higher in a latitude band between 30º and 40º for all isentropic surfaces used in the study (310 to 390 K).

Based on the fact that χ_{O_3} and PV are highly correlated in the lower stratosphere, Vaughan and Price (1991) derived a theoretical relationship between total ozone and relative vorticity. They found that the ozone column Ω can be written as

$$\Omega = \frac{1}{M}\overline{\left(\frac{\chi}{q}\right)}\left\{ f(\theta_p - \theta_t) + \int_{\theta_t}^{\theta_p} \zeta_\theta d\theta \right\} + \Omega_T + \Omega_U \qquad (2.16)$$

where the overbar indicates mean value, θ_t and θ_p are the potential temperature at the tropopause and at the level where χ_{O_3} and PV are no longer positively correlated, Ω_T is the tropospheric ozone column, Ω_U is the residual ozone column above θ_p, and M is the mass of an air molecule. Given that the troposphere typically contributes with only 10% to the ozone column, and that integration of typical profiles above θ_p (about 24 km, Danielsen, 1985) is almost constant at all latitudes, Ω_T and Ω_U can be regarded as constants in eq. 2.16. As a result, Vaughan and Prince (1991) argued that when there is

little phase propagation with height, the integral of ζ_θ with height is directly related to the value of ζ_θ at the base of the stratosphere. Therefore, at synoptic scales and smaller, a correlation between Ω and relative vorticity is expected. Clearly, given the assumptions, a correlation between total ozone and potential vorticity is also expected.

Allaart et al. (1993) followed a slightly different approach. They statistically compared column integrated potential vorticity (taken from ECMWF analyses) with total ozone (as seen by the TOVS instrument). They showed that the total ozone field can be reconstructed from the PV distribution by using a discrete version of

$$\Omega(t) = \Omega_0 + K(t)\int_{400hPa}^{50hPa} q(p)dp \; + \; \varepsilon(t) \tag{2.17}$$

In this equation Ω_0 is a constant value of 240 DU, *K(t)* is a slowly varying function of time (to account seasonal variations in the correlation) and ε is the amount of ozone column not explained by the ozone-PV correlation. The RMS of ε is of the order 10-20 DU which is of the same order of the reported error of ozone retrieved by TOVS (Planet et al., 1984).

Davis et al. (1999) used the total ozone-PV correlation to retrieve winds from the Total Ozone Mapping Spectrometer (TOMS) data. In this case, they defined the column integrated PV, Σ, as follows,

$$\Sigma = \frac{1}{\Delta p}\int_{p_1}^{p_2} q(p)dp \tag{2.18}$$

where $\Delta p = p_2 - p_1$, with p_2=50 mb and p_1=500 mb. PV data was obtained from the NCEP/NCAR (National Centers for Environmental Prediction/National Center for Atmospheric Research). Equation (2.18) shows that Σ is basically the average PV within

the layer Δp . In their study, Davis et al. (1999) showed that the correlation between ozone and PV is variable from day to day, and that it is has a strong latitudinal dependence, with essentially no correlation in the tropics and high correlation in mid-latitudes.

All these results clearly indicate that PV and ozone are highly correlated in regions around the extratropical tropopause (lower stratosphere/upper troposphere), suggesting that the dynamical information present in the total ozone field mainly concerns this region. Such a good correlation is impressive given the fact that sources and sinks of ozone and PV are not identically distributed. As mentioned before, ozone is produced mainly in the middle and high tropical stratosphere, and is destroyed at the surface (WMO, 1986). In contrast, because PV can neither be created or destroyed within a layer bounded by two isentropic surfaces (Haynes and McIntyre, 1987), sources or sinks of PV can only exist on isentropes that intersect the lower boundary. However, that is not the only way that the PV column can change. If the isentropes become closer (farther apart) from each other, reflecting the increase (decrease) of static stability, then the PV column also increases (decreases). This effect may be interpreted as the sources and sinks for PV being diabatic heating (cooling) (Riishøjgaard and Källén, 1997).

2.6 Total Ozone and Meteorological Regimes

From the discussion in the previous sections, it is clear that total ozone and the tropopause height change relatively abruptly in regions near the upper-level jets, especially during cyclogenesis events. The question is, what is the behavior of these two quantities in areas far from regions where cyclogenesis is occurring? Shalamyanskiy (1980), and Shalamyanskiy and Romashkina (1980) analyzed aircraft data collected by

the Main Geophysical Observatory of the former Soviet Union. These flights intersected the polar and subtropical jets-fronts 32 times between 1974 and 1977 (Shalamyanskiy and Romashkina, 1980). All these cross-sections confirmed the fact that the zones of jet streams always coincided with regions of large gradients in total ozone. However, in flights with lengths from 500 km to 2000 km outside the jet stream region, total ozone gradients were found to be small and without a definite sign in the meridional, or the latitudinal direction (Shalamyanskiy and Romashkina, 1980). As they pointed out, this implies that the quasi-synoptic meridional section of the total ozone field is not smooth (as a zonal average would indicate), but rather a stepwise rise in total ozone from the tropics to the poles. This pattern was observed in all flights in the meridional direction with the "steps" corresponding to the position of the upper-level jets.

The observations suggest, therefore, that the ozone field can be classified into regions whose boundaries are the polar and subtropical jets. In order to see if this was true over the whole Northern Hemisphere and not only over regions where the aircrafts were flown (the former Soviet Union), Shalamyanskiy and Romashkina (1980) analyzed charts of geopotential height for every day between 1975 and 1976. They used isobaric surfaces of 200 mb and 300 mb to identify isohypses (height contours) that corresponded to regions with the highest winds. The 300 mb surface was used to identify the polar jet and the 200 mb surface to identify the subtropical jet. The resultant isohypses were then compared with isopleths of total ozone previously identified from the aircraft data. The agreement between them was remarkably good, indicating that both fields can be separated into three regions or *regimes*[6]. Interestingly, Shalamyanskiy and Romashkina

[6] They designated these regions as *air masses*. We will call them *regimes* throughout this work.

(1980) noted that the isohypses taken as the boundaries of these regimes in the geopotential height field clearly separated the total ozone field over the entire Northern Hemisphere and not only in regions where the jet streams were present. That is, these isohypses separate the ozone field not only in regions of very strong winds (where they were determined) but also in locations where the wind speed is slow.

Additional analyses of the characteristics of these regimes (Karol et al., 1987) show that the variability of ozone and temperature is reduced by a factor of 1.5 or 2 within a regime as compared to the variability along the same latitudinal band. Even further, they showed that despite the extremely variable configuration of the regime boundaries, many of their characteristics are stable and show certain regularity. For instance, geopotential heights that identify the upper level jets exhibited little day-to-day variability and their mean monthly values show little interannual variability (Karol et al., 1987).

Independently of these findings, Shapiro et al. (1982) suggested that the position and intensity of upper-level jet streams could be identified from satellite instruments that measure the ozone column. They used data from TOMS on board of Nimbus-7, aircraft measurements, and rawinsondes in order to study a few cases. Aircraft and rawinsonde data were used to produce cross-sections of regions where strong upper-level jets were present. As expected from the discussion in sections 3.2 and 3.3, these analyses show the characteristic tropopause folds and, maybe more important for this case, the horizontal discontinuities in both the depth of the stratosphere, and ozone (Shapiro et al., 1982). When TOMS ozone maps were inspected looking for mesoscale discontinuities in the total ozone field, it was found that these discontinuities coincided with the axis of the jet

streams. The intensity of the ozone gradients appeared to be proportional to the magnitude of the jet wind speed (Shapiro et al., 1982).

Just recently, Hudson et al. (2003) used total ozone from TOMS to identify the location of the upper-level fronts and therefore, following Shalamanyanskiy and Romanshkina (1980), classify the Northern Hemisphere atmosphere into meteorological regimes. Based on the fact that total ozone variability is much smaller within a regime than in a latitudinal band (Karol et al., 1987), Hudson et al. (2003) used an iterative approach to calculate the ozone values used to define the regime boundaries for every day. They confirmed the smaller total ozone spatial variability within a regime, and the little day-to-day ozone variability. In addition, they showed that the tropopause height, calculated from daily synoptic rawinsonde measurements, shows clearly distinct values for every regime. This fact is true not only for the thermal tropopause but also for the chemical tropopause defined by ozone concentration. Since the work of Hudson et al. (2003) is the basis of the present paper, a much more detailed explanation and discussion of their method is given in Chapter 3.

3. METHOD

The results obtained by Shalamyanskiy and Romanshkina (1980) and Hudson et al. (2003) show that the meteorological regimes are bounded by the upper-level subtropical and polar jets. A very important part of this work is the correct identification of these jets and their spatial location. For that reason, the method to obtain the total ozone boundary values that mark their location as well as the methods used to test their accuracy and reliability will be described in detail in this and the next chapters.

Hudson et al. (2003) named the regions bounded by the upper-level jets as follows:

1) Tropical regime – the region between the Equator and the subtropical jet
2) Midlatitude regime – the region between the subtropical jet and the polar jet
3) Polar Regime – the region between the polar jet and the polar vortex when the latter is present or up to the pole otherwise

The region inside the polar vortex is treated separately (in fact, excluded from the present analysis) because it exists only in winter/spring and its characteristics, from a total ozone point of view, are very different from the remainder of the hemisphere.

3.1 Data Used to Identify the Upper-level Jets

Total ozone (Ω) level-3 hierarchical data format product from the Total Ozone Mapping Spectrometer (TOMS) instruments is used in this paper[7]. The time period covered by each of the TOMS instruments is shown in Table T5.1. The level-3 data set is an average ozone value on a 1-degree latitude by 1.25 degrees longitude grid. In addition,

[7] The data can be found at http://toms.gsfc.nasa.gov/.

level-2 hierarchical data format product is also used here. This data set contains the measurements made at each of the observation points of the instrument. The resolution of each point varies from 50x50 km to 50x150 km, depending on the viewing geometry. The data is collected around local noon everywhere and is therefore not synoptic data (for a more detailed description of the TOMS data see Appendix A).

Potential vorticity fields were obtained from the reanalysis data set from the National Centers for Environmental Prediction/ National Center of Atmospheric Research (NCEP/NCAR) (Kalnay et al., 1996; Kistler et al., 2001). The reanalysis data set is a combination of observational data and model analysis. All available data is assimilated and interpolated into the model after a careful quality control process (Kalnay et al., 1996) in order to estimate the "true" state of the atmosphere. The resulting product, therefore, is neither the original data nor the pure model results, but an optimal balance between them. Although satellite data is part of the input data, the analysis strongly depends on profile information gathered mainly by rawinsondes (Kalnay et al., 1996). The reanalysis data set has global coverage with synoptic fields at 0, 6, 12, and 18 Z in a grid of 2.5 x 2.5 degrees. In order to compare data from the reanalysis to total ozone data from TOMS, the former was interpolated in time to produce a "TOMS-centered" data set.

3.2 Gradients in the Total Ozone Field

The discussion in chapter 2 suggests that the natural way to locate the upper-level jets using total ozone data would be to examine the spatial gradient of this field. Figure 3.1 shows total ozone from TOMS for 5 September 1990. This day was chosen because many typical features are clearly observed in the data, but at the same time other

characteristics that could affect the accuracy and reliability of the method are also present.

The first thing that is clearly distinguishable in figure 3.1 is a large area near the pole with very low total ozone ($\Omega < 220$ DU). This area is the Antarctic Polar Vortex. As established by extensive field experiments and theoretical studies, ozone depletion due to heterogeneous chemical processes occurs within the vortex (Solomon et al., 1999 and references therein). In the context of the present study the polar vortex is a source of "noise" and therefore its location is important only to try to isolate it from the remaining hemisphere.

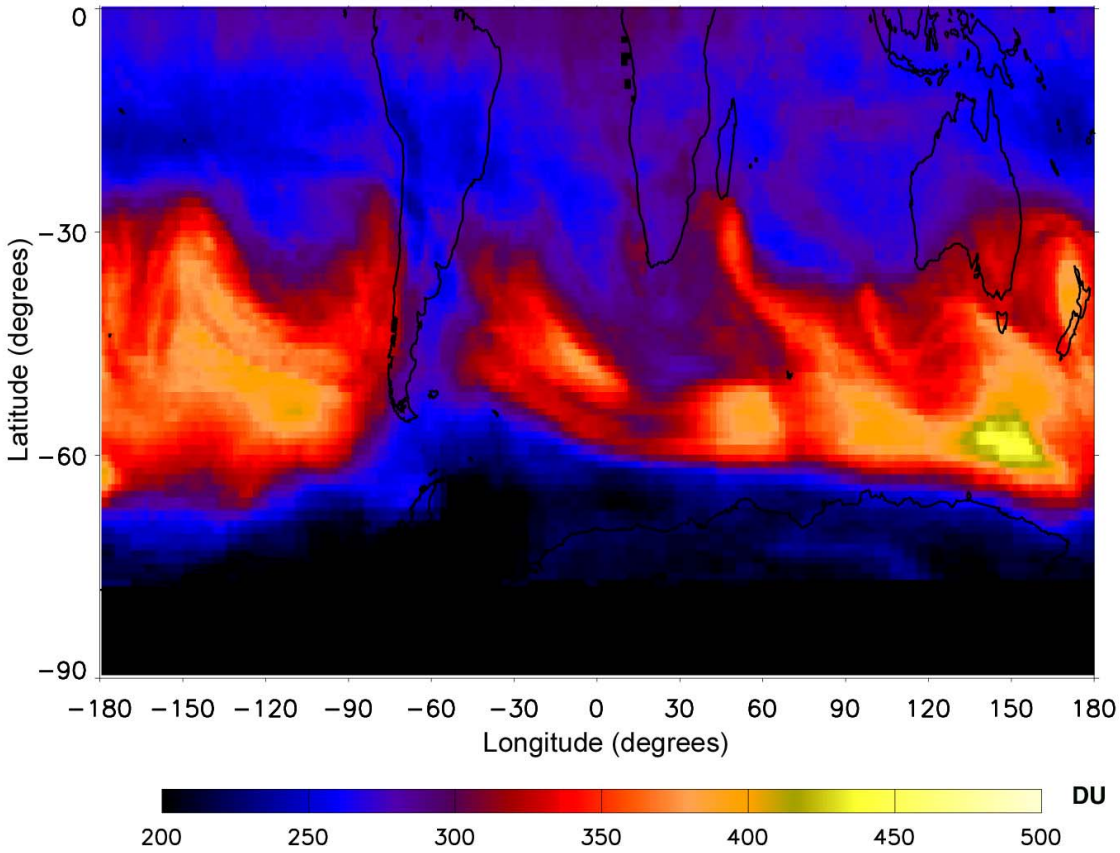

Figure 3.1 Southern Hemisphere total ozone field (in Dobson Units) for 5 September 1990. Data was collected by TOMS aboard Nimbus-7 and is reported in a 1.25º longitude x 1.0º latitude grid using TOMS version 8 algorithm.

Figure 3.2 shows the spatial ozone gradient computed from the total ozone field depicted in figure 3.1. This gradient was only computed between 70ºS and the equator because at high latitudes every two adjacent pixels in longitude have the same ozone value. As expected, a large gradient can be observed around 60ºS. This feature corresponds to the edge of the Antarctic Polar Vortex and therefore it should not be associated with the tropospheric upper-level jets. Other regions where the ozone gradient is large can be observed in fig 3.2. As it will be shown later, these gradients correspond to regions of high winds and changes in the tropopause height.

As suggested by Shalamyanskiy and Romanshkina (1980) and Hudson et al. (2003) two ozone values are expected to delineate the location of the subtropical and

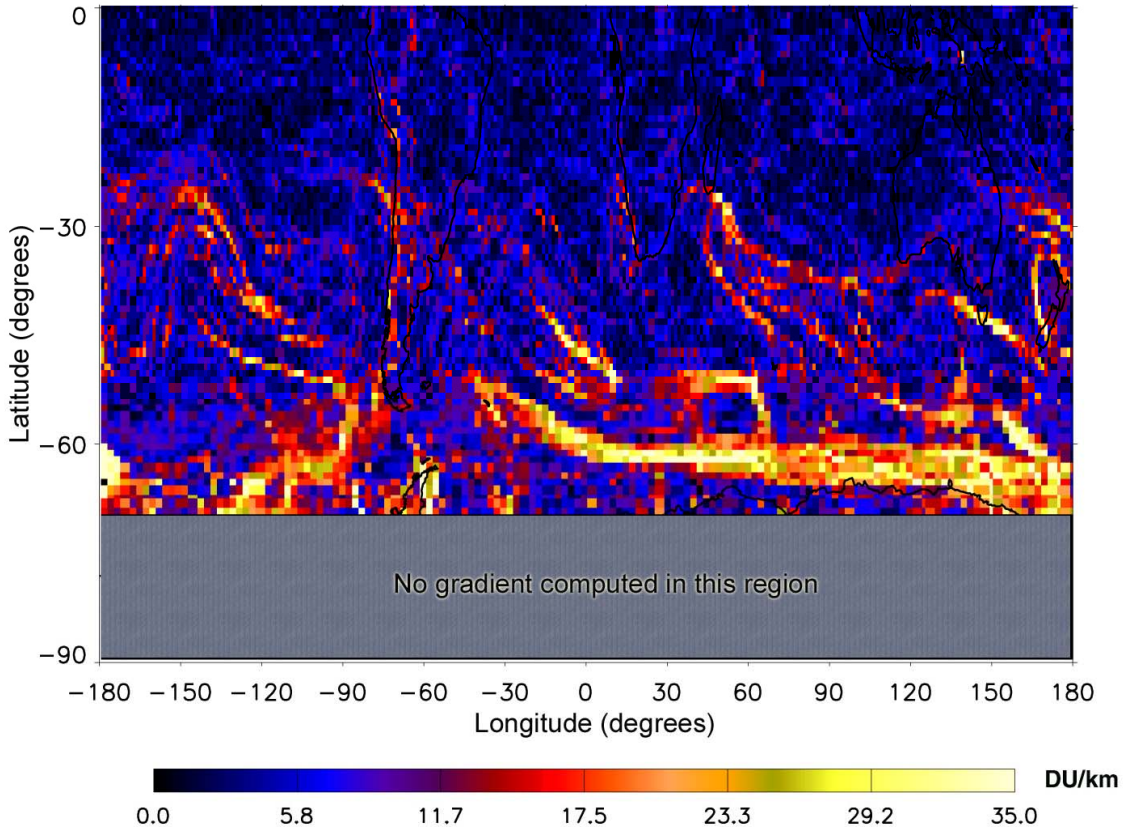

Figure 3.2 Total ozone spatial gradient obtained from TOMS data for 5 September 1990. Note that there is no data available at high latitudes for that day.

polar jets. In order to objectively find those values from the total ozone gradient field, histograms of the ozone gradient field binned by total ozone were produced. For example, all pixels with total ozone greater than 300 DU but smaller than 302 DU, and gradient larger than 10 DU/km, were selected. Then, their gradient magnitudes were added and later normalized in order to produce the "relative frequency" for this ozone interval. Figure 3.3a shows one of such histograms for 5 September 1990. Although no clear peak can be observed, there is some indication that there is one about 300 DU and another around 330 DU. In order to improve the statistics, TOMS level-2 data was used to produce the histogram (not for computing the gradients). Figure 3.3b shows this "enhanced" (by the number of points used) histogram. Now, three peaks can be clearly observed. The most pronounced, centered around 330 DU, corresponds to the gradient at the edge of the polar vortex as can be verified by inspection of figure 3.1. The other two peaks are associated, as will be shown ahead, with the subtropical and polar boundaries (~297 and ~375 DU respectively). It should be stressed here that the when the spatially averaged (gridded) data is used, the peaks in the histogram are not unmistakably defined,

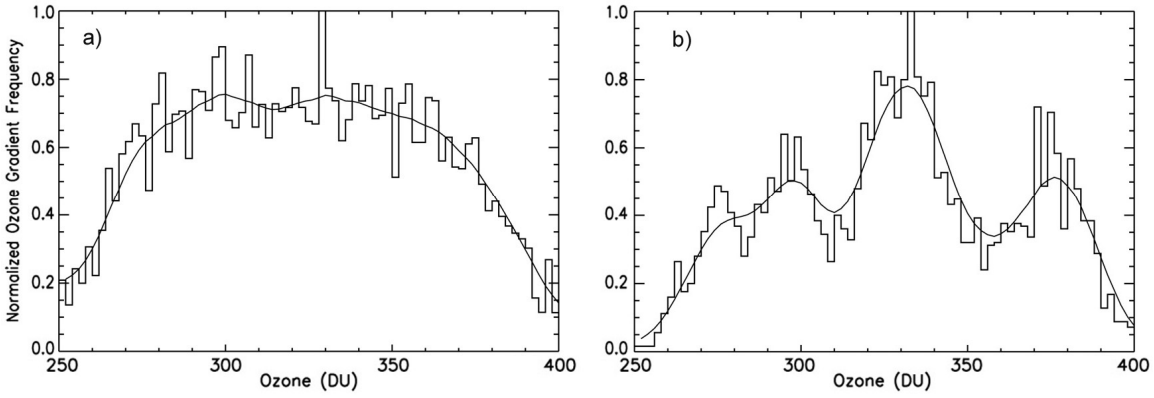

Figure 3.3 a) Normalized histogram of total ozone corresponding to regions with large spatial ozone gradient (pixels with a gradient magnitude larger than 10 DU/km in figure 3.2). The data corresponds to TOMS level-3 data for 5 September 1990 and has been binned in 2 DU intervals. b) Same as 3.3a but for TOMS level-2 data.

whereas when the high resolution data set is used, the peaks are clearly identifiable. This suggests that the averaging process smoothes some of the spatial features present in the original data.

Note that the Full Width at Half Maximum (FWHM) of the peaks in figure 3.3b is of the order of ~15-20 DU, indicating that the uncertainty in the determination of the ozone frontal boundaries is of the order of 10 DU for this particular day. This is a relatively large error for the boundaries especially in summer time. In addition, and even more importantly, the estimation of the local maxima shown in figure 3.3b is often not as easy as suggested by this figure. Since the frontal boundaries have to be computed on a daily basis, an "objective" method needs to be employed. The fitting option used does not guarantee the detection of both peaks, especially because they are weak in some months (usually during the fall). Furthermore, even when the method does detect both peaks, there are occasions that the FWHM is larger than 20 DU. Clearly this is not a very precise method and another, more robust and reliable technique, would be preferred.

3.3 Identification of the Polar Vortex

From the previous section it is clear that the stratospheric polar vortex, when present (from approximately June to November), could interfere with the determination of the ozone frontal boundaries. Traditionally, potential vorticity on isentropic surfaces has been used to determine the boundaries (and extension) of the polar vortex (Nash et al., 1996; Schoeberl et al., 1992). Although different potential temperature surfaces have been used for this purpose, PV on the 450 K or 550 K surfaces have been widely used. Following Nash et al. (1996) the 450 K isentropic surface was initially chosen to calculate the boundaries of the polar vortex. However, unlike Nash et al. (1996), a

simpler algorithm was used for this purpose. Spatial gradients on the PV field were computed for every day, and then the PV value that best defined the region with the largest PV gradient was used to delineate the boundary of the polar vortex. In order to reduce the noise, a five-day running average was used instead of the actual value. Subsequent analysis of these data showed that the same method but applied to the PV on the 550 K surface produced a better definition of the Antarctic polar vortex boundary. In any case, despite the simplicity of the method employed to determine these boundaries, sensitivity analyses indicates that, at least for the 25º-60ºS region, the results are robust and reliable. Figure 3.4 shows the PV field on the 550 K isentropic surface for 5 September 1990.

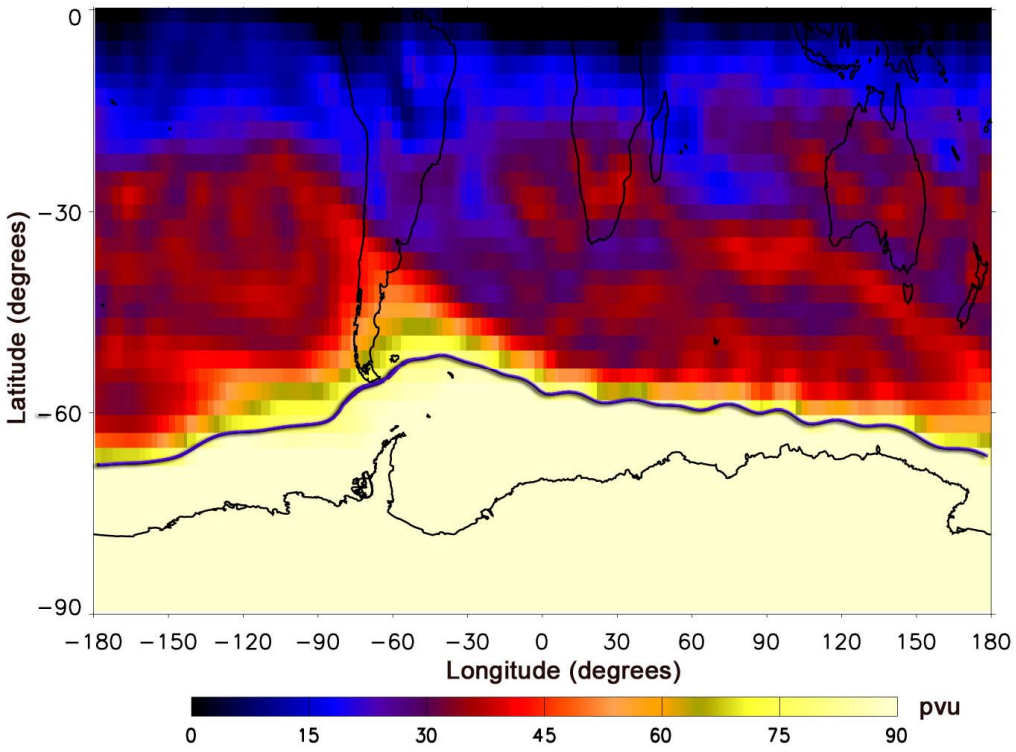

Figure 3.4 Potential vorticity on the 550 K isentropic surface for 5 September 1990 obtained from the NCEP/NCAR reanalysis data. The solid blue line marks the border of the Antarctic vortex corresponding to the largest PV gradient region on this surface.

3.4 Identification of the Upper-level Jets

The fact that, as shown by Hudson et al. (2003), total ozone is relatively constant within each regime suggests the possibility of computing the ozone boundary values from an iterative scheme. Following Hudson et al. (2003) the procedure indicated in figure 3.5 was applied. However, before explaining the method, there are a few things that should be explained in some detail.

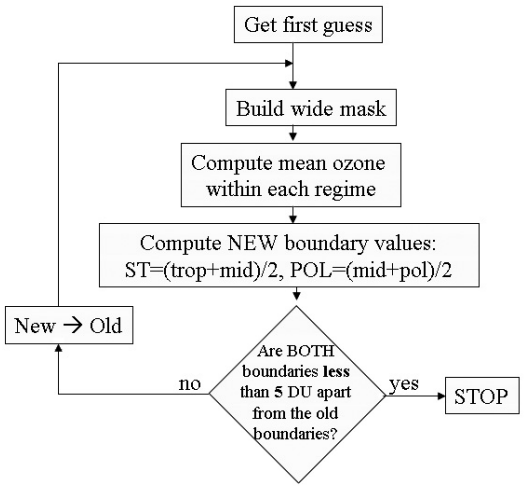

Figure 3.5 Flow chart of the algorithm used to determine the total ozone boundaries from the TOMS level-3 data.

The latitude interval used for this approach was 25º-60ºS in order to adequately weight the presence of the three regimes. If one regime is too dominant in terms of area, the values obtained for the frontal boundaries would typically have a much larger uncertainty.

The limit of 60ºS has been chosen for two additional reasons. First, because TOMS uses backscattered radiation, it cannot retrieve total ozone in regions with no direct sunlight. Therefore, an upper limit of 60ºS ensures a latitudinal band with data over the entire year. The second reason for choosing this latitude is related to the polar vortex. The Antarctic vortex grows much larger and lasts longer than its counterpart in the Northern Hemisphere. For this reason, excursions of vortex air north of 60ºS are more frequent in the Southern Hemisphere than south of 60ºN in the Northern Hemisphere. As will be discussed later, these events introduce “noise” that makes the determination of the

frontal boundaries less accurate. As a consequence, using a latitude higher than 60º would introduce even more noise into the data.

In the case of the Northern Hemisphere, Hudson et al. (2003) used "climatological" values of total ozone as a first guess to initiate the computations. This climatology was obtained from ground-based instruments as well as from concurrent rocket-sondes and ozonesondes from the former Soviet Union network (A. Frolov, 2001; personal communication, based on the Karol et al. (1980) analysis). Although the values of the first guess are not important for most months of the year, when the difference between the ozone values that define the frontal boundaries is small (in summer), values that are too far from the actual value could lead to non-convergence. Hence, for those months, it is important to have a reasonable estimation of the ozone frontal boundaries either by using experimental data (as in the case of the Northern hemisphere) or reanalysis data.

For the Southern Hemisphere, however, there was no information that could be used as a "first guess". For that reason, a meteorological variable that could aid in estimating and validating the ozone frontal boundaries was sought. After trying different options such as PV on different isentropic surfaces, geopotential height on 200 and 300 mb isobaric surfaces, and potential temperature on constant PV surfaces, we found that the best meteorological quantity for the "pre-identification" of the upper-level jets was the mean vertically integrated potential vorticity (MPV). Details about how and why this quantity was chosen are given in section 3.5. Suffice to say at this moment that this MPV field was used to obtain the "first guess" in ozone for the subtropical and polar regimes.

The algorithm used to calculate the ozone values that define the frontal boundaries is shown in figure 3.5. The first iteration took the “first guess” (obtained from MPV in this case) and classified the total ozone field by regimes. In order to perform this classification, masks with the same resolution as the TOMS level-3 data were used. A description of these masks is detailed in section 3.6. The only difference between the final mask described there and the masks used at this stage were the ozone values used to delineate the regime boundaries. During the iterations, the values computed at every step were used for that purpose.

Once the regions corresponding to the regime boundaries were identified, they were enlarged by 1º in latitude and 1.25º in longitude in order to exclude as many pixels close to the boundary regions as possible. The exclusion of these pixels assures a faster convergence of the procedure as well as the proper determination of the “true” ozone boundary values. In the next step, mean total ozone within each regime was computed and the “midpoints” between regimes were calculated. For example, the midpoint associated with the subtropical jet would be the arithmetical average of the mean total ozone for the tropical regime and the mean total ozone for the midlatitude regime. These “new” values for ozone were then compared with the “old” ones (the first guess in the case of the first iteration). If the difference between them was larger than 5 DU (for either of the two boundaries) the process was repeated until convergence was reached. In this way, the method estimates the ozone frontal boundaries with a precision of 5 DU. There are two reasons for not making this value smaller. First, in order to reduce the noise in the daily data, a 30-day running average is used instead of the obtained daily values. The standard deviation around the smoothed curve is of the order of ~3-4 DU. Second, a

value smaller than 2 DU produces some “instabilities” on some days (especially when one of the regimes is dominant), which in turn could lead to non-convergence. Therefore, the choice of 5 DU is a good compromise between precision and reliability using this approach.

As an example let us consider the values obtained for 5 September 1990. After convergence was achieved, the results indicate that the 309 DU isopleth delineates the subtropical jet, whereas the 363 DU isopleth marks the location of the polar jet for that day. Contours for these two values as well as the isopleth that delineates the polar vortex on the 550 K isentropic surface are plotted onto the ozone field in figure 3.6. The yellow

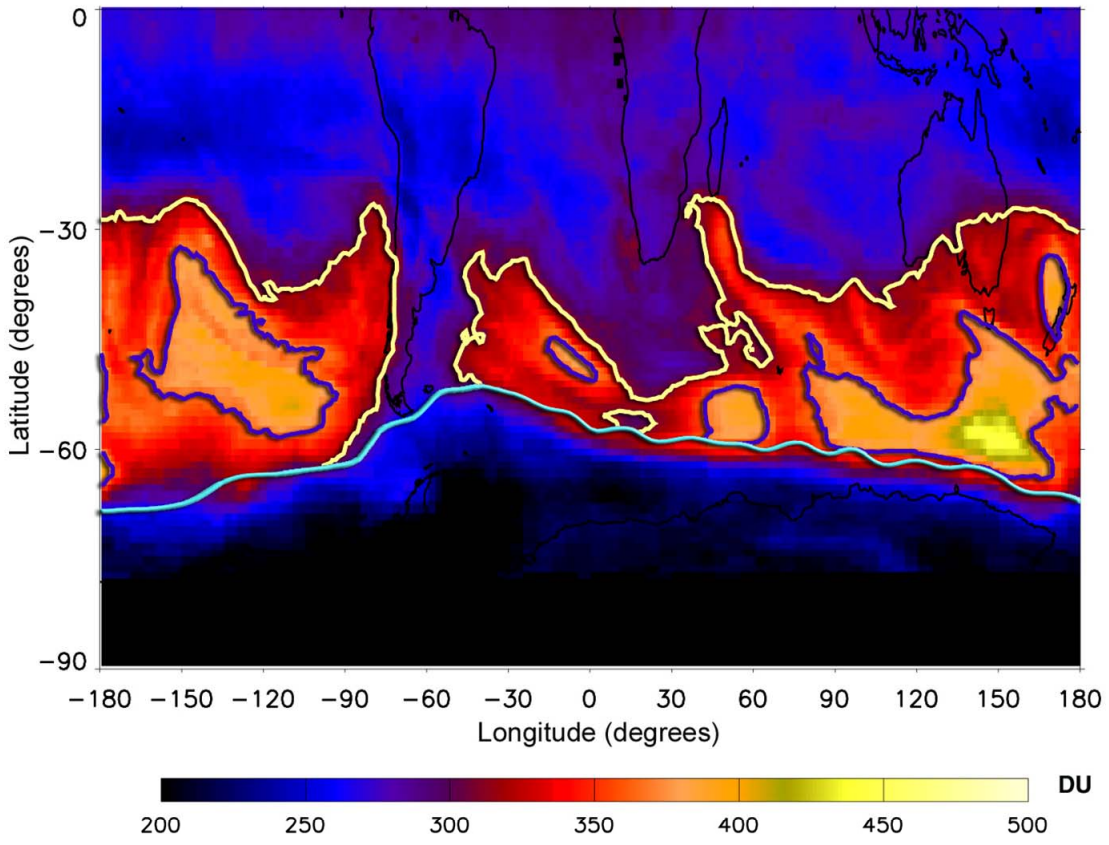

Figure 3.6 TOMS level-3 data for 5 September 1990. The light blue-green line denotes the position of the Antarctic polar vortex. The yellow contour indicates the location of the subtropical jet (except at latitudes higher than 60º, where in some places the Antarctic boundary is not delineating its edge correctly), the dark blue contour shows the location of the polar jet. See text for explanation on how these contours were calculated.

contour identifies the location of the subtropical jet (except at latitudes higher than 60º, where in some places the Antarctic boundary is not delineating its edge correctly), the dark blue line corresponds to the polar jet, and the light blue contour designates the edge of the polar vortex. Note that both ozone values correspond reasonably well to the regions of largest gradients in ozone shown in figure 3.3b (~297±10 for the subtropical jet, ~375±10 for the polar jet). After the 30-day running average, the numbers used for subsequent analyses are 310 DU for the subtropical jet and 368 DU for the polar jet.

The precision and accuracy with which these boundaries are computed are also related to the choices made for the latitudinal band used for the analysis, and the isentropic surface used to define the polar vortex. In order to estimate the error introduced by those choices, the ozone boundary values were computed for different latitude bands and isentropic surfaces. Potential vorticity on the 450 K and 550 K isentropic surfaces were used to define the Antarctic vortex; 20º, 25º, and 30ºS were used as the lower limit of the band, and 55º, 60º, and 65ºS were used for the upper limit. The boundary values obtained from the combination of these parameters differed by less than 5 DU with respect to the values used in this thesis. In addition, the mean difference throughout the year is less than 2 DU. This clearly indicates that the ozone boundary values calculated for the band 25º-60ºS and 550 K isentropic surface, are robust and reliable.

3.5 Masks and Meteorological Regimes

The 30-day running average of the total ozone values computed from the iterative scheme were used to classify the total ozone field into meteorological regimes for every

day that TOMS data was available. In order to facilitate the process and apply this classification to other meteorological data, masks at the same resolution of TOMS level-3 data were produced. In these masks, every "pixel" is ascribed to one regime, boundary region, or the stratospheric polar vortex region. The boundary regions on these masks are marked by computing contours of the ozone frontal boundaries values on the total ozone field. All pixels "touched" by the contour were marked as "boundary or transition zones". Thus, the width of these frontal boundaries was implicitly defined as one pixel (1.25º longitude x 1.0º latitude). The remaining pixels were ascribed to the meteorological regimes based on their total ozone value. For instance, if total ozone within a pixel was smaller than the value that identified the subtropical jet, the pixel was ascribed to the

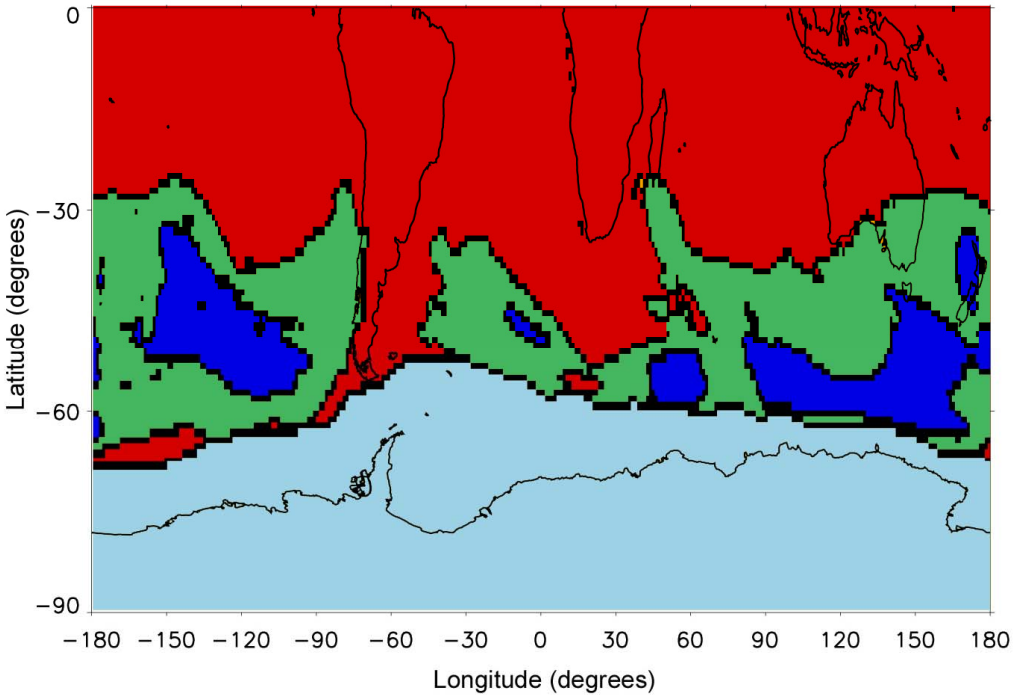

Figure 3.7 Mask created for 5 September 1990 using the smoothed boundary values computed following the procedure described in figure 3.5. The position of the Antarctic boundary was obtained from the region with the largest PV-gradient on the 550-K isentropic surface from the NCEP–NCAR reanalysis data. Each black pixel represents a 1º latitude by 1.25º longitude area. The colors indicate the 3 regimes: red for the tropical regime, green for the midlatitude regime, and dark blue for the polar regime. The light blue region corresponds to the polar vortex, while black pixels correspond to the boundary regions.

tropical regime, whereas if its value was larger than that, but lower than the value for the polar jet, it was classified as a midlatitude pixel. When the polar vortex was present, a similar procedure could be used on the 550 K isentropic surface, only using PV instead of ozone.

Figure 3.7 shows a mask for 5 September 1990. There, colors indicate the 3 regimes: red for the tropical regime, green for the midlatitude regime, and dark blue for the polar regime. The light blue region corresponds to the polar vortex, while black pixels correspond to the boundary regions. In this way, these masks not only delineate the location of the upper-level jets, but identify those pixels that are within each regime. The masks built in this way are referred as "narrow masks". However, some studies required the use of all data available. In this case, half of the pixels were assigned to one regime, and the other half were assigned to the other. These masks with no-boundary pixels are referred as "zero masks". For some of the analyses carried out in this paper it was important to reduce the influence of these transition zones. Consequently, the boundary regions were enlarged by 'n' pixels in both latitude and longitude. These masks will be referred as "broad masks".

3.6 Mean Vertically Integrated PV (MPV)

3.6.1 Definition and relation to total ozone

As discussed in Chapter 2, vertically integrated PV has been correlated with total ozone. Different pressure levels have been used to define this PV column. For instance, Davis et al. (1999) integrated PV between 500 and 50 mb, whereas Allart et al. (1993) used the 400-50 mb interval. The lower limit (in altitude) is usually chosen because PV is very small below those pressures, and therefore it does not contribute significantly to the

integral. The upper limit, on the other hand, was implicitly suggested by Danielsen (1985) who showed that a high positive correlation (>0.9) between ozone mixing ratio and PV in the upper troposphere/lower stratosphere changes abruptly to a negative one at about 24 km altitude.

Following Davis et al. (1999) and Shapiro et al. (1999) the vertically integrated PV has been normalized in order to obtain a "mean vertically integrated PV" or MPV as follows,

$$\mathrm{MPV} = \left| \frac{1}{\Delta p} \int_{p_1}^{p_2} q(p)dp \right| \tag{3.1}$$

with $\Delta p = p_2 - p_1$. Note that MPV is nothing more than the absolute value of the integral in height of the density-weighted PV, normalized by Δp. As a consequence, MPV has the same units as PV, in this case pvu.

Reanalysis data from the European Centre for Medium Weather Forecast (ECMWF)[8] was used to find and verify the optimum pressure interval to compute MPV. The reason for choosing this data set for this particular task, in lieu of the NCEP/NCAR reanalysis, is related to the availability of PV on isobaric surfaces from the ECMWF as opposed to PV on isentropic surfaces for the case of NCEP/NCAR. Potential vorticity on 10, 20, 30, 50, 70, 100, 150, 200, 250, 300, 400, and 500 mb isobaric surfaces were used for the analysis in this section.

As a first step, MPV for the entire globe was computed between 500 and 50 mb to verify that high spatial correlation between this field and the total ozone field is observed as suggested. Figure 3.8a shows the MPV field for 5 September 1990. The region

[8] http://www.ecmwf.int/

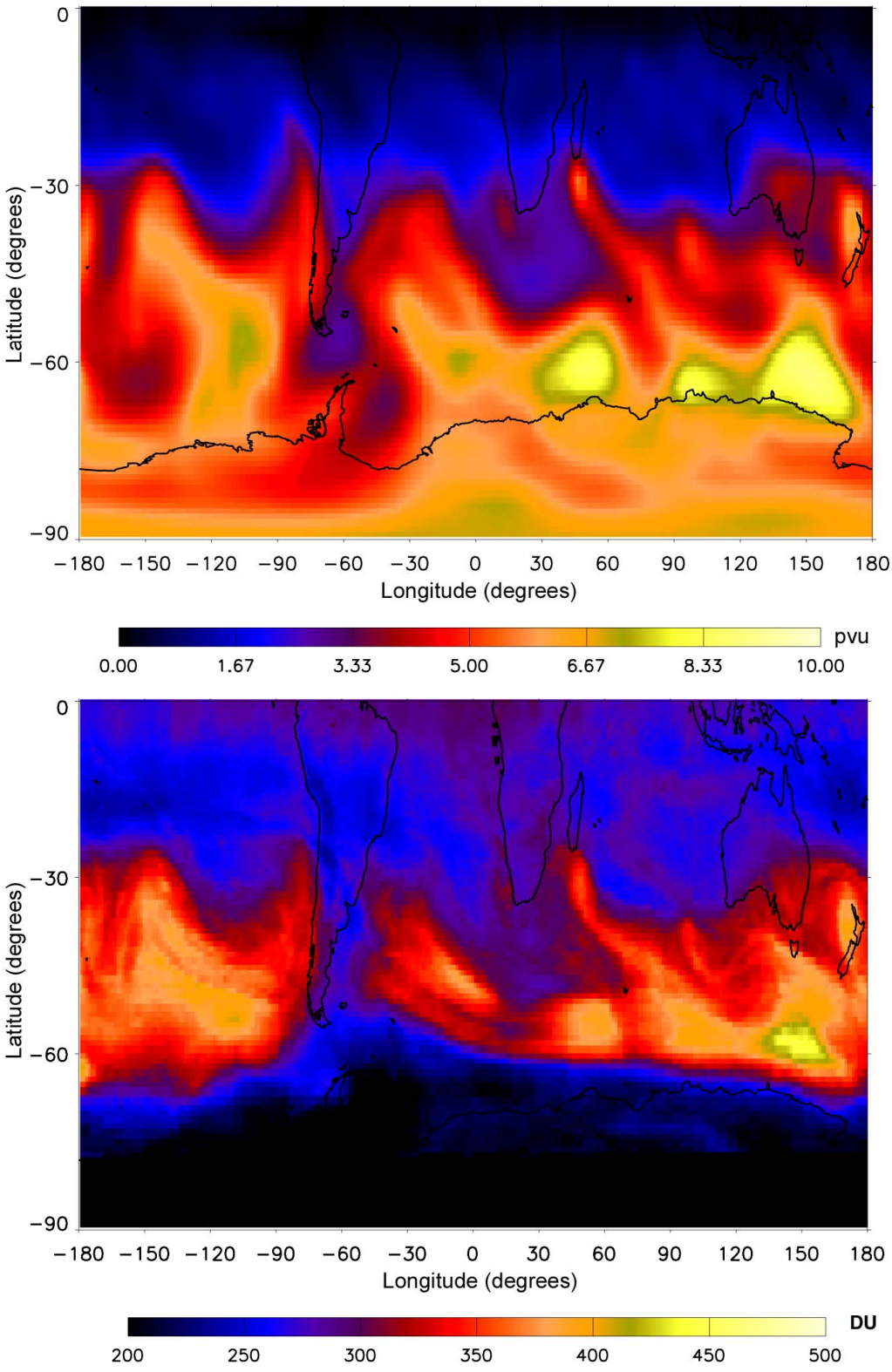

Figure 3.8 a) Mean Integrated PV (MPV) between 500 and 70 mb calculated from ECMWF data for 5 September 1990. For comparison, TOMS total ozone data has been plotted in b) for the same day (figure 3.1).

between 20º and 60ºS shows many similarities between the MPV and ozone fields. For instance, two elongated "tongues" of relative high ozone/MPV (red color) extending equatorward are clearly visible on both fields (figure 3.8b) at approximately 90ºW and 45ºE. By the same token, two poleward intrusions of "tropical" air (low MPV/ozone) can be observed at approximately 75ºW and 15ºE in both fields. The region of largest disagreement between these two fields is the one corresponding to the polar vortex. Nevertheless, from 3.8 it seems evident that if the polar vortex was excluded, the MPV and ozone fields would be linearly related. In order to explore this relationship, MPV was plotted against total ozone for the 25º-60ºS band in figure 3.9a (no data was excluded). The colors indicate the latitude of every pixel and the solid line was obtained from a simple linear regression between MPV and ozone. Despite the relatively large dispersion of the points, it is clear that most of them are concentrated along the solid line (the area-

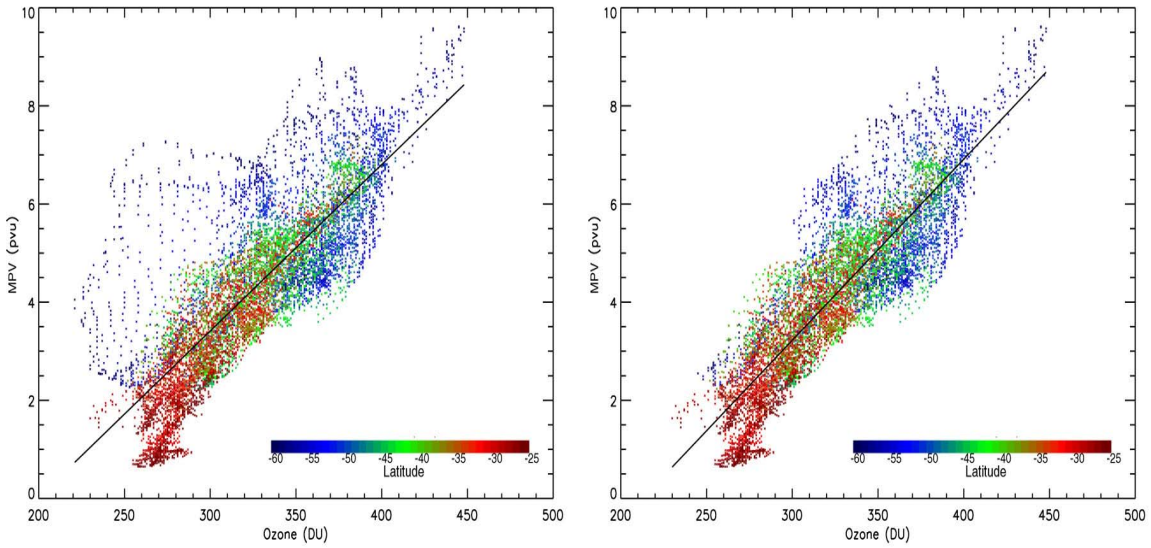

Figure 3.9 Scatter plot of MPV against total ozone for the 25º-60ºS band on 5 September 1990. The colors indicate the latitude of every pixel. MPV data has been interpolated to the TOMS resolution in order to compute their correlation. a) The polar vortex region is included. b) The polar vortex data is excluded.

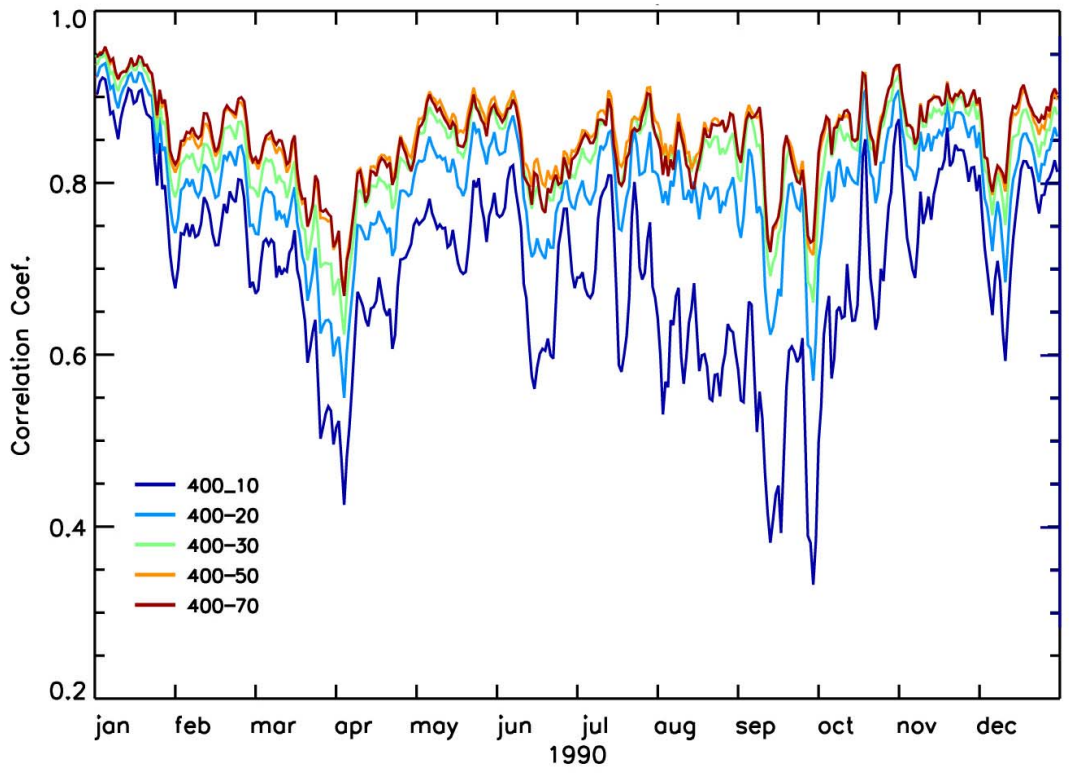

Figure 3.10 Daily spatial pattern correlation between total ozone and MPV for the year 1990. The correlation coefficient has been computed for the 25º-60ºS band and for five different pressure intervals.

weighted pattern correlation coefficient, r_w, is 0.83). However, it is also clear that their behavior is not linear everywhere. For instance, low latitude pixels clearly depart from the solid line. However, the largest deviation from this linear behavior is observed for a relatively small number of high latitude pixels. Based on the previous discussion, these pixels are expected to be associated with the Antarctic polar vortex. When data within this region was excluded from the analysis, a smaller variability around the solid line and a higher pattern correlation coefficient (r_w=0.88) is observed (figure 3.9b). In any case, the largest variability still occurs for high latitude pixels.

In order to determine what pressure levels produce the “best” MPV in terms of correlation with total ozone, different levels were tested for every day of 1990. The MPV

field, originally at a spatial resolution of 2.5 x 2.5 degrees, was linearly interpolated to match the TOMS resolution. Then, the daily pattern correlation coefficient between 25º and 60ºS was computed and plotted on figure 3.10. For all cases, data within the polar vortex was excluded from the analysis. Preliminary studies indicate that using 400 or 500 mb as the lower limit produces negligible differences in MPV. The 400 mb level was chosen as the lower limit. The upper limit was varied from 150 to 10 mb. Interestingly, all layers show a high correlation coefficient (>0.7 in average), with the highest values for p_2=50 mb and p_2=70 mb, and the lowest for p_2=10 mb. Careful comparisons suggested that p_2=70 mb produces slightly better results than 50 mb. Consequently, 70 mb was chosen as the upper level of the integration. The annual mean correlation coefficient for 1990 for the layer 400-70 mb is ~0.85 which indicates the high correlation between MPV and total ozone throughout the year.

3.6.2 Boundary values from MPV: First guess for total ozone

Given the fact that the highest correlation between MPV and total ozone occurs for the layer 400-70 mb (a region that covers the tropopause), and that the tropopause height correlates well with total ozone, the location of the upper-level jets was expected to be found following an analogous approach to the one used for ozone. In this way, essentially the same algorithm shown in figure 3.5 was used to estimate MPV values that delineate regions of high upper-level winds. The main difference with respect to total ozone is that for the MPV case, two *a priori* (and relatively arbitrary) values were used as first guess in the algorithm. In the first stage of the procedure, these two MPV values were used to delineate the location of the subtropical and polar jets and, consequently, to

classify the MPV field into five regions (seven when the polar vortex is included): three meteorological regimes (and the polar vortex) and two (three) transition zones corresponding to the upper-level jets (and the edge of the polar vortex). Then, the mean MPV within each regime was computed and "new" boundary values were calculated as the arithmetic average of these MPV mean values for two "adjacent" regimes as in the case of total ozone (i.e. the subtropical MPV boundary is equal to the average of the mean MPV for the tropical regime and the mean MPV for the midlatitude regime). If the new boundary values differed by more than 0.05 pvu from the old ones, then the process was repeated until convergence was reached. In this way, two MPV values were obtained for every day between 1979 and 1993. Figure 3.11 shows the MPV field for 5 September 1990 with the red solid line corresponding to the subtropical jet, the white line to the

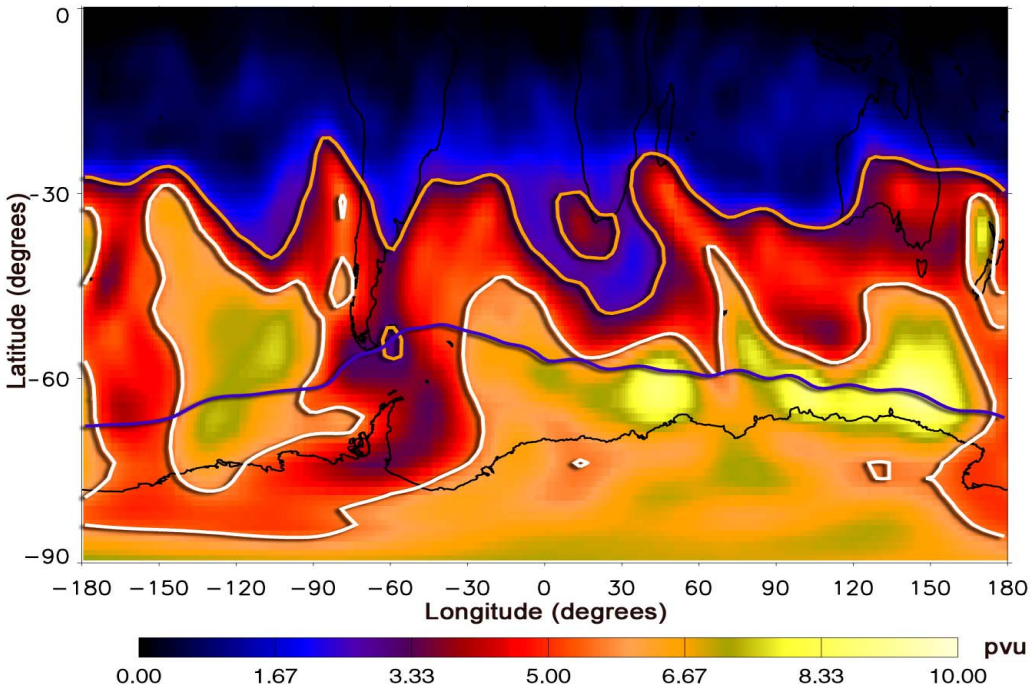

Figure 3.11 Mean Integrated PV (MPV) between 400 and 70 mb calculated from NCEP/NCAR data for 5 September 1990. The solid lines indicate the position of the regime boundaries according to this data set: red for the subtropical boundary, white for the polar boundary. The same procedure depicted in figure 3.4 has been used to calculate these values. The Antarctic polar vortex boundary (dark blue) is also plotted for completeness.

polar jet, and the dark blue to the edge of the polar vortex. It is worthwhile to note that these two values break the MPV field into “regimes” which have relatively constant MPV (figure 3.12) as in the case of total ozone (see figure 4.1). The most evident difference between total ozone is the behavior of the MPV tropical regime which shows (at least for this particular day) a strong dependence with latitude.

These values were used to build MPV masks as in the case of ozone. In order to find which total ozone values correspond to the boundary regions of these masks, the transition zones were widened by one pixel in latitude and one pixel in longitude and the mean total ozone within each of the boundary regions was computed. These mean ozone values were used later to build a “climatology” for both the subtropical and polar boundaries. These climatological values are the ones used as “first guess” for the final estimation of the ozone frontal boundaries following the method illustrated by figure 3.5.

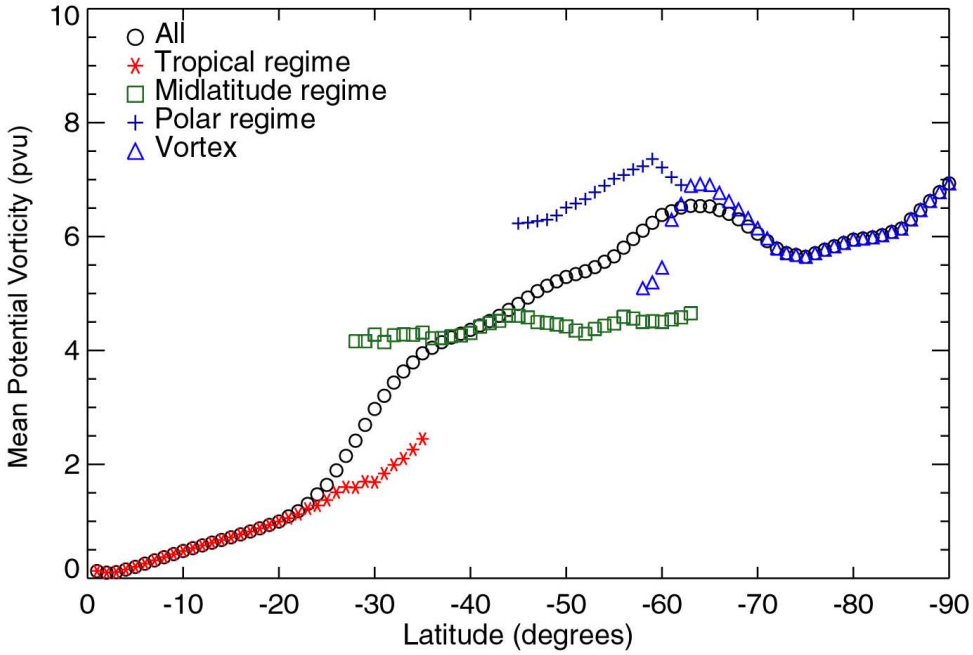

Figure 3.12 Zonally averaged MPV values over 1º latitude bands for 5 September 1990. The average of all the data is shown as circles. The average for the tropical regime is shown as asterisks, the midlatitude as squares, the polar as pluses, and the Antarctic as triangles.

4. VALIDATION

In order to validate that the boundaries defined by total ozone identify the upper-level jets correctly, total ozone itself, its gradient, reanalysis data, and information from ground-based and satellite instruments were used. Data sets that have not been mentioned in Chapter 3 are briefly described in section 4.1.

4.1 Data

Upper-level winds were obtained from the NCEP/NCAR reanalysis data set[9]. The data is calculated on a regular grid with a resolution of 2.5º in longitude and 2.5º in latitude and is presented in zonal and meridional components.

Rawinsondes were kindly provided to us by Wesley Ebisuzaki from NCEP. This data set is essentially the same used by the NCEP/NCAR in the data assimilation process. These profiles were collected at (or close to) 00, 06, 12, and 18 Z. It should be noted that not only the mandatory levels are reported in this data set, but all data available from each rawinsonde.

Data from the Stratospheric Aerosol and Gas Experiment II (SAGE II) instrument, on board the Earth Radiation Budget Satellite (ERBS), was also used for this validation. Ozone profiles were obtained from solar occultation measurements at sunrise and sunset with an approximate vertical resolution of 0.5 km. SAGE II was placed in a mid-inclination, 57º, in order to provide nearly global coverage (complete seasonal sampling from 55°S to 55°N). Two measurements are made during each orbit producing approximately 15 sunrise and 15 sunset profiles for every day. Although some reports

[9] http://www.cdc.noaa.gov/cdc/data.ncep.reanalysis.html

indicate that there are differences between the sunrise and sunset data sets (SPARC, 1998) this difference appears to be significant only above 1 mb (SPARC, 1998). Consequently, all available data was used for the present analysis. In spite of that, there are some days in which there was data for only one hemisphere because, during those periods, both sunrise and sunset profiles were collected in only that hemisphere. It should be stressed that when the analysis is performed in a particular latitudinal band, as in this thesis, the number of available profiles can be small.

4.2 Zonal Mean Ozone within Regimes

From the analysis of the Northern Hemisphere presented by Hudson et al. (2003), a *stepwise* function for the zonal total ozone mean is expected when this field is classified by meteorological regimes. This is exactly the case when the same analysis is performed in the Southern Hemisphere. Figure 4.1 shows the zonal average for 5 September 1990 in

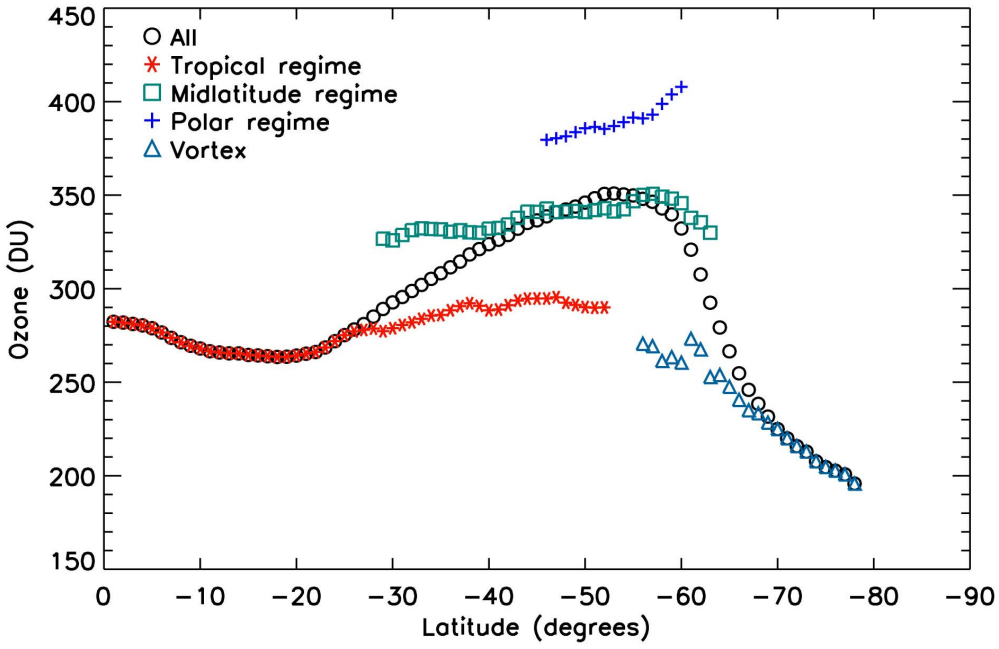

Figure 4.1 Zonally averaged total ozone values over 1º latitude bands for 5 September 1990. The average of all the data is shown as circles. The average for the tropical regime is shown as asterisks, the midlatitude as squares, the polar as pluses, and the Antarctic as triangles.

1-degree latitude bands when total ozone is classified by regime. These zonal means, in red, green, and blue for tropical, midlatitude, and polar regimes, respectively, are compared with the zonal average when no classification is performed (open circles). For this figure, the frontal regions were broadened by 1º in latitude and 1.25º in longitude and the data within them excluded from the average. In addition, only bands with more than 50 points were plotted. The similarity between figure 4.1 and the schematic in figure 4.2, showed by Hudson et al. (2003), is remarkable. The total ozone field is nearly constant with latitude within each regime, especially in the midlatitude regime. There is a slow increase of total ozone with latitude for all regimes, with a more pronounced dependence for the polar regime. The polar vortex region shows a clear depletion of ozone with a rapid decrease in total ozone towards the pole. Notice also the spatial overlapping among regimes between 30º and 60ºS and the nearly constant separation in total ozone among

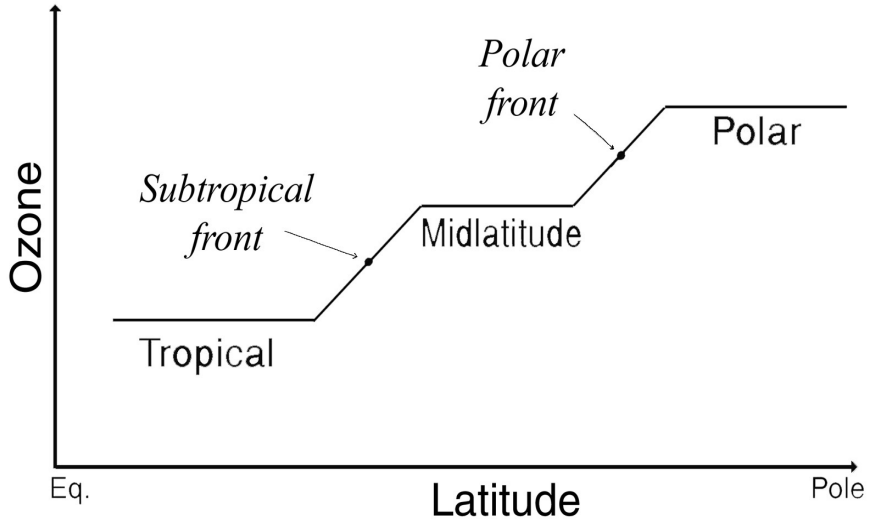

Figure 4.2 Schematic showing total ozone as a function of latitude. The position of the subtropical and polar fronts, as determined by total ozone, are also depicted here (from Hudson et al., 2003)

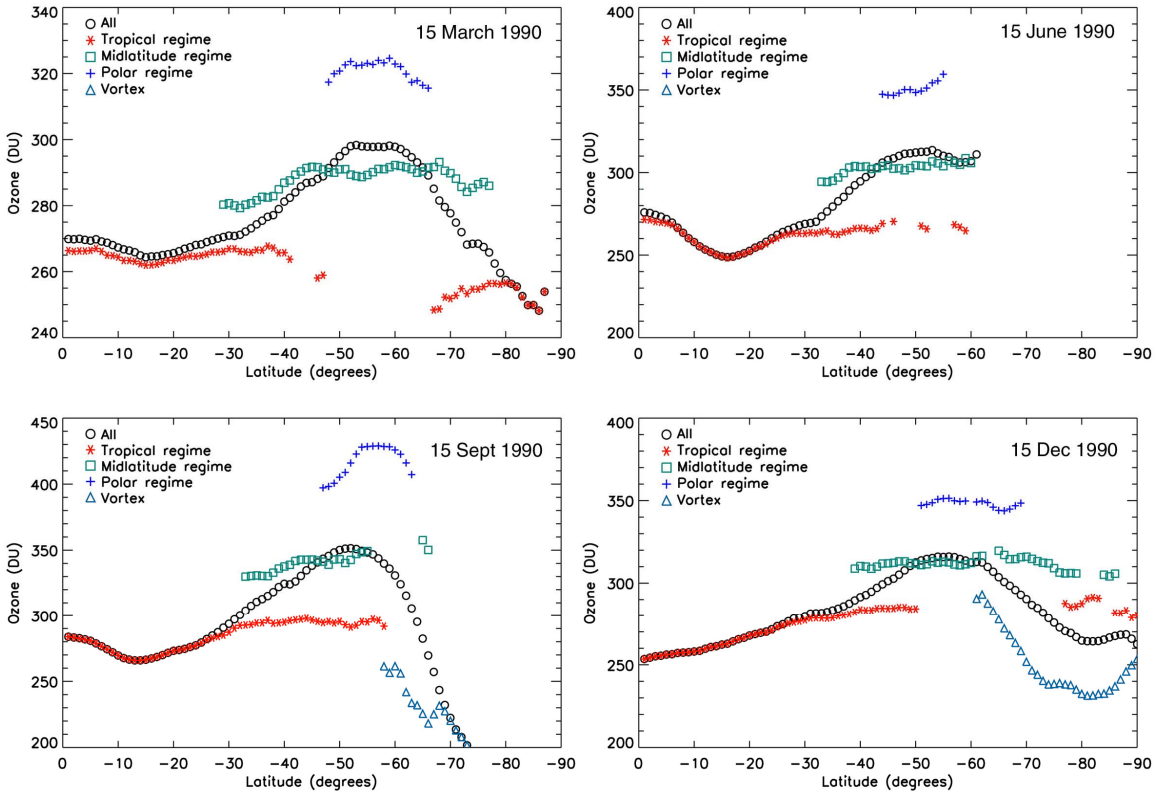

Figure 4.3 Zonally averaged total ozone values over 1º latitude bands for four different days in 1990. Symbols and colors are the same as in figure 4.1. Note the different scales for the y-axis.

them. This behavior is not exclusive of 5 September 1990. Figure 4.3 shows the zonal averages for different days of that year in March, June, September, and December of 1990. The total ozone field within each regime is relatively constant, resembling the schematic of figure 4.2.

4.3 Upper-level Winds

In order to verify whether the ozone boundary values produced by the iterative approach described in Chapter 3 do in fact delineate regions of high winds in the upper-troposphere, NCEP/NCAR reanalysis data was used. Shalamyanskiy and Romanshkina (1980), and Shapiro et al. (1999) suggested that the 200 mb isobaric surface would be the

best surface to find the subtropical jet whereas the 300 mb surface would be best for the polar jet.

Figure 4.4a shows 200 mb wind vectors plotted onto the total ozone field for 5 September 1990. The size of the arrows is proportional to the wind speed. Regions with high winds can be observed almost everywhere along the interface between “low” (blue regions) and “high” (red-orange regions) ozone. This is especially evident west of South America, south of Africa, and over Australia. An area of special interest is the low ozone region south of South America connecting the tropics and the polar vortex (figure 4.4b).

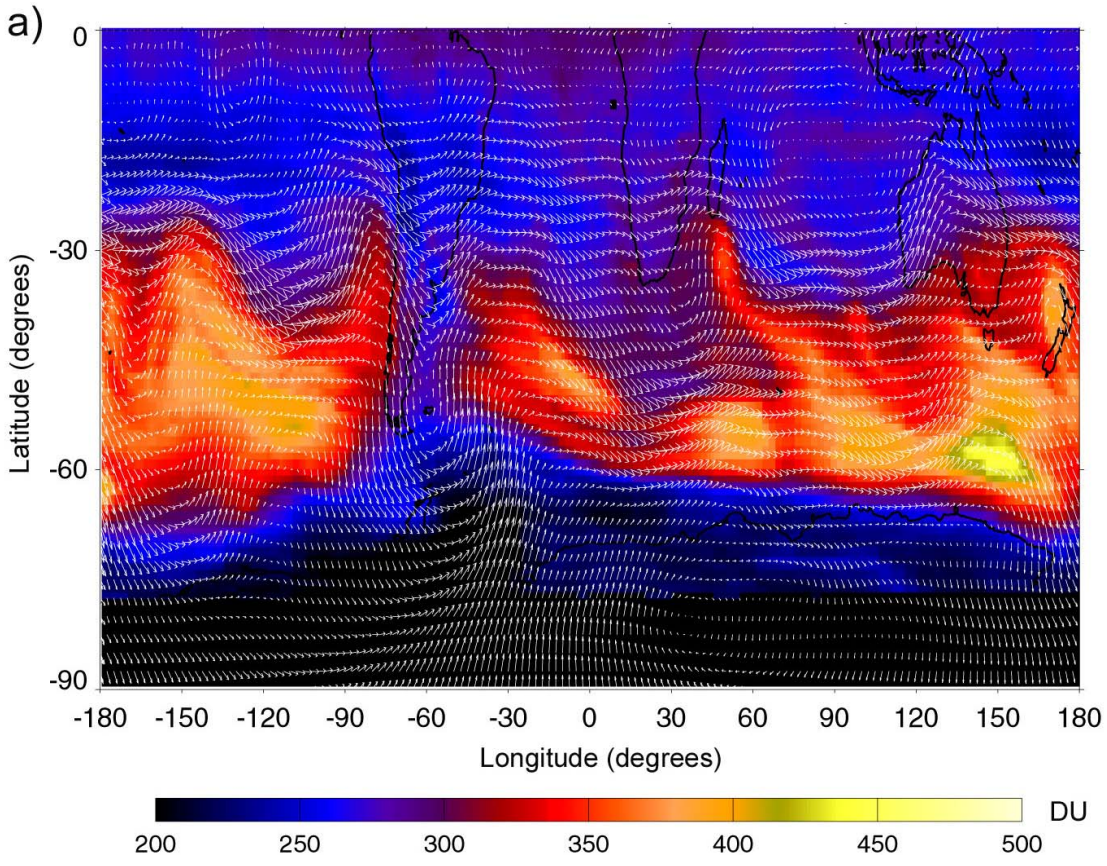

Figure 4.4 a) Wind vectors on the 200 mb isobaric surface superimposed onto the total ozone field for 5 September 1990. a) Southern Hemisphere.

b)

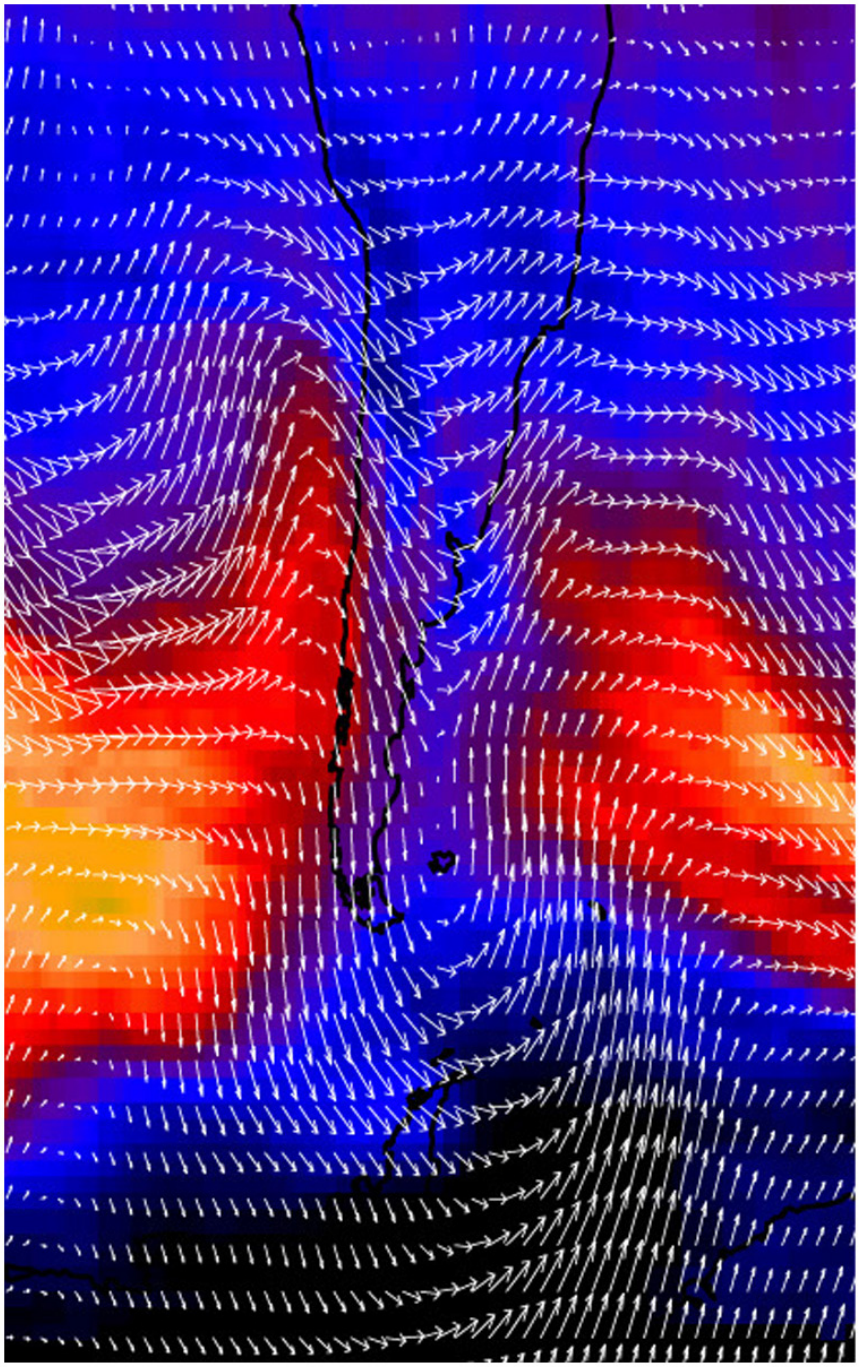

Figure 4.4 (cont) b) Same as a) but zoom in on South America.

By looking at ozone alone, the origin of this low ozone could be thought of as an intrusion of tropical air deep into the mid-latitudes, or an intrusion of polar vortex air into mid-latitudes as a result of a dilution event. The wind field, however, strongly suggests that it is more likely that tropical air is being transported into mid and high latitudes.

Against expectations, winds on the 300 mb surface (not shown here) did not add new information about the upper-level jets, especially the polar jet. Because this wind field is almost identical to the 200 mb, the latter can be used to explore the relation between high winds and ozone gradients in the case of the polar jet. A closer look at figure 4.4a reveals that relatively narrow regions with high winds correspond to high total ozone gradients. For instance, south of Australia, near Antarctica, strong winds "surround" the northern part of a high ozone area (yellow area). West of this region, in between the orange areas, a relatively small amount of total ozone corresponds to a region with weak winds. A more extensive inspection of figure 4.4a confirms that, in general, there is a good agreement between the ozone gradient and wind fields. That is, high gradients in total ozone are associated with relatively small regions with high winds, whereas weak ozone gradients correspond to weaker winds.

4.4 Mean Position of the Upper-level Jets

From the preceding section, it is evident that, at least for the day studied, regions delineated as the upper-level jets by total ozone correspond indeed to regions of high winds. Although the same connection is observed for other days and years, a simple way to confirm if this relationship holds for longer periods of time is to analyze monthly means of upper tropospheric winds and ozone gradients along the frontal boundary regions. The basic idea behind this method was suggested by Shapiro et al. (1982), who

noted that the magnitude of the total ozone gradient is proportional to the wind speed in the vicinity of the upper-level jets.

In order to determine if this is the case, pixels along the subtropical and polar jets were identified for every boundary and every day separately. Then these regions were enlarged by 1.0 degree in latitude and 1.25 degrees in longitude. Only the magnitudes of the ozone gradient within these regions were considered for this analysis. In order to estimate the monthly behavior from these daily fields[10], all the data for a month was

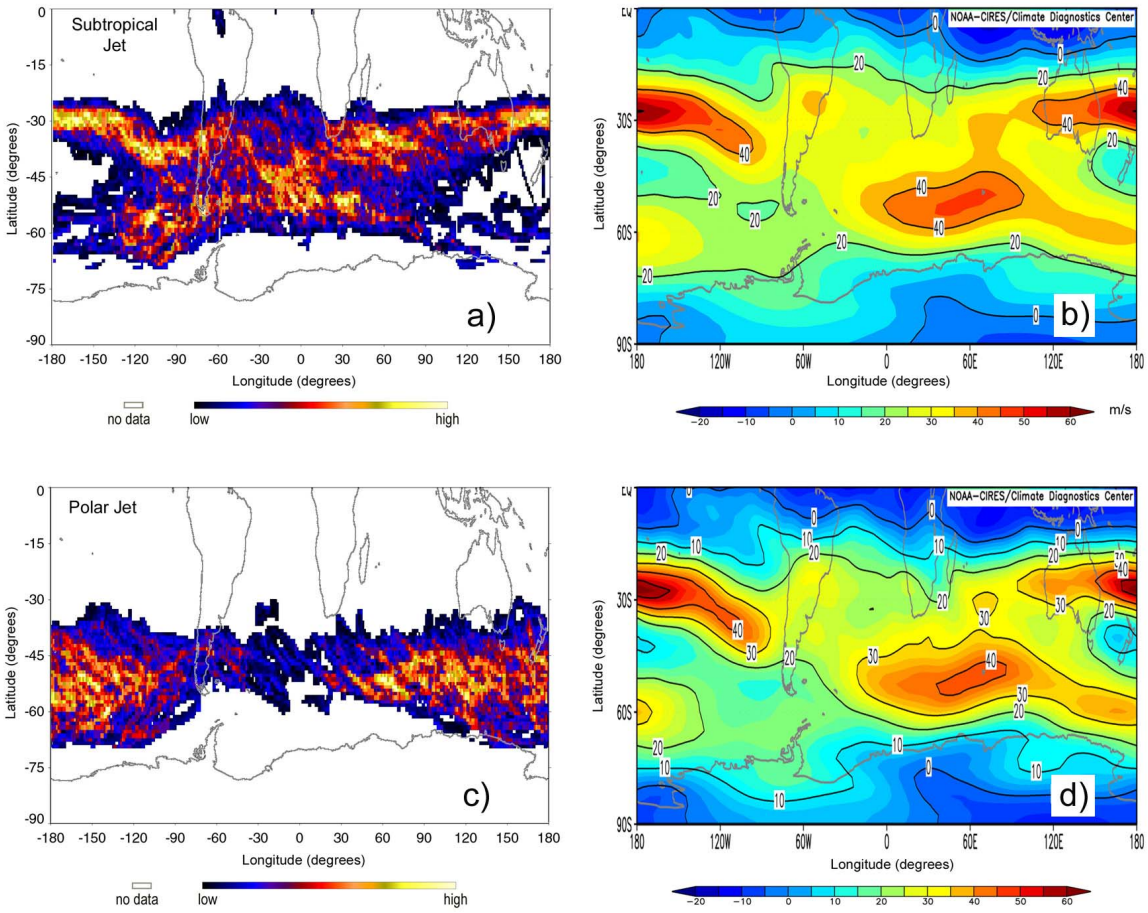

Figure 4.5 Monthly mean ozone gradients for the (a) subtropical and (c) polar regime boundaries, and monthly zonal winds on the (b) 200 mb isobaric surface and (d) 300 mb isobaric surface for September 1990.

[10] These "fields" contain information along the ozone boundaries only.

added, and the resulting field normalized to its maximum value. As an example, this method was applied to September 1990. Figure 4.5a shows the result for the subtropical jet. A continuous and almost completely zonal region with persistent high gradients around 30ºS over the Pacific is clearly seen in this figure. Near South America and Africa, the high gradient areas show less zonal behavior with a local maximum around 45ºS. Note the small area with high ozone gradients southwest of South America. These gradients are related to deep migrations of the subtropical jet into high latitudes as discussed previously for 5 September 1990. It is interesting to observe the large extent of the latitudinal meandering of the subtropical jet during September 1990. According to the ozone data, the subtropical jet migrated between 25º and 65ºS for most longitudes except for a region over the western Pacific where, at least for this particular month, no strong indications of this jet were observed.

In order to confirm if these results were realistic, daily 200 mb zonal winds from NCEP/NCAR reanalysis were used to compute monthly mean zonal winds for September 1990. Figure 4.5b shows the results for this case. The quasi-zonal region over the Pacific at about 30ºS observed from the ozone analysis is also clearly seen in this case. Even the shape of this strip is similar in both cases. That is, this “mean jet” bends southward at about 120ºW. Another high wind region is also depicted south of Africa (~55ºE, 50ºS) in figure 4.5b. Although there is not a clear equivalent in the ozone gradient field, a small area of high ozone gradient is present west of this region, with smaller (but still high) gradients extending to the west.

When the same procedure was applied to the polar jet, a much broader region with relatively high ozone gradients was observed (figure 4.5c). In this particular case,

this band is almost zonal at about 55ºS but has a latitudinal extent of almost 30º, and a longitudinal coverage of approximately 200º (60ºE to120ºW). This jet appears to meander in a narrower region (~35º to 65ºS) than its subtropical counter part. It must be kept in mind, however, that the stratospheric polar vortex limits our ability to use ozone poleward of its edge during the austral spring.

Following Shalamyanskiy and Romanshkina (1980) and Shapiro et al. (2002), 300 mb winds instead of the 200 mb winds were used to compare the mean polar jet from ozone with the reanalysis winds. Figure 4.5d shows the monthly zonal winds for this isobaric surface. As noted for the case of 5 September 1990, the monthly means for 200 and 300 mb surface winds show very little difference. For that reason, using winds on these surfaces alone, it seems that it would be difficult to determine if a region of maximum monthly mean winds corresponds to the subtropical or polar jet, or if it has "contributions" from both. For example, the region with high winds around (60ºE, 50ºS) (figure 4.5d) appears in both isobaric surfaces, but does not become visible either in the ozone subtropical or ozone polar jet analyses (figures 4.5a and 4.5c). It should be noted, however, that figure 4.5c does show a region with a relative maximum at about (60ºE, 50ºS), which resembles the high winds region mentioned before. There is a local maximum in the ozone gradient field for the subtropical case slightly west of this area (figure 4.3a). Given the fact that both wind surfaces show the influence of the subtropical and polar jets, it seems plausible that a combination of both upper-level jets (not attempted here) could produce a result with more similarities to both mean wind fields.

4.5 Rawinsondes and Meteorological Regimes

Hudson et al. (2003) showed, in the Northern Hemisphere, that vertical temperature profiles could also be sorted into regions with clear distinctive characteristics. For instance, each regime showed a unique tropopause height that had a much weaker dependence with latitude than if the profiles had been classified purely by latitude. A dense ground-based network helped Hudson et al. (2003) to perform the analysis for every day of 1990 when TOMS data was available. It is not possible to perform a similar analysis in the Southern Hemisphere, not only because there is much less land in this hemisphere, but also because the ground-based network has a much lower density than its counterpart in the Northern Hemisphere (see figure 4.6). In spite of that, we can use rawinsonde data for a particular day to investigate the consistency of the classification.

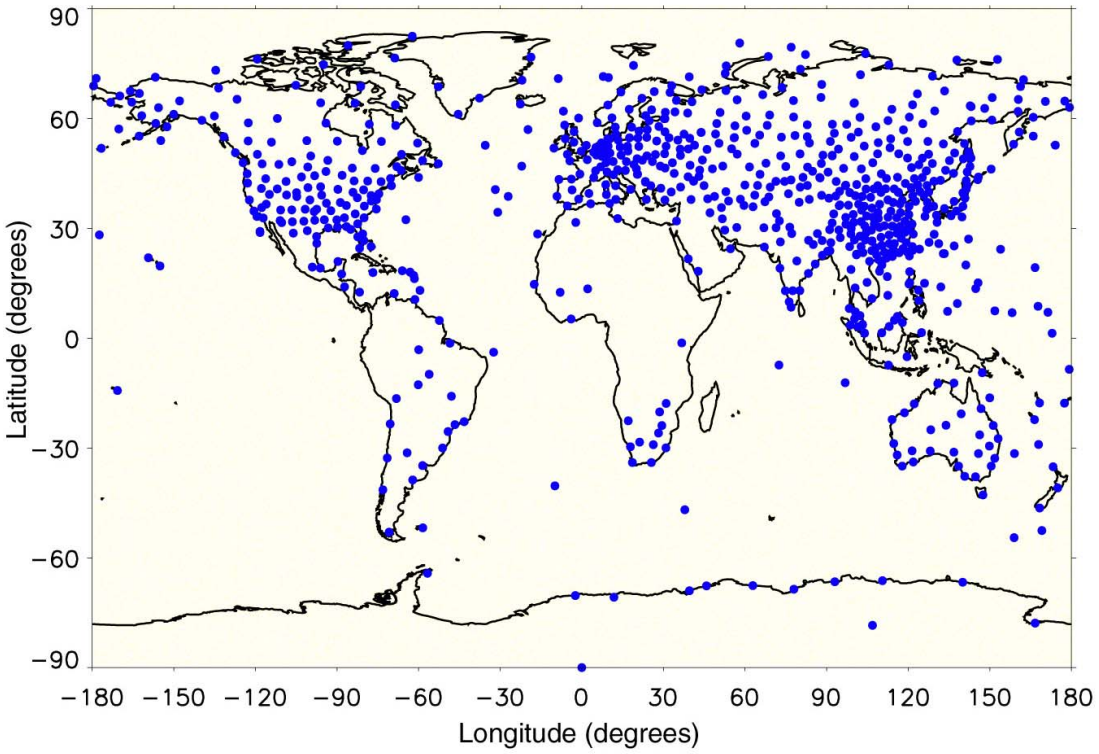

Figure 4.6 Spatial distribution of the rawinsondes used in the analysis for 5 September 1990.

4.5.1 Profiles for one day

Figure 4.7a shows the region around South America for 5 September 1990. Only ten rawinsondes were available for that day. The white circles indicate their location, whereas red crosses identify rawinsondes that lie within the tropical regime, and white circles without crosses indicate rawinsondes that are "too close" to the boundary regions (about two degrees from them), and, therefore, were marked to be excluded in subsequent analyses (but will be used in the present discussion). No rawinsonde in this region was classified within the midlatitude or polar regime for this particular day. The numbers beside every data point are used to identify the profiles in figure 4.7b. Table T4.1 contains their location as well as their estimated tropopause heights.

Tropopause heights were calculated for all profiles. Two techniques were combined for this purpose. One followed the WMO definition (1957) of the tropopause. The other technique used the intersection of the tropospheric and stratospheric lapse rates. Points between 900 and 400 mb were used to calculate the former, whereas points above 100 mb were used to compute the latter. The tropopause height was assumed to be correctly estimated when the two techniques produced results within 1.5 km. Profiles that did not meet this criterion were not used for subsequent tropopause height analysis.

Figure 4.7a shows that seven profiles were classified as belonging to the tropical regime, whereas the other three were assigned to the transition zones. The first thing to note is the large latitudinal extension of the tropical regime. Although it seems reasonable that points 2, 4, 5, 6, and 9 were classified within the tropical regime, this is not the case for points 1 and 3, which were almost 15 degrees south of the former group. Looking at

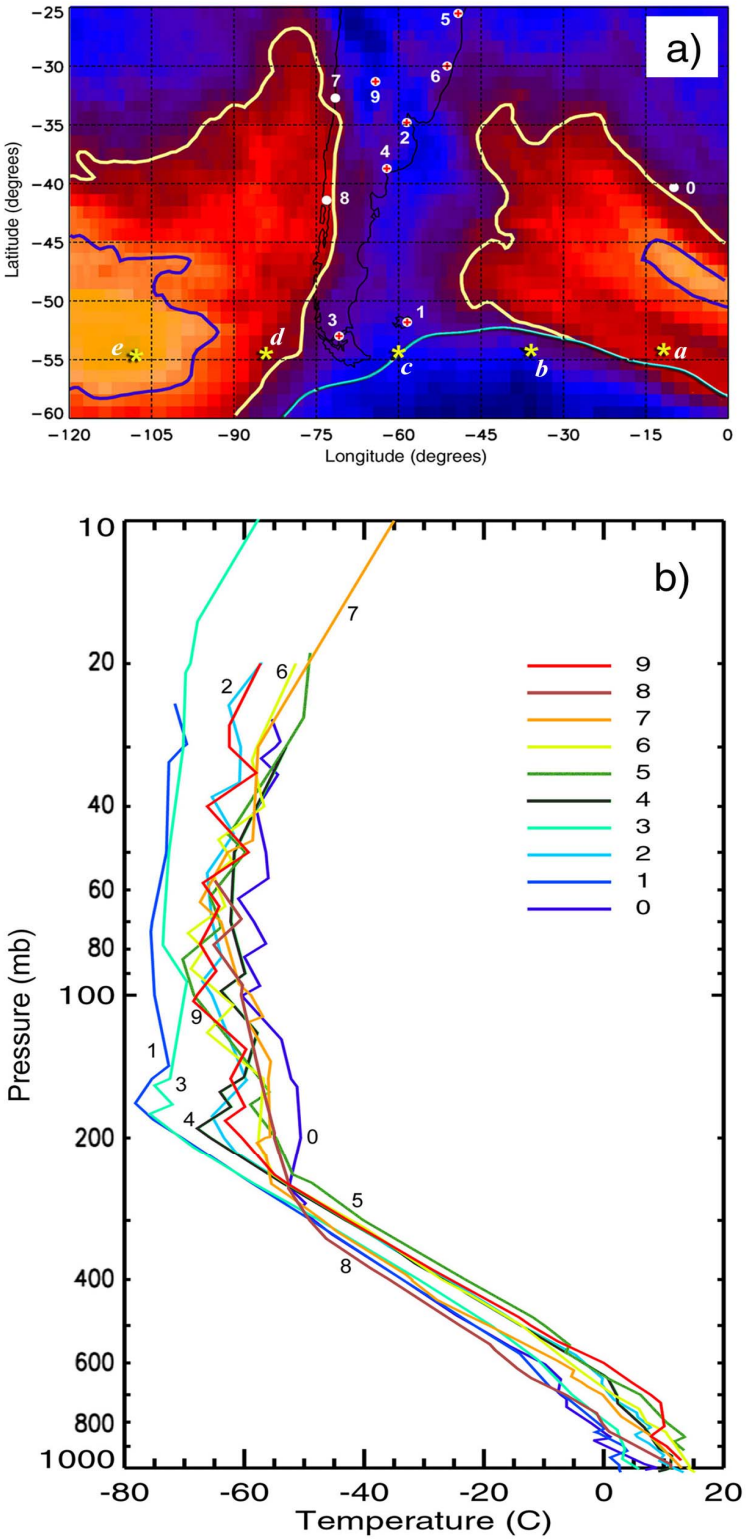

Figure 4.7 a) Spatial distribution of rawinsondes (circles) and SAGE II profiles (stars) used in the analysis for 5 September 1990. The meaning of the color scale and solid contours is as described in figure 3.6. b) Temperature profiles obtain from the rawinsonde data set. Numbers and colors are used to distinguish among the different profiles.

Profile	Lon (º)	Lat (º)	P (mb)	H (km)
0	-9.88	-40.34	250	10.5
1	-58.45	-51.81	177	12.5
2	-58.53	-34.81	198	12.2
3	-70.85	-52.99	179	12.5
4	-62.17	-38.72	195	12.2
5	-49.17	-25.51	110	16.0
6	-51.18	-29.99	183	12.7
7	-71.53	-32.72	198	12.1
8	-73.12	-41.42	262	10.1
9	-64.22	-31.31	180	12.8

Table T4.1 Location of the rawinsonde data used in figure 4.5. Tropopause height, both in pressure and altitude, are also indicated for each profile.

the temperature profiles (figure 4.7b), it is evident that profiles 2, 4, and 9 had very similar shape. Tropopause heights for all of them were located around 190 mb (approximately 12.3 km). Above the tropopause their temperatures were almost constant with altitude except for profile 4, which shows a slight warming above 50 mb. Similarly, profiles 1 and 3 are also alike, and despite being much further south (almost 1500 km away), they present a tropopause height at about 180 mb (~12.5 km). Their shape is also similar to profiles 2, 4, and 9, but because they have a colder starting point at the surface, their profiles seem to be "shifted" to lower temperatures. Profiles 5 and 6, also "tropical" profiles this day, show a different shape. They present a sudden change in tropospheric lapse rates about 250 mb, but both have the tropopause at higher altitude: ~180 mb for point 6 and ~110 mb for point 5, which is the most "equatorial" of all points.

Probably the most interesting profiles are those of points 0, 7, and 8, which are close to the boundary between tropical and midlatitude regimes. These three points are at a latitude comparable to points 2, 4, and 9 and more than 10º north of points 3 and 1, but in spite of that, they have the lowest tropopause heights of all of the points: ~250 mb for points 0 and 8, and ~200 mb for point 7. Note that the latter is located more into the

tropical regime (although still into the wide transition zone) than the other two points. These profile shapes look like a mix of tropical and midlatitude regimes as expected.

The analysis of the temperature profiles for 5 September 1990 present a consistent picture of the relationship between the meteorological regimes and the ground-based rawinsonde data.

4.5.2 Monthly profiles

In order to obtain monthly mean profiles, all available rawinsondes for the Southern hemisphere between 25º and 60ºS were classified every day by using 2-degree broad masks, and then amalgamated for the month. About half of the profiles were within the enlarged transition zones and therefore not used in the monthly profile calculations. Figure 4.8 shows the classified profiles for the month of September 1990. Out of 1290 profiles available for this month, 469 were classified as tropical, 197 as midlatitude, and 26 as polar profiles. The remainder 598 profiles were found to be in the transition zones.

Figure 4.8 clearly shows that temperature profiles can be sorted into three distinct groups, corresponding to the three meteorological regimes, by using the masks based on total ozone. Each regime shows a distinct profile shape, tropopause height, and temperature at sea level. The tropical regime, for example, shows profiles that tend to increase in temperature with altitude above 100 mb, whereas both midlatitude and polar regimes show a relatively constant temperature with altitude above their respective tropopause. Furthermore, despite the similarity between midlatitude and polar profiles, it is evident that the latter shows a lower tropopause than the former.

The tropical regime shows two other interesting characteristics for this month. First, some profiles have low temperatures at about 20 mb compared to the bulk of profiles which show an increasing temperature with altitude at that pressure. In principle, these low temperature profiles could be thought of as misclassified by our method and therefore they would have to be assigned to the midlatitude or polar regimes. However, a closer inspection of figure 4.8 reveals that neither midlatitude nor polar regimes have profiles with such low temperatures about 20 mb. Recalling that a similar case occurred for 5 September 1990, where the two tropical profiles observed at high latitudes (~52ºS) had similar characteristics, these "cold profiles" can be described as "high latitude tropical profiles". Second, a small group of the tropical profiles appears to have a lower tropopause, comparable in fact to the one found in the midlatitude regime. Although some of these profiles are indeed high latitude tropical profiles as mentioned above, analysis of SAGE II data (to be discussed later) indicates that some misclassification has

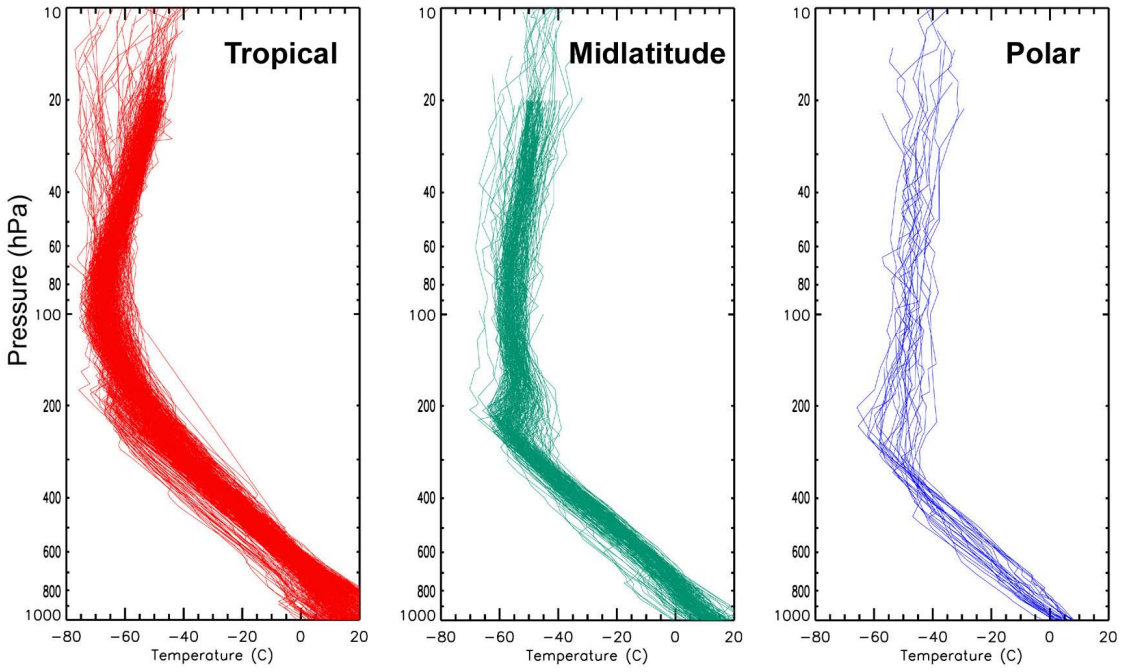

Figure 4.8 Temperature profiles between 25º and 60ºS for September 1990 classified by meteorological regime as defined by total ozone.

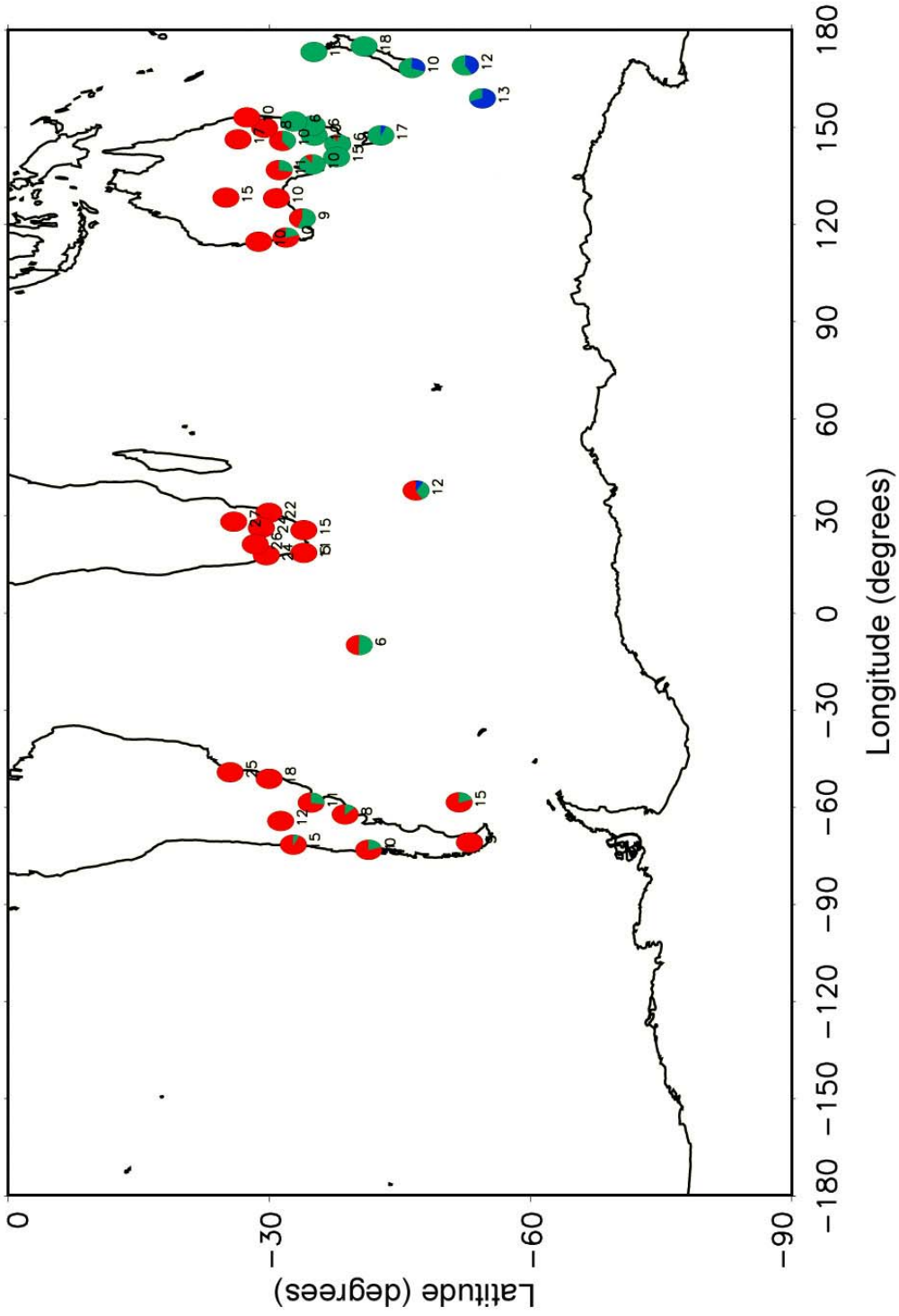

Figure 4.9 Rawinsonde stations in the 25º-60ºS band that measured temperature profiles for September 1990. The colors indicate the percentage of data classified within each regime.

occurred. Inspection of daily data for September 1990 showed that small errors in the location of the polar vortex could explain this “anomalous” profiles in the tropical regime.

Figure 4.9 shows the spatial distribution of the rawinsondes used for computing mean profiles for September 1990. Profiles within transition zones were not taken into account to produce this figure. The circles indicate the relative contribution from each regime at any given station. For example, the station at (35ºE, 45ºS) measured 12 profiles classified within a regime. Of these, more than half are ascribed to the tropical regime and therefore a proportional area of the circle for this station is colored red. The other two colors are proportional to the midlatitude (green) and polar (blue) contribution. The figure shows some interesting facts. First, it seems that poleward intrusions of tropical air were relatively common over South America for September 1990. Second, no midlatitude profiles were observed over South Africa; and third, a clear spatial separation can be observed between tropical and midlatitude profiles over Australia, with very few intrusions of tropical air south of this continent. The latter reflects a persistent and zonal subtropical jet in this region.

4.5.3 Monthly mean profiles

Once the daily profiles were classified by regime, monthly mean temperature profiles were computed for each month of 1990. All available profiles were used for this purpose, even those with very few points, i.e. profiles with data in the lowest 4 km only. The atmosphere was divided into layers of 1 km height, and the mean temperature within each layer was computed separately. For this reason, the number of points used for every layer was not constant. Approximately 500 data points per layer were used in the case of

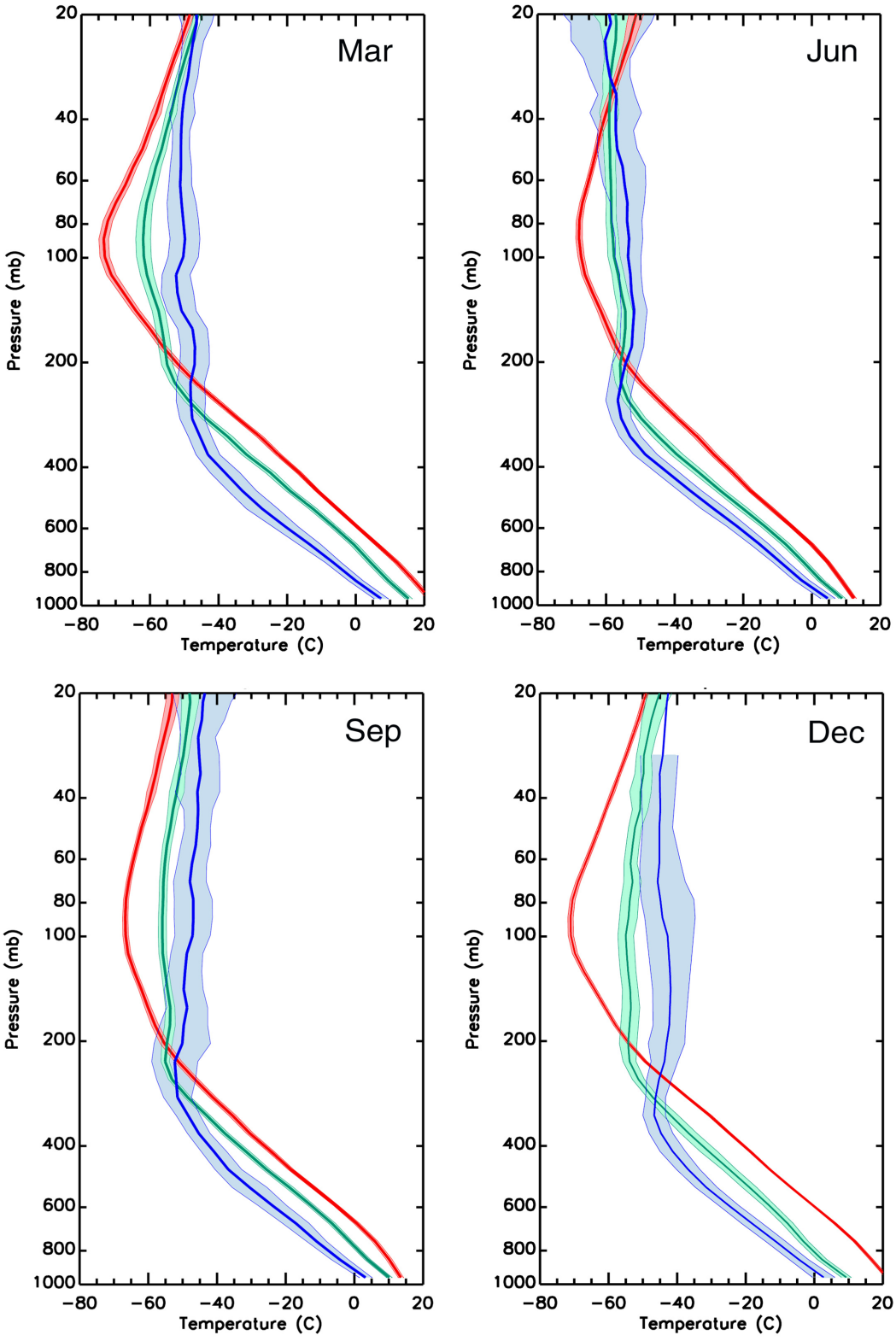

Figure 4.10 Monthly mean temperature profiles within each regime for March, June, September, and December of 1990. Red profiles correspond to the tropical regime, green to the midlatitude regime, and blue to the polar regime. Shaded areas indicate the standard error at 95% confidence interval.

MONTH	OVERALL					TROPICAL					MIDLATITUDE					POLAR				
	Prof	Press	SE	Alt	SE	Prof	Press	SE	Alt	SE	Prof	Press	SE	Alt	SE	Prof	Press	SE	Alt	SE
Jan	1129	136	3	15.0	0.1	461	111	1	16.2	0.1	68	198	10	12.2	0.4	10	291	23	9.4	0.6
Feb	986	140	3	14.8	0.1	237	129	4	15.3	0.2	106	171	10	13.4	0.4	3	322	57	8.6	1.2
Mar	1070	140	3	14.8	0.1	236	112	2	16.1	0.1	88	175	10	13.2	0.4	16	296	39	9.4	1.0
Apr	1064	163	4	13.8	0.1	328	128	3	15.2	0.2	83	221	12	11.5	0.4	6	350	44	8.0	1.0
May	1082	178	4	13.2	0.1	401	133	3	14.9	0.1	117	237	7	10.9	0.2	22	322	16	8.6	0.4
Jun	1010	179	4	13.1	0.2	334	131	4	15.0	0.2	110	236	8	10.9	0.3	23	298	13	9.0	0.3
Jul	1007	188	4	12.8	0.2	265	140	5	14.6	0.2	158	235	7	10.9	0.2	16	307	22	8.9	0.5
Aug	1016	178	4	13.2	0.2	373	135	4	14.9	0.2	112	246	7	10.6	0.2	18	274	19	9.6	0.5
Sep	1029	182	4	13.0	0.1	393	142	4	14.6	0.2	152	237	5	10.9	0.2	16	324	23	8.5	0.5
Oct	1057	176	4	13.2	0.1	419	137	3	14.8	0.1	151	238	7	10.9	0.2	12	318	28	8.6	0.6
Nov	1057	158	3	14.0	0.1	560	126	2	15.3	0.1	56	247	9	10.6	0.3	3	324	55	8.5	1.4
Dec	1113	145	3	14.6	0.1	663	119	2	15.7	0.1	48	241	13	10.8	0.4	6	359	23	7.7	0.5

Table T4.2 Monthly mean tropopause heights for 1990. Number of profiles used in the calculations, mean and standard error at 95% confidence interval, in pressure (mb) and altitude (km), are reported for each month.

the tropical regime; 300 points for midlatitude profiles; and about 30 for the case of the polar regime. Monthly mean profiles for March, June, September, and December of 1990 are depicted in figure 4.10. In all cases red, green, and blue colors represent tropical, midlatitude, and polar regimes, respectively. Shaded areas about the mean profiles indicate the standard error at 95% confidence interval. These mean profiles show distinct shapes, tropopause heights, and temperatures at sea level. This distinction between sea level temperatures is especially evident for December and March. It is important to note that the monthly mean tropopause height was not estimated from the mean profile. Instead, the tropopause height was computed independently for every profile as described before, and then (and only then) the monthly mean tropopause was determined.

The fact that figure 4.10 shows that the tropopause heights are distinct for these four months strongly suggests that this is also the case for every month of 1990. To verify this, monthly mean tropopause heights were calculated for every month of the year. Table T4.2 shows the corresponding results and the values are displayed in figure 4.11 where the bars indicate the standard error at 95% confidence interval about the mean. Note that,

in general, the three regimes show a very distinct tropopause height for every month. Notable exceptions are November, when the polar tropopause height shows large variability and its distribution almost overlaps with the midlatitude regime distribution; and August when the midlatitude and polar tropopause heights are closer than other months.

In addition, figure 4.11 shows no clear seasonal behavior for any regime, contrary to the Northern hemisphere (not shown here). Despite that, the midlatitude regime presents the highest tropopause height in the Southern Hemisphere summer months (as in the case of Northern Hemisphere) but shows an almost constant tropopause height the

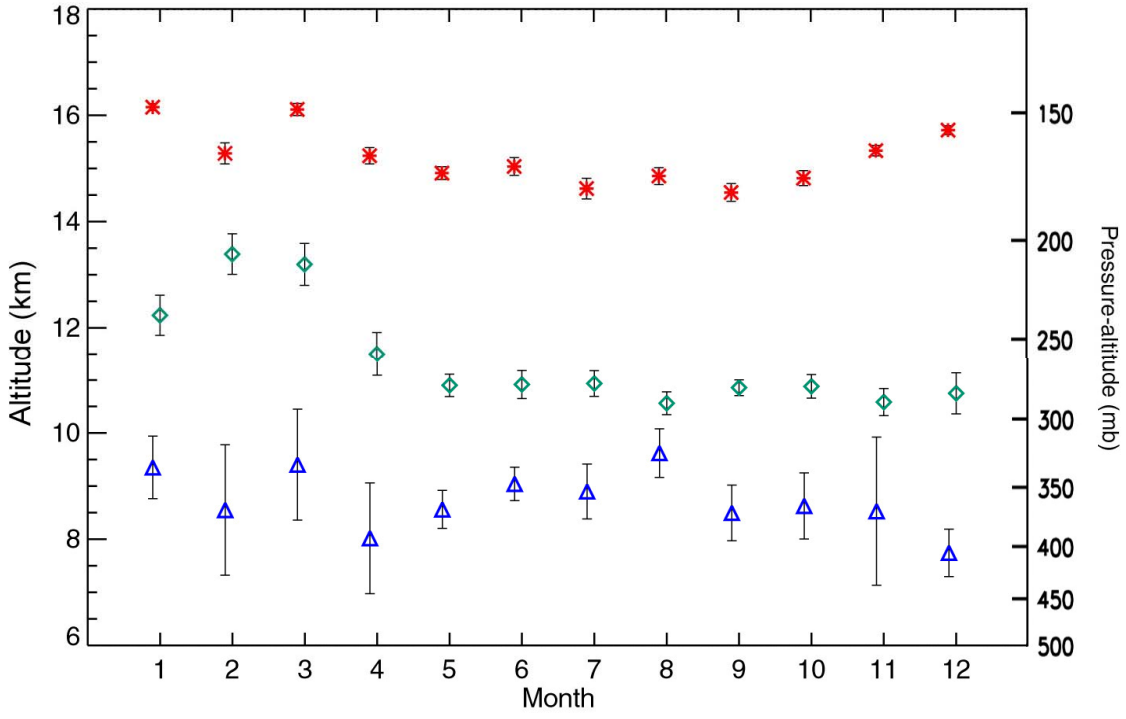

Figure 4.11 Monthly mean tropopause heights within each regime for the 25º-60ºS band for 1990. Red asterisks show tropopause height within the tropical regime, green diamonds within the midlatitude regime, and blue triangles show tropopause heights within the polar regime. Error bars indicate the standard error at 95% confidence interval.

rest of the year. Data for the tropical regime also suggests that the highest tropopause heights occur in summer but with only one year of data this argument is difficult to make. However, in the case of the midlatitude regime, the mean tropopause is clearly highest in summer and almost constant the rest of the year. Tropopause heights for the polar regime profiles do not show a clear maximum in any month. In this case, not only large variability but also lack of information (few profiles) could contribute to this behavior.

4.6 SAGE II Data and Meteorological Regimes

In addition to rawinsonde data, Hudson et al. (2003) investigated the behavior of ozonesonde profiles within a meteorological regime. They confirmed that if total ozone within a regime is relatively constant, then the ozone profiles within the regime should show little variability. In our case, given the clear separation of temperature profiles by the ozone masks, it is reasonable to expect that ozone profiles would also show similar characteristics when sorted by meteorological regime. For the Southern Hemisphere, however, the use of ozonesondes for that purpose is almost impossible. The low density of stations compared with their northern counterparts, as well as the presence of much less land, will produce a poor statistical sampling. For this reason, SAGE II ozone profiles were used to explore the behavior of stratospheric ozone.

For the month of September 1990, 288 profiles distributed over 15 days were available for the Southern Hemisphere. From those, 223 corresponded to sunrise and 65 to sunset. Because the analysis was performed in the 25º-60ºS band, only sunrise measurements were used (all sunset measurements occurred in regions outside this band). Figure 4.12 shows the spatial distribution of all available SAGE ozone profiles. Red, green, and blue circles indicate that these profiles were ascribed to the tropical,

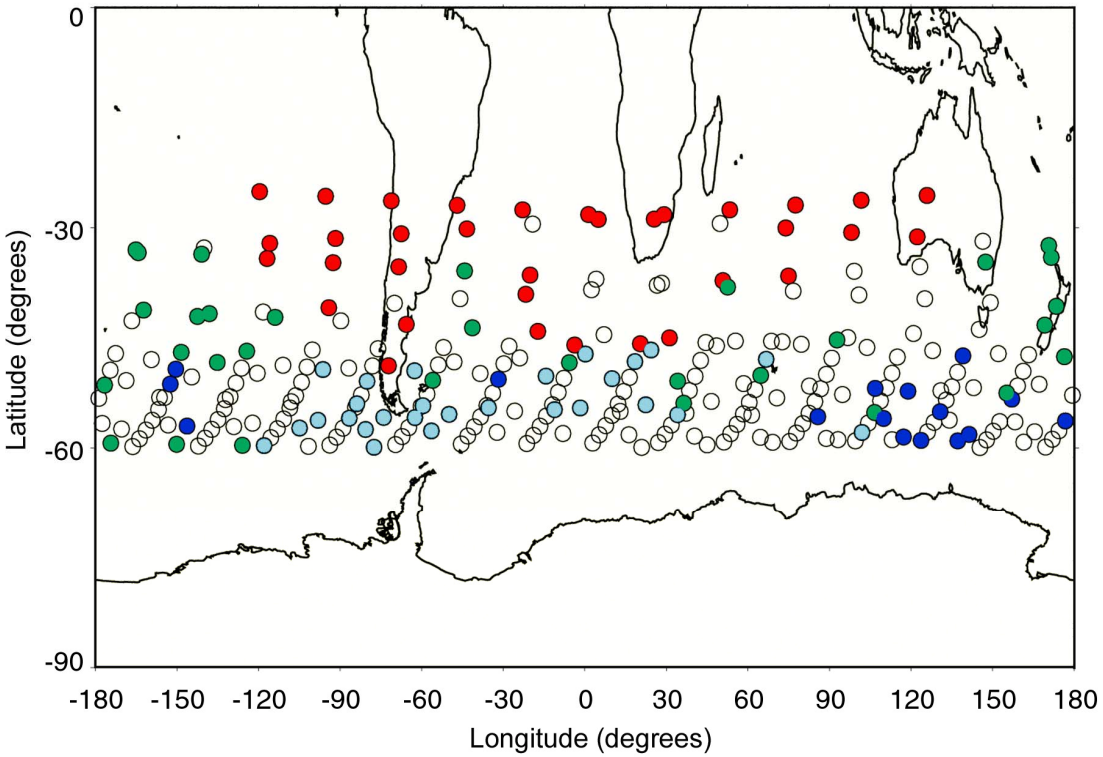

Figure 4.12 Spatial distribution of SAGE II profiles between 25º and 60ºS for September 1990. Red, green, and blue circles correspond to tropical, midlatitude, and polar regimes, respectively. Light blue circles mark profiles with strong influence from the polar vortex, and open circles correspond to profiles that lay in the broadened boundary regions or within the polar vortex.

midlatitude, and polar regimes, respectively; light blue circles mark profiles with strong influence from the polar vortex as described later; and open circles correspond to profiles within or too close to the boundary regions, or within the polar vortex. The SAGE II algorithm assumes that the atmosphere is homogeneous along the tangent path (Chu et al., 1989). “Too close” means these profiles were derived from tangent paths clearly inhomogeneous, especially for layers in the lower stratosphere. In order to avoid this problem, an additional restriction was imposed on the ozone profiles. Those profiles closer than 300 km in any direction of the boundary regions were also excluded.

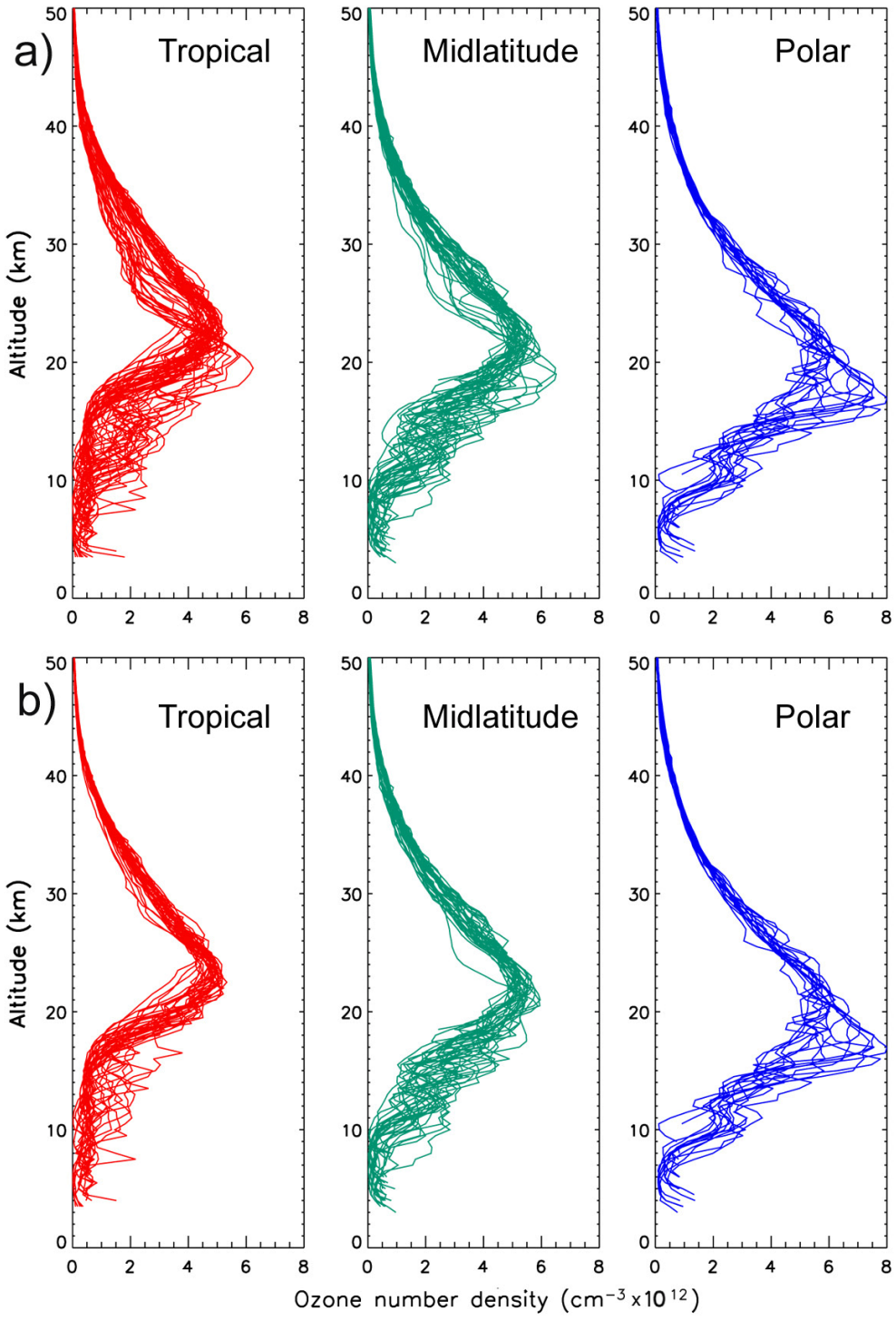

Figure 4.13 SAGE II ozone profiles for September 1990 classified by meteorological regimes using 2-degree masks. a) All available profiles. b) Same as a) but with profiles who suffered strong influence from the Antarctic polar vortex removed from the data set. See text for details.

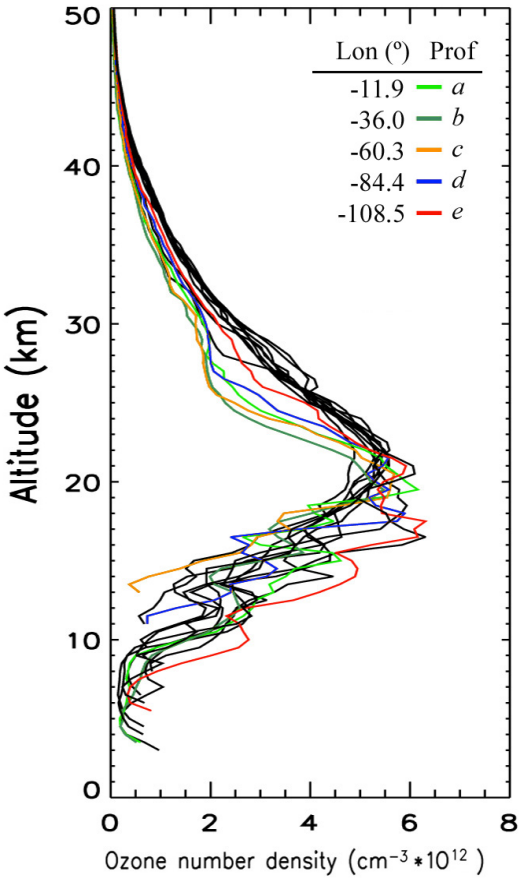

Figure 4.14 Southern Hemisphere SAGE II ozone profiles for 5 September 1990. Profiles in color correspond to the region between 120ºW and 0º. The longitude of these profiles is indicated in degrees beside a color and letter in order to identify them. Their actual position is depicted by stars in figure 4.5a.

Classified SAGE II profiles show distinct characteristics for every regime (figure 4.13a). Polar profiles, for example, display the lowest tropopause heights and the highest ozone concentrations as expected. However, the difference between midlatitude and polar profiles is not as clear as anticipated. These profiles indicate that the tropopause height is distinct between them, but at the same time they show large variability between 10 and 20 km. Nonetheless, the three regimes show a surprising similarity. All of them have a group of profiles with consistently different shapes from their respective means. In particular, some of the midlatitude and tropical profiles show ozone depletion occurring about 27 km of altitude, and a maximum in concentration at lower altitudes than their mean profile peaks. Examining other months, similar kind of profiles were observed in

June, July, August, October, and November of that year, however in much smaller proportion than in September.

In order to investigate this behavior, all SAGE profiles for 5 September 1990 were plotted in figure 4.14, but only those profiles between 120ºW and 0º were plotted in color. Their longitude is also indicated in this figure. The location of these five profiles is indicated by yellow stars in figure 4.7a. The important feature to note in figure 4.14 is the shape of the profiles that lie within or close to the polar vortex. In particular, four of these five profiles (*a*, *b*, *c*, and *d*) show a large ozone depletion in a layer between 22 and 30 km. According to figure 4.7a, only one of these profiles is within the Antarctic polar vortex. Two of them are close to the Antarctic boundary, and one is within the midlatitude regime although close to the subtropical boundary. Time differences between the total ozone data (which is quasi-synoptic data set) and the time-interpolated reanalysis data used in this analysis could help to explain some of these misclassifications. This is, the boundary edges could be slightly displaced from their "correct" location. The problem is, however, that even a profile that is relatively far from the vortex edge (profile *d*) shows a strong ozone reduction in the aforementioned layer. According to ozone, profile *d* is close to the transition zone between midlatitude and tropical regimes. However, if the surrounding area is under the influence of the stratospheric polar vortex, and therefore suffering ozone depletion, the boundary determined from total ozone could have been placed in the wrong location. If in addition, as figure 3.6a suggests, the vortex edge is not correctly delineated along all its length, then some regions could be erroneously ascribed to the tropical regime when in fact they should have been assigned to the polar vortex. There is one more fact to be taken into account in the case of SAGE

data. SAGE profiles are measured either at local sunrise or local sunset. TOMS data, on the other hand, is taken close to local noon. Therefore, there is an almost 6-hour difference between the data of these two instruments. Differences in ozone pattern between these two times could explain some of the errors in classifying SAGE profiles.

In order to calculate the monthly mean profiles for September 1990, a manual identification of all polar vortex profiles was performed. Total ozone, 200 mb winds, MPV, and the profiles themselves were used for this process. Figure 4.11b shows the final classification after these polar vortex profiles were removed. The profiles show a much clearer separation and a more defined tropopause height. Despite that, the midlatitude and tropical profiles still show a relatively large variability between 10 and 15 km.

Figure 4.15 shows monthly mean ozone profiles for March, June, September, and December of 1990. Polar vortex profiles were identified and removed only for September. In general, all months display a reasonable separation of the ozone profiles by regime. These monthly mean profiles clearly suggest distinct tropopause heights and concentration peak altitudes, as expected from the temperature profiles. In addition, the shapes are different, with polar profiles having a broader altitudinal distribution than the midlatitude, which in turn show similar behavior with respect to tropical profiles.

In order to see if the tropopause height defined from SAGE II ozone profiles is consistent with the thermal tropopause obtained from the rawinsonde profiles, a simple comparison was performed. A definition similar to the one used by Bethan et al. (1996) was followed. The tropopause height is assumed to be the lower altitude where the volume mixing ratio is 80 ppbv or higher, and its vertical gradient is higher than

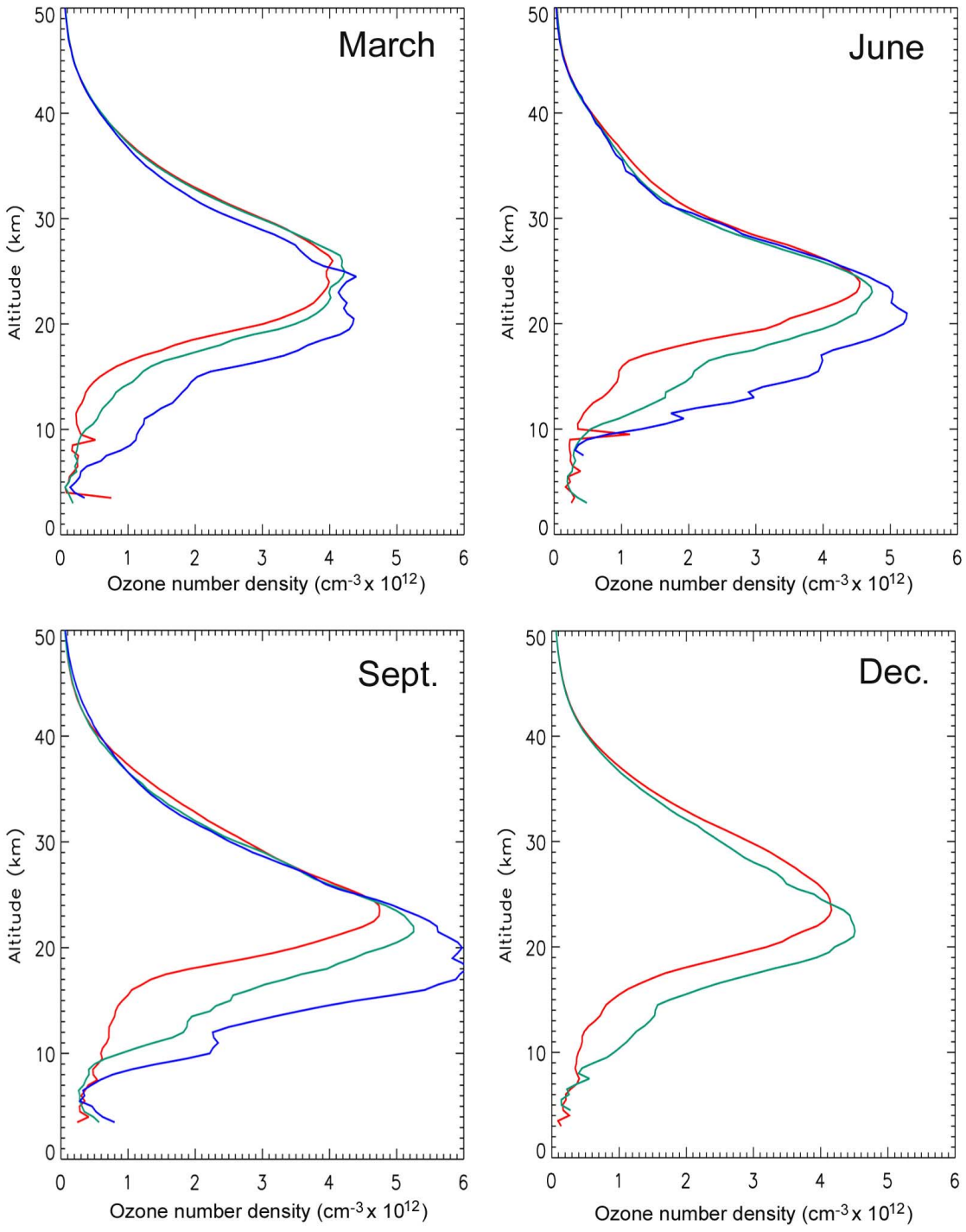

Figure 4.15 Monthly mean ozone profiles obtained from SAGE II data for the months of March, June, September, and December of 1990. These profiles were classified by using 2-degree masks. Red profiles correspond to the tropical regime, green profiles to the midlatitude regime, and blue profiles to the polar regime. In December there were not enough profiles within the polar regime to compute the monthly mean.

Month	TROPICAL			MIDLATITUDE			POLAR		
	η	Hraw	Hsage	η	Hraw	Hsage	η	Hraw	Hsage
March	0.32	16.2	15.0	0.44	13.5	11.5	0.77	9.3	8.5
June	0.36	15.1	16.5	0.63	10.9	10.5	0.75	9.2	9.5
Sept	0.39	14.5	15.5	0.62	10.9	9.5	0.84	8.5	8.0
Dec	0.33	15.9	16.0	0.60	11.1	10.0	0.89	7.8	

* η in molec cm^{-3}, H_{sage} and H_{raw} in km

Table T4.3 Monthly mean tropopause heights (H_{sage}) for March, June, September, and December of 1990 obtained from SAGE II data. The number density η was obtained from eq. 4.1 for a mixing ratio of 80 ppbv, and for a pressure and temperature corresponding to the tropopause calculated from the rawinsonde data. For comparison purposes, their corresponding altitude (H_{raw}) is also displayed here. H_{sage} were estimated with 1 km of uncertainty. There were not enough SAGE II profiles within the polar regime to compute reliable monthly mean values for December.

0.15×10^{12} molec cm^{-3} km^{-1} in the 1.0 km layer above this point[11]. From the equation of state it can be shown that the number density, η, can be written as follows,

$$\eta = 7.248 \times 10^{16} C \frac{P}{T} \quad \left[\frac{\text{molec}}{\text{cm}^3} \right] \tag{4.1}$$

where η is given in molec cm^{-3}, C is volume mixing ratio, P is the pressure in Pa, and T is the temperature in K. Table T4.3 shows the tropopause heights (H_{sage})computed using the criteria discussed above. The table also shows the number density for a mixing ratio of 80 ppbv, calculated at the tropopause level (H_{raw}), as indicated by the rawinsonde data. Reasonably good agreement between these two estimations is found. The agreement holds for all months and regimes. Given the relatively arbitrary definition of the "chemical" tropopause used for ozone, and that only mean temperature profiles were used for these calculations, the agreement is remarkable.

[11] The actual lapse rate in ozone concentration depends on regime.

5. TOTAL OZONE: TEMPORAL VARIABILITY WITHIN THE REGIMES

So far, the validation analysis indicates that the method is working as expected: it is classifying the ozone field into three distinct regimes each with a distinct tropopause height, total ozone column, and ozone profile. In this section, the characteristics of each regime as well as their ozone boundary values will be presented. The analyzed period covers almost 25 years, from January 1979 to December 2003, with a gap between December 1994 and August 1996 when no TOMS instrument took measurements (see Table T5.1). Despite the fact that three different instruments collected the measurements presented below, no attempt has been done to intercalibrate or homogenize the data. As will be discussed later, the precision to which the upper-level jets are determined is not expected to be affected by small systematic or random errors in total ozone. Similarly, the relative areas should not be sensitive to the instrument used because their boundaries are determined by gradients in the total ozone field and do not depend on the absolute value of total ozone. On the contrary, instrumental or retrieval errors could affect total ozone trends. For example, systematic differences between two instruments could introduce an artificial trend. More about this topic is discussed in section 5.4.

Satellite	Begin	End
*Nimbus-7**	Nov-78	Apr-93
*Meteor-3***	Aug-91	Nov-94
*Earth Probe****	Aug-96	Today

* Data retrieved with algorithm version 8

** Data retrieved with algorithm version 7

*** Version 8 until Aug 03, version 7 from then on

Table T5.1 Satellites that carried TOMS instruments and periods when ozone data was collected by them.

At this point it is important to mention that this is the first time that total ozone has been analyzed by meteorological regimes in the Southern Hemisphere. Almost all previous studies have used latitudinal bands or, to a lesser extent, equivalent latitude, to

perform analyses of ozone trends. The basic quantity used in either case was mean total ozone within the designated latitude band. However, by classifying the ozone field by regime, this basic quantity now becomes the result of total ozone contributions from each regime weighted by their corresponding spatial extent. For this reason, the temporal behavior these two quantities will be studied in this chapter. The goal, in any case, is to try to better understand what factors contribute to the observed trends in total ozone, and how they do it.

5.1 Boundary Values

As discussed in chapter 3, daily values for the ozone boundaries were computed using an iterative procedure for every day when TOMS data was available. These daily values show a strong seasonal dependence. In order to compute a "climatology", a two-harmonic function (annual and semi-annual components) was fitted to the data. The seasonal behavior for the two boundaries is depicted in figure 5.1. As mentioned earlier,

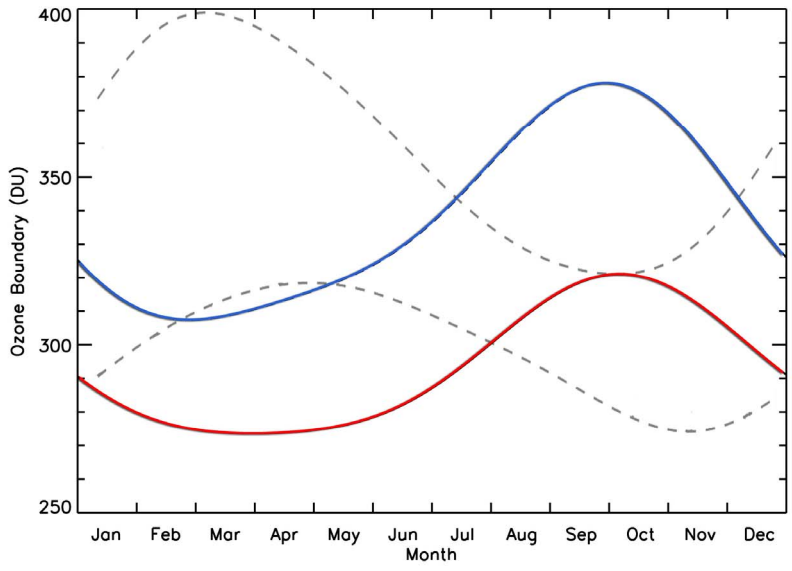

Figure 5.1 Climatological polar (solid blue line) and subtropical (solid red line) ozone boundaries deduced from 25 years (1979 to 2004) of TOMS data for the 25º-60ºS band. The corresponding NH values are shown by the dash lines.

these curves show a strong annual cycle with the lowest values in the fall and the highest in spring. The mean separation between the two boundaries also varies with season, with a minimum of 30 DU in the fall and a maximum at the beginning of spring with an approximate separation of 60 DU. These climatological values can be compared with the ones shown by Hudson et al. (2003) for the Northern Hemisphere (NH). For comparison, those values are also displayed in figure 5.1. As expected, there is almost a 6-month phase difference between the Northern and the Southern Hemispheres. However, the Southern Hemisphere (SH) polar boundary has smaller values than its NH counterpart. In addition, the SH boundaries are almost in phase with each other, whereas the NH boundaries have a phase difference of about two months. Finally, it should be noted that the SH subtropical boundary has an almost constant value during the fall showing an abrupt increase about June. The NH subtropical boundary does not show this kind of behavior.

Figure 5.2a shows daily values of the SH ozone boundaries after the annual and semi-annual climatology has been removed. The standard deviations for these data are 7 and 3 DU for the polar and subtropical boundaries, respectively. This indicates that the variability of the boundary values was relatively small during this period. There are, however, three peaks that show values well above 3σ. Data for 1979, 1981, and 1988 show very large total ozone values for periods of almost one month between September and October of those years. The fact that these peaks occurred at the same time of year makes them suspect. When the data for the anomalous days was analyzed in more depth, two facts were evident: a) these were years with very high total ozone, and b) the large total ozone

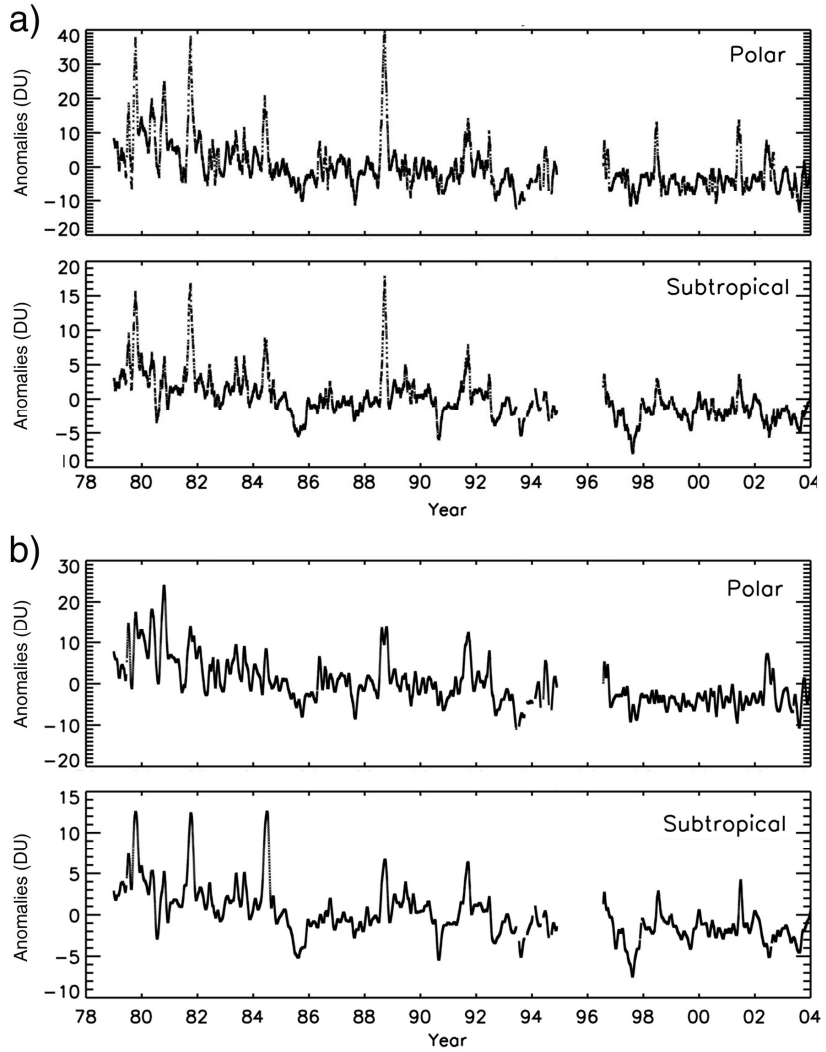

Figure 5.2 Deseasonalized daily total ozone values for the polar and subtropical boundaries for 1979 to 2004. Panel a) shows original values after the procedure described in the text was applied to the TOMS data. Panel b) shows the same data after the area-weighted mean was used to compute the ozone boundaries during the periods indicated by table T5.2. The latter was used in the analysis of this paper.

regions were concentrated in relatively small regions. In particular, ozone within the polar regime exhibited a much larger latitudinal dependence than other years. This fact forces the iterative method to shrink the polar regime, pushing its mean total ozone to higher (and unrealistic) values, and eventually producing these anomalous large boundary values. In order to avoid this problem, the polar boundary for these anomalous days was computed as the weighted mean of the polar and midlatitude ozone

averages with their corresponding relative areas as weights. In addition to the periods already mentioned, this procedure was applied to a few days in 1984, 1998, and 2001. Table T5.2 shows the periods when this correction was applied. Figure 5.2b shows the residuals for the boundary values once the correction was performed. Although, there are still some relatively large fluctuations, no extreme outliers are now observed. Further, the corrected values show a better agreement with the values obtained from the ozone gradient method (not shown here). The climatology for the boundaries changed very little with the corrected boundaries.

Begin	End
15-Sep-79	05-Nov-79
04-Sep-81	28-Oct-81
01-May-84	31-Jul-84
26-Aug-88	11-Oct-88
27-May-98	22-Jul-98
10-May-01	12-Jul-01

Table T5.2 Periods in which area-weighted means where used to determine ozone boundaries.

5.2 Ozone

Area-weighted total ozone means were computed for all regimes for every day that TOMS data was available. The zero-masks were used for this purpose (see chapter 3). In order to include all the data, half of the boundary pixels were assigned to one regime and the other half to the other regime. Although in this way the mean ozone values are slightly "contaminated" by the boundary values, no data is excluded from the analysis. This fact is important when comparing the regime results with those obtained from conventional analysis using latitude bands when no separation is performed. At this point, it should be stressed that the Antarctic region has been excluded from the process of calculating the ozone boundaries. The destruction of ozone within this region is controlled to a large extent by chemical processes (Solomon, 1990 and references therein) and therefore total ozone within the Antarctic region does not act as a dynamical tracer. As a result, total ozone within the vortex does not have a narrow distribution, and

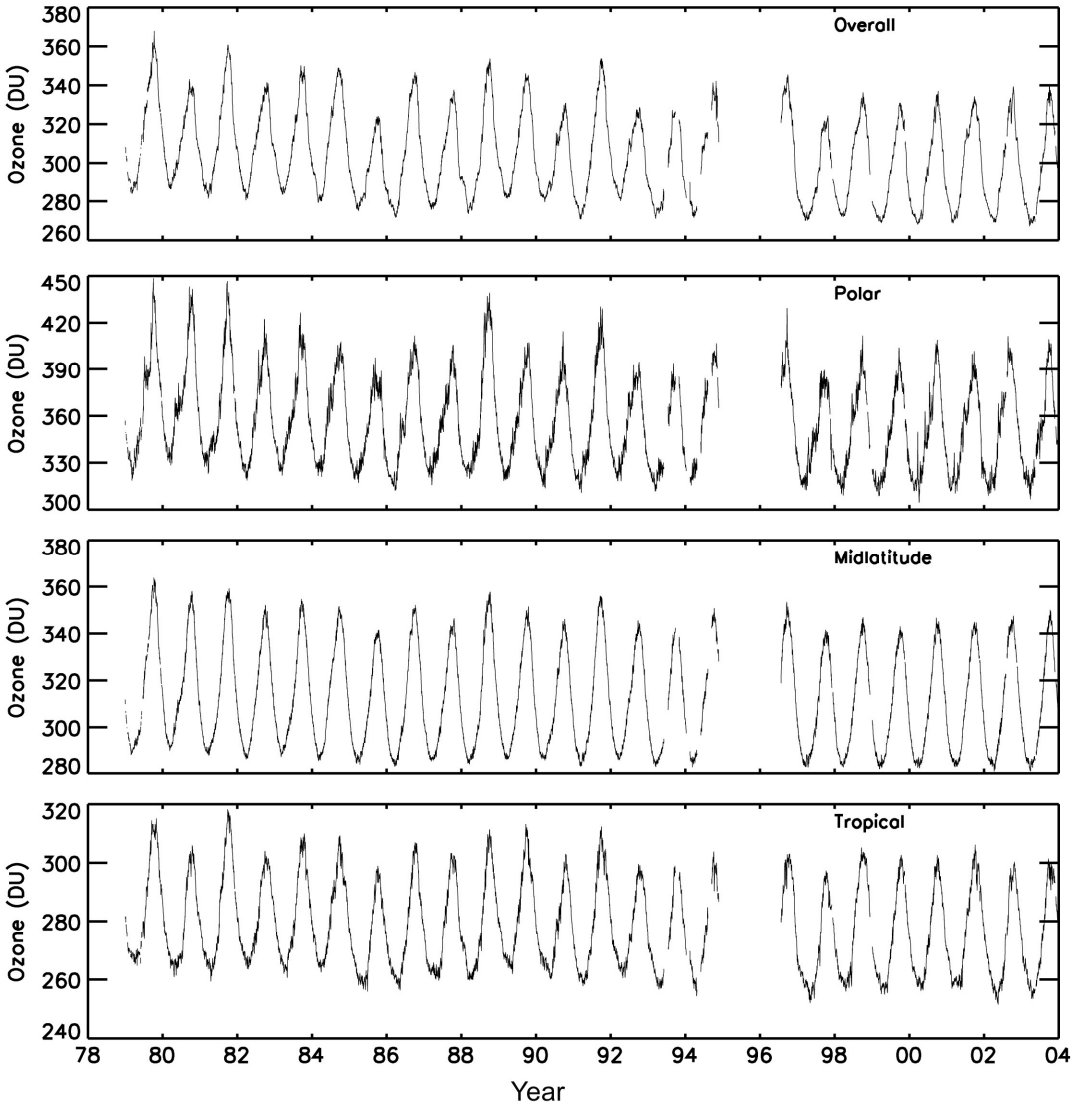

Figure 5.3 Daily mean total ozone within the 25-60ºS band for the overall data and the polar, midlatitude, and tropical regimes. The data spans from January 1979 through December 2003.

the iterative method used to determine the ozone boundaries cannot be applied for this case.

The daily total ozone for years 1979 through 2003 are shown in figure 5.3. Four time series are depicted. The top panel shows the data without any classification (hereinafter referred to as "the overall data"). The other panels show daily total ozone for the three regimes. The overall data is used basically for comparison purposes, i.e. to show

that those results agree with previous studies. Due to the seasonal nature of the Antarctic vortex, its inclusion in the calculation of the overall ozone mean does affect the result of the statistical analysis. Results when the Antarctic is included or excluded from the statistical analysis are presented later in order to estimate the influence of this region over the ozone trends in the 25º-60ºS region.

Figure 5.3 shows a very strong seasonal cycle for all four time series. During this 25-year period, the annual ozone range was 267-368 DU for the overall data, and 304-448 DU, 281-364 DU, and 251-318 DU for the polar, midlatitude, and tropical regimes, respectively. Note the similarity in the ozone domain between the overall data and the midlatitude regime.

Total ozone climatologies for every regime as well as for the overall data were calculated using the entire ozone record from 1979 through 2003. Figure 5.4 shows these

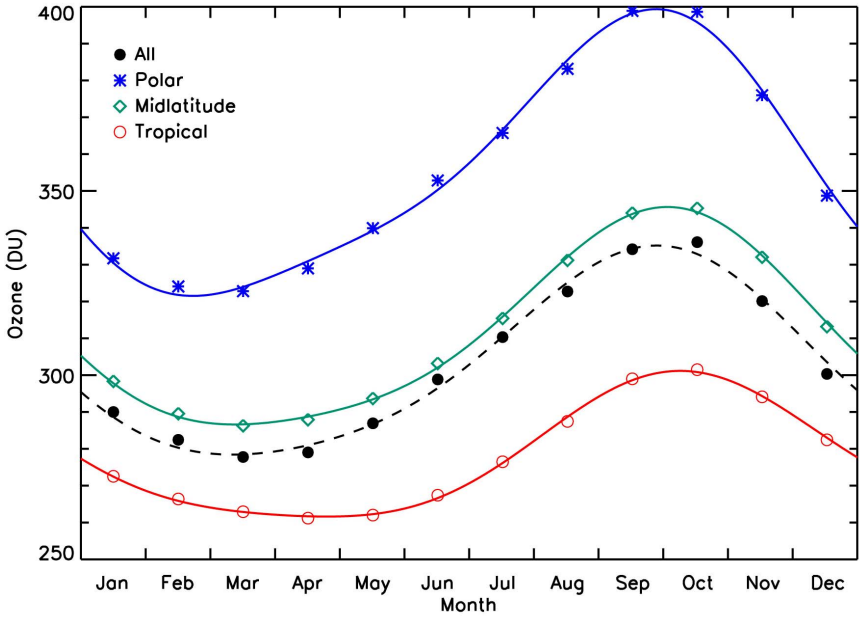

Figure 5.4 Monthly climatological values of total ozone for the overall data (black) and the meteorological regimes (red for tropical; green for midlatitude, and blue for polar regime). A two-harmonic sinusoidal function has been fitted to the monthly values in each case.

climatologies obtained from two independent methods. The symbols represent monthly mean values of total ozone within the regimes for each month of the year. The curves, on the other hand, show climatologies obtained by fitting sinusoidal functions with annual and semi-annual periods (two-harmonics) to the data. In both cases, the overall mean is also included for comparison. Figure 5.4 shows that the agreement between these two methods is good. The two-harmonic fitting will be used in subsequent analyses.

These climatologies show, as expected, that total ozone is at a maximum in spring and a minimum in fall. The data also indicates that the three regimes are in phase, a feature that is different in the NH case (Hudson et al., 2003). The mean total ozone within each regime is also smaller in the SH than in the NH. This difference is most marked for the polar regime.

In order to investigate ozone variability, the ozone residuals were computed for every day. Figure 5.5 shows the total ozone residuals for the overall data as well as for the meteorological regimes. The standard deviation of these residuals are 8.8 DU for the overall, and 10.9 DU, 4.3 DU, and 4.8 DU for the polar, midlatitude, and tropical regimes, respectively. In percent, these numbers correspond to 2.9% for the overall, 3.1% for the polar regime, 1.4% for midlatitude regime, and 1.7% for the tropical regime. This data shows that the ozone variability is small during these 25 years. In spite of that, several aspects of figure 5.5 also suggests that this signal carries additional information. First, the data shows positive values for the anomalies at the beginning of the record (1979-1984) in all data sets. In contrast, at the end of the record most of the anomalies are close to zero or negative, suggesting a negative trend in total ozone. Second, the data shows strong and relatively long anomalies which are clearly above the "noise" level. An

interesting thing to note here is that the amplitude of these anomalies within the regimes is not the same as within the overall data. In general, the anomalies in the midlatitude and tropical regimes are almost half of the corresponding anomalies in the polar regime or the overall data. Even in the case of the regime with the largest variability, the polar regime, the amplitude of its anomalies almost never exceeded the anomalies shown by the overall data. Furthermore, some strong anomalies are present in one regime or another but not

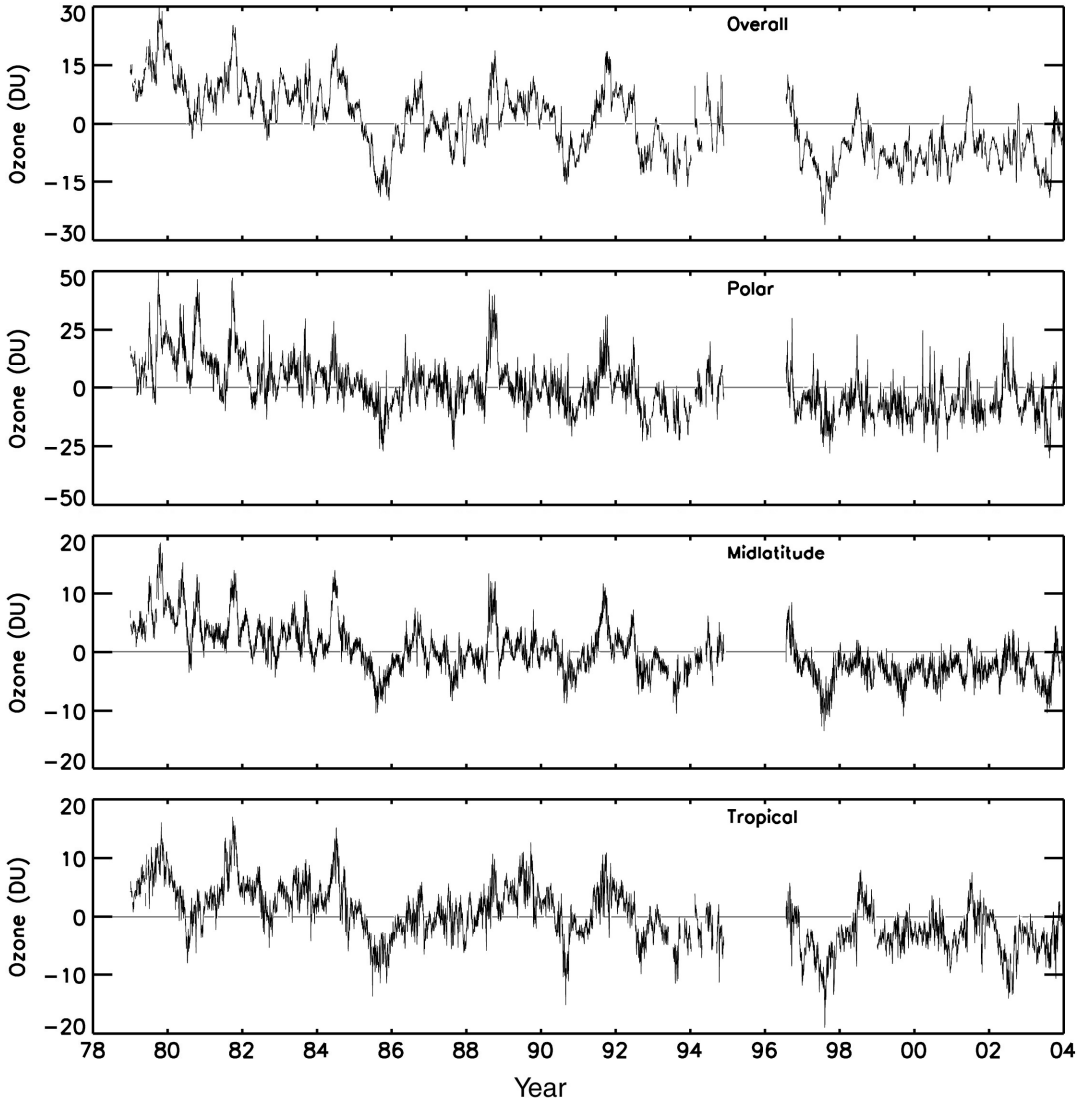

Figure 5.5 Daily total ozone residuals for the overall data and the meteorological regimes for data measured between January 1979 and December 2003 in the 25º-60ºS band.

in all of them. This suggests that the observed variability in the overall data is the result of fluctuations in total ozone within each regime, plus fluctuations of at least one additional factor as will be shown later.

There is abundant literature about the influence of climate-related phenomena upon the total ozone column (WMO, 1988; Hollandsworth et al., 1995; Chandra and Stolarski, 1991). In particular, it has been shown that the quasi-biennial oscillation (QBO) and the solar cycle have strong influence over the overall total ozone (WMO, 1998; Randel and Wu, 1996). In order to investigate if these phenomena also affect total ozone within the regimes, the power spectrum of the ozone residuals were analyzed. The daily ozone residuals between January 1979 and December 1993 were processed using a Fast Fourier Transform (FFT) in order to identify the main frequencies present in them. No filtering of any kind was applied to the data. This time interval was chosen because the data is almost continuous in this period (118 days missing out of 5114). For the days when no data was collected, a climatological value was used in order to avoid gaps in the input data. Figure 5.6 shows the Power Spectrum Density (PSD) for the lowest frequencies (up to 5 cycles/year). Higher frequencies show much smaller values of the PSD and therefore are not considered statistically relevant. The dotted lines in this figure show the PSD for a reference signal with an 11-year period, and a 27-month period, in addition to the annual, semi-annual, and 4-month periods. These spectra suggest the existence of frequencies close to the 11-year, associated with the solar cycle, and the 27-month, associated with the QBO. An additional frequency in between is also observed. A peak related to a 4-month period, which will be taken into account in the deseasonalization procedure, is also present.

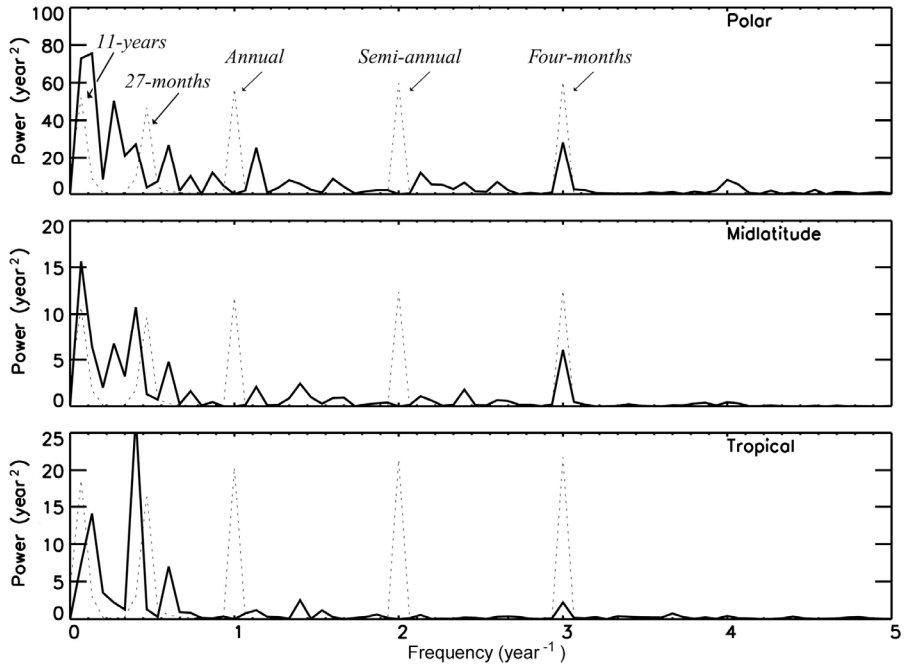

Figure 5.6 Power spectrum densities (PSD) of the daily ozone residuals depicted in figure 5.5 for the period 1979-1993. Dotted lines show the PSD for a reference signal with 11-year, 27-month, annual, semi-annual, and 4-month periods.

In order to estimate which peaks were statistically significant, the following procedure was applied. A sinusoidal function with only one harmonic was fitted to the data for each regime. The variance of the new residuals was computed and compared with the original ozone residuals. The explained variance (EV), defined as,

$$\mathrm{EV} = 1 - \frac{\mathrm{Var}(r_{new})}{\mathrm{Var}(r_{ori})} \tag{5.1}$$

was used to establish the significance of the given frequency. In equation 5.1, r_{new} are the residuals after the fitting was applied, and r_{ori} are the original residuals shown in figure 5.5. Only frequencies that explained more than 5% were considered statistically significant. Figure 5.7 shows EV as a function of frequency (in cycle/year) for the overall data as well as for each regime. Four peaks are higher than 5% and present in almost all regimes. These peaks are centered about 0.11, 0.25, 0.40, and 0.59 cycles per year which

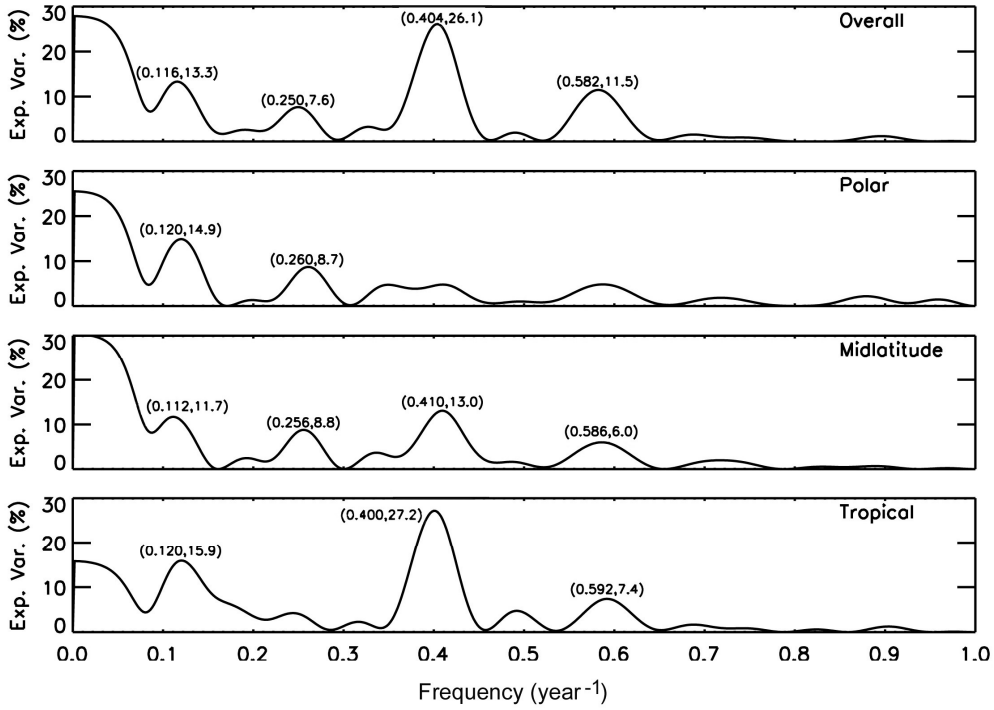

Figure 5.7 Explained variance as a function of frequency (in year^{-1}) for the ozone residuals shown in fig 5.5. Numbers in parenthesis are the frequency of the local maximum and its corresponding EV in percent.

correspond to periods of 9 years, 4 years, 30 months, and 20 months, respectively. Note that small uncertainties in frequency will produce relatively large uncertainty in the corresponding periods. For example, for the frequency of 0.11 cycles/year, an uncertainty of 0.01 will produce a period interval of 8.3-10 years. Taking that into account, the 9-year and 30-month peaks can be thought to represent the influence of the solar cycle and QBO over total ozone. The other two peaks do not seem to have an obvious relation with these two phenomena. However, Tung and Yung (1994) showed that the 20-month peak is related to the seasonal modulation of the QBO phenomenon. They argued that this modulation is much stronger in the extratropics than in the equatorial regions, which led them to suggest that the 20-month frequency is a signature of a QBO circulation anomaly in the extratropics. The 4-year oscillation peak has not been associated with QBO or the

solar cycle but has been noted before by Hasabe (1984) in a 10-year record of Solar Backscatter Ultraviolet (SBUV) data**.**

The important point outlined by the previous analysis is that both the solar cycle and QBO seem to play a role in modulating total ozone within the meteorological regimes. Figure 5.7, however, shows that this influence is not the same in all regimes. The 30-month and 9-year oscillations emerge clearly in the tropical regime, but are weak in the polar regime. Conversely, the 4-year oscillation is strong in the polar regime but has a relative small signature in the tropical regime. The 9-year oscillation, presumably related to the solar cycle, is present and significant in all regimes. For these reasons, the influence of QBO and the solar cycle must be taken into account in order to compute the ozone trends correctly.

A statistical linear regression model of the form

$$\Omega_i = \alpha \cdot t_i + \beta \cdot \mathrm{Solar}(t_i) + \gamma \cdot \mathrm{QBO}(t_i) + \varepsilon_i \qquad (5.2)$$

was applied to the monthly ozone residuals in each regime. Here, t_i is the time corresponding to the *i–th* month, Solar(t_i) is the solar index related to the solar flux at that time, and QBO(t_i) is the QBO index at the same moment. The terms α, β, and γ are constants to be determined from the regression analysis. In the present thesis, the Mg-II index is used as a proxy of the solar flux (Heath and Schlesinger, 1986; DeLand and Cebula, 1993). Normalized winds at 50-mb from NCEP are used to represent the QBO. It should be noted that a lag difference of a few months between the westerly zonal winds at 50-mb and total ozone has been reported previously (Hollandsworth et al., 1995). In our case, a 3-month lag of ozone with respect the equatorial QBO produced the best correlation between the QBO data and total ozone residuals.

TROPICAL				MIDLATITUDE				POLAR			
lin	QBO	Mg-II	EV	lin	QBO	Mg-II	EV	lin	QBO	Mg-II	EV
		x	14.6			x	9.3			x	9.7
	x		16.9		x		8.1		x		2.3
	x	x	31.5		x	x	17.3		x	x	12.0
x			37.4	x			41.6	x			35.7
x		x	50.4	x		x	49.5	x		x	44.0
x	x		53.2	x	x		48.9	x	x		37.7
x	x	x	66.2	x	x	x	56.8	x	x	x	46.0

Table T5.3 Explained total ozone variance, in percent, for different combinations of the coefficients in equation 5.2. The 'x' indicates that the corresponding parameter has been taken into account in the statistical model.

Table T5.3 shows the explained variance for different combinations of the coefficients in equation 5.2. The x's in this table indicate that the parameter is included in the statistical model. For example, for the tropical regime, when only the Mg-II index is used ($\alpha=\gamma=0$), the model explains 14.6% of the original variance. On the other hand, when all parameters are used, the EV is 66.2%. The results shown in Table T5.3 suggest that the QBO and Mg-II indices act like statistically independent variables for the total ozone residuals because the summation of their respective EVs is almost exactly the same as the EV when both parameters are included into the statistical model simultaneously. This is not true when the linear term α is included in the model. In this case, the summation of the EVs for each individual parameter is smaller than the EV when the full model is used. The difference between these two quantities, however, is less than 2% for all regimes, indicating that the three parameters used in eq. 5.2 behave as statistically quasi independent variables.

The other interesting thing to note in table T5.3 is that the Mg-II, QBO, and linear terms explain more variance in the tropical regime than in the polar regime, together or

individually. Although the linear term produces EVs of the same order of magnitude for both polar and tropical regimes, the EV for the QBO in the tropical regime is almost eight-times larger than the corresponding EV in the polar regime. This is consistent with what is shown in figure 5.7, where the 30-month peak is much stronger in the tropical regime than in the polar one. When the model is applied as described in eq. 5.2, that is,

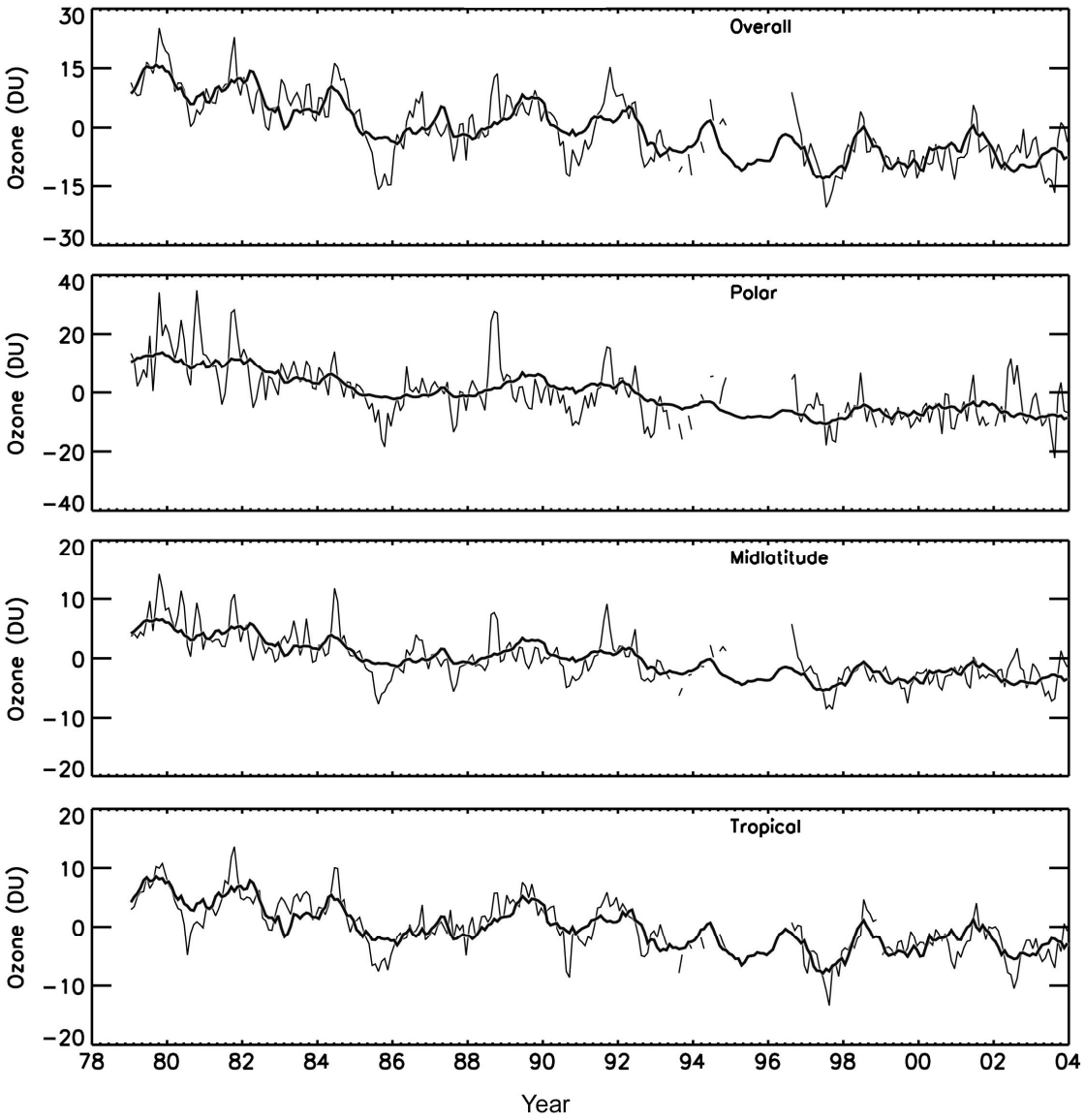

Figure 5.8 Monthly ozone residuals (thin solid line) for the overall data as well as the meteorological regimes. The thick curve is the fit obtained from eq. 5.2 including all terms.

using all terms of that equation, 66% of the original variance can be explained for the tropical regime. In contrast, only 46% of the variance is explained by this model for the polar regime, while 37% is explained for the midlatitude regime. For reference, when the same statistical model is applied to the residuals of the overall data, 69% of the variance is explained. Figure 5.8 shows the monthly ozone residuals for the overall data and the three regimes. The thick solid line is the fit to the data. These curves follow the data reasonably well, especially in the tropical regime. The linear term α in equation 5.2 indicates a decline in total ozone for all regimes as well as for the overall data for the period 1979-2004. These trends are: -2.4%/decade for the overall data, -2.1%/decade, -1.1%/decade, and -1.3%/decade for the polar, midlatitude, and tropical regimes, respectively. Note that all regime trends are smaller than that of the overall data.

5.3 Relative Areas

Relative areas were computed for all regimes for every day when TOMS data was available. If A_i is the area of the *i-th* regime, and $A_{25\text{-}60}$ is the area for the band 25-60ºS, then the relative area for the *i-th* regime is defined as:

$$R_i = \frac{A_i}{A_{25-60}} \tag{5.3}$$

for the latitudinal band 25º-60ºS. In this case the polar vortex area was included in the analysis to guarantee that the fluctuations in the relative areas were real changes in the actual areas of the regimes, and not an artifact of the normalization procedure. In this way, the summation of the regime relative areas and the polar vortex area always add up to one (the boundary regions are ascribed to each regime in the same way as ozone). Given the fact that the TOMS data contains days where some pixels are missing or, as in

the case of EP-TOMS, large regions contain no data due to the satellite orbit, total ozone was interpolated from MPV (see section 3.5 for more details). In this way no "holes" were left on the data. At least 50% of the band was required to have valid data in order to perform such interpolation. If this criterion was not fulfilled, the data was not used in the analysis. Using MPV to fill gaps in the data makes an important difference in terms of relative area only during the period when the Earth Probe satellite was at 700 km altitude (August 1996 to December 1997). For other periods or satellites there is almost no difference whether the missing data is taken into account or not.

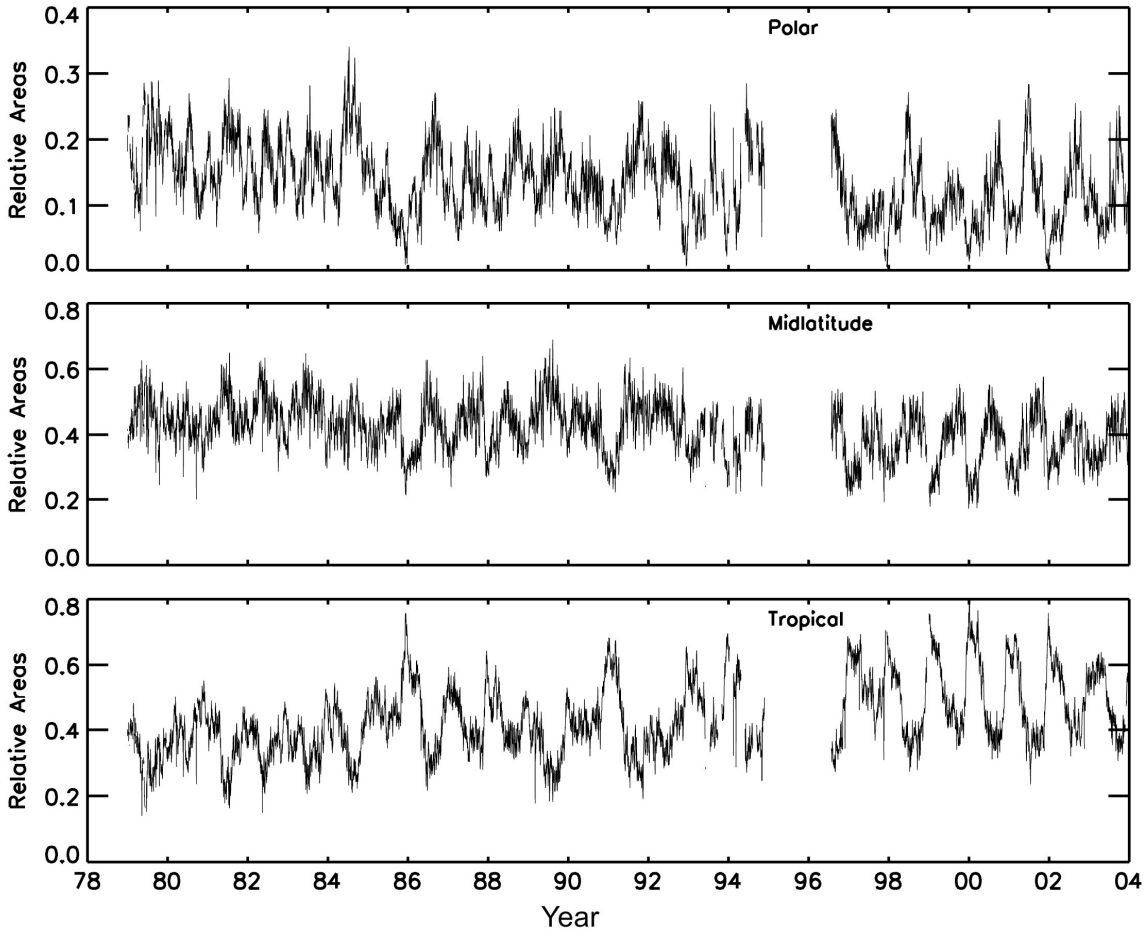

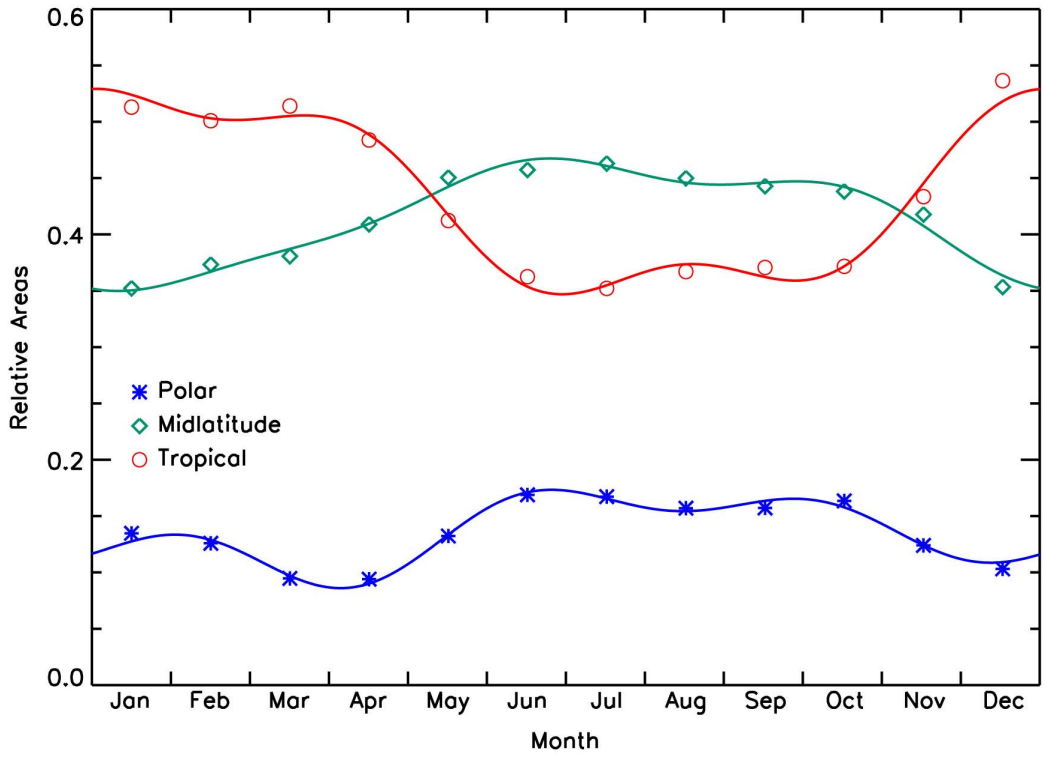

Figure 5.10 Monthly climatological values of relative areas within each regime. Red open circles for the tropical regime, green diamonds for the midlatitude regime, and blue stars for the polar regime A sinusoidal function with 3 harmonics has been fitted to the monthly values in each case.

The daily relative areas are plotted in figure 5.9. Compared to the total ozone data, the relative areas are much more variable. The mean relative areas during the period 1979-2004 were 0.13 for the polar regime, 0.42 for the midlatitude regime, and 0.43 for the tropical regime. The corresponding standard deviations were 0.05, 0.08, and 0.11. These numbers indicate that the area of the polar regime in the band 25-60ºS is not as large as in the Northern Hemisphere (Hudson et al., to be submitted) for the corresponding latitudinal band. In addition, the seasonal cycle is not as strong as in the case of total ozone. This is evident when the climatology of the relative areas is computed. Figure 5.10 shows the monthly mean relative areas for the three regimes. The solid curves were obtained by fitting three-harmonic functions to the daily data,

whereas the symbols were computed as the average relative area for every month. A good agreement between the two methods is observed. As in the case of ozone, the sinusoidal function will be used as climatology for the relative areas from now on. These climatologies confirm the fact that the polar regime contributes about 20% of the relative area between 25º-60ºS throughout the year. Small seasonal dependence for this regime can be observed, with a minimum in relative area at the beginning of the austral fall. The other two regimes show a much stronger dependence with season. The "peak-to-peak" amplitude for the polar regime is 0.087, while the same parameter has a value of 0.117 for the midlatitude, and 0.182 for the tropical regime. As expected, the tropical regime has its maximum extent in summer and minimum in winter. The midlatitude regime behaves almost exactly the opposite of the tropical regime.

Figure 5.11 shows the daily residuals for the three regimes after the deseasonalization. The standard deviations of these three data sets are 0.048, 0.070 and 0.088 for polar, midlatitude, and tropical regime, respectively. These numbers represent a variability of 35%, 17% and 20% with respect to their mean values. Compared with the variability of ozone residuals, the relative areas are almost 10-times more variable. Despite that, the relative area residuals show some structure, as in the case of total ozone. In fact, some periodicity is clearly evident in the data. These residuals also show something that was evident in the ozone residuals. The relative areas seem to be almost constant between 1979 and mid 1984, when an abrupt change occurs. Then, between 1985 and 1992, the data shows large variability and structure. Finally, between 1999 and 2003, another period of relative tranquility is observed. The mean value for the latter period is clearly different from the one at the beginning of the record

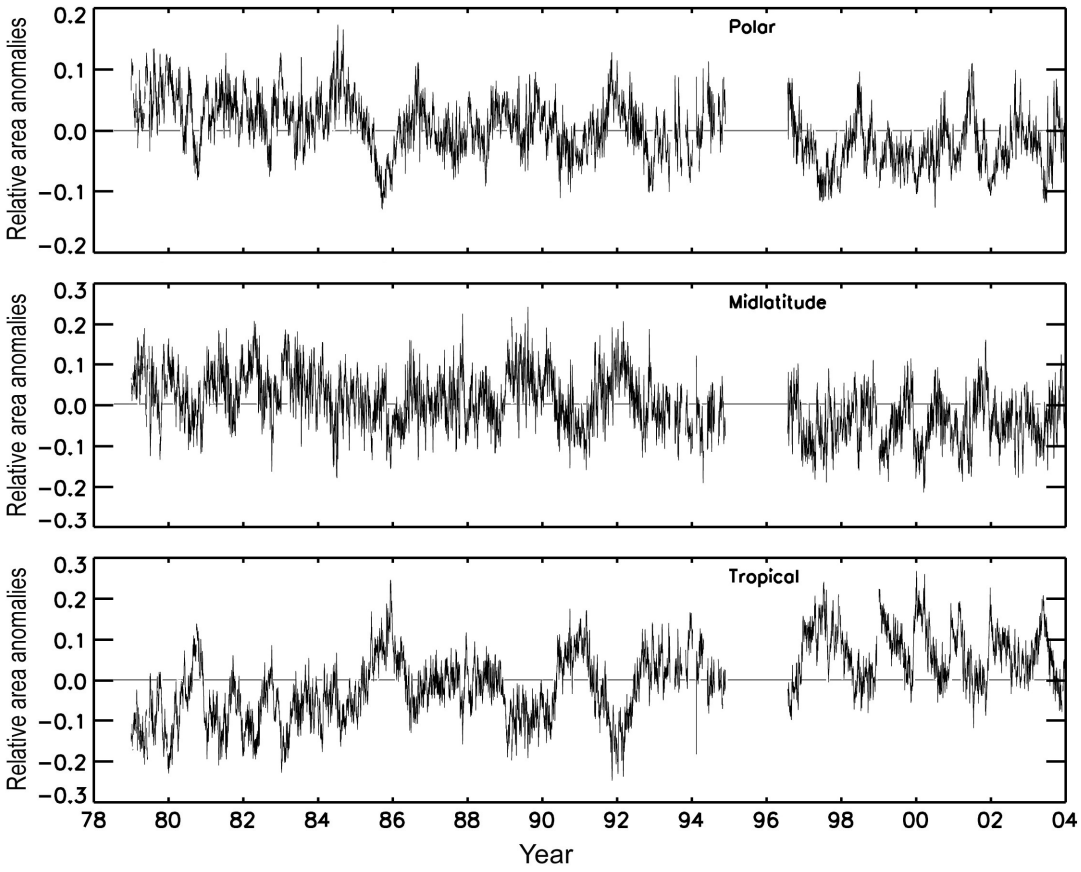

Figure 5.11 Daily relative area residuals in the band 25º-60ºS for the polar, midlatitude, and tropical regimes. The data spans from January 1979 to December 2003.

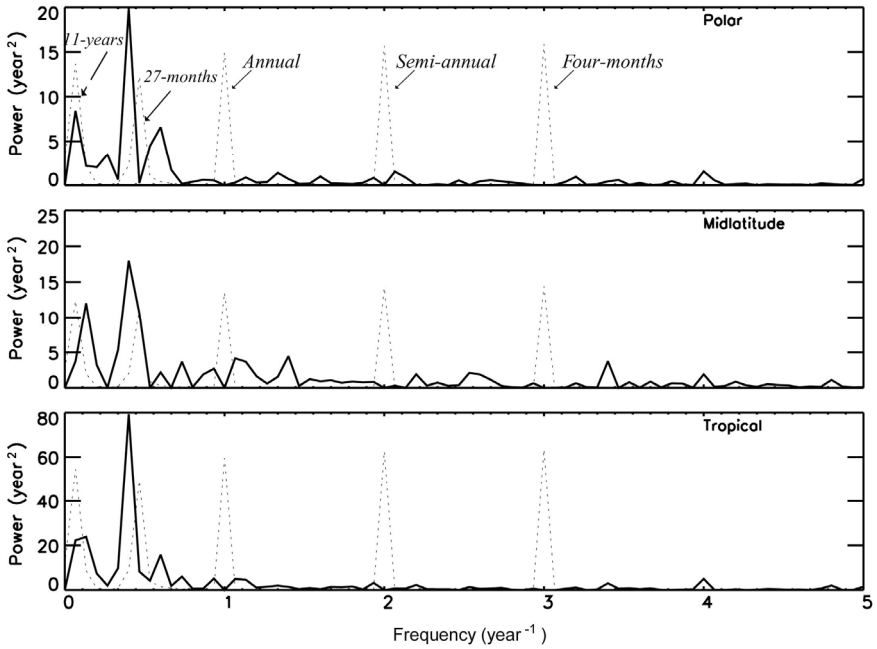

Figure 5.12 Power spectrum densities (PSD) of the daily relative areas depicted in figure 5.11 for the period 1979-1993. Dotted lines show the PSD for a reference signal with 11-year, 27-month, annual, semi-annual, and 4-month periods.

In order to identify the periodic signals an FFT was applied to the residuals. Figure 5.12 show the resulting PSD for the lowest frequencies. Higher frequencies show smaller peaks than those illustrated in this figure and are not considered statistically significant. A reference PSD is also depicted in the figure (dotted lines). This synthetic signal contained five harmonics with periods of 1-year, half-year, 4-month, 27-month, and 11-year. These PSDs suggest the presence of the solar cycle and QBO signatures in the relative areas. Given the fact that the record used to calculate this PSD is only 15 years long, the 11-year cycle was expected to have small statistical significance. As in the case of total ozone, a one-harmonic function was fitted to the data and the explained variance, computed from equation 5.1, was used to establish the statistical significance of that harmonic. Figure 5.13 shows basically the same three peaks as in the total ozone

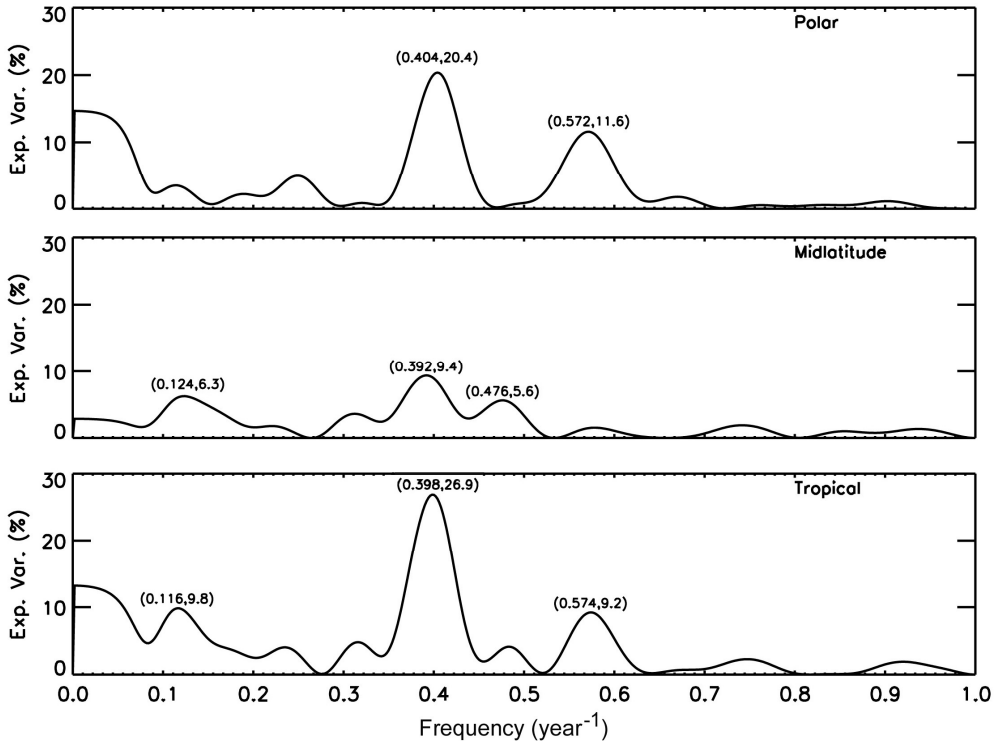

Figure 5.13 Explained variance as a function of frequency (in year^{-1}) for the relative-area residuals shown in fig 5.11. See text for details. Numbers in parenthesis are the frequency of the local maximum and its corresponding EV in percent.

TROPICAL				MIDLATITUDE				POLAR			
lin	QBO	Mg-II	EV	lin	QBO	Mg-II	EV	lin	QBO	Mg-II	EV
		x	7.3			x	7.0			x	2.7
	x		14.9		x		5.3		x		18.3
	x	x	22.2		x	x	12.2		x	x	21.0
x			37.3	x			28.6	x			27.8
x		x	43.5	x		x	34.6	x		x	29.9
x	x		51.2	x	x		33.4	x	x		45.2
x	x	x	57.4	x	x	x	39.4	x	x	x	47.3

Table T5.4 Explained relative area variance, in percent, for different combinations of the coefficients in equation 5.2. The 'x' indicates that the corresponding parameter has been taken into account in the statistical model.

case. That is, frequencies around 0.11, 0.40, and 0.58 corresponding roughly to 9-year, 30-month, and 20-month oscillations, respectively. This figure suggests that the influence of the 9-year period is less pronounced than in the total ozone case.

In order to determine what role the solar cycle and the QBO play in the regime's relative area behavior, a statistical model of the form of eq. 5.2 was applied to the relative area residuals. As in the case of ozone, table T5.4 shows the results for different combinations of the coefficients in eq. 5.2. This table indicates that the Mg-II and QBO indices act like statistically independent variables, and that they are weakly correlated with time. In addition, this table shows that the linear term explains a large portion of the variability for all regimes, whereas the influence of the solar cycle on the relative areas seems to be small, especially over the polar regime where the EV for the QBO is not considered to be statistically significant.

Figure 5.14 shows the monthly relative area residuals (thin solid lines) for the 1979-2004 period. The fitted data is shown by the thick solid lines. It can be observed that the fitted curve follows the residuals reasonably well. In fact, according to table T5.4, these curves explain 47% of the observed variability in the case of the polar regime, 39%

in the case of the midlatitude regime, and 57% for the tropical regime. The linear term α of eq. 5.2 is equal to -0.00289, -0.00399, and 0.00660 for the polar, midlatitude, and tropical regimes, respectively. These quantities, given in units of relative area per year, suggest that in these 25 years the tropical regime has grown at the expense of the polar and midlatitude regimes in the band 25º-60ºS.

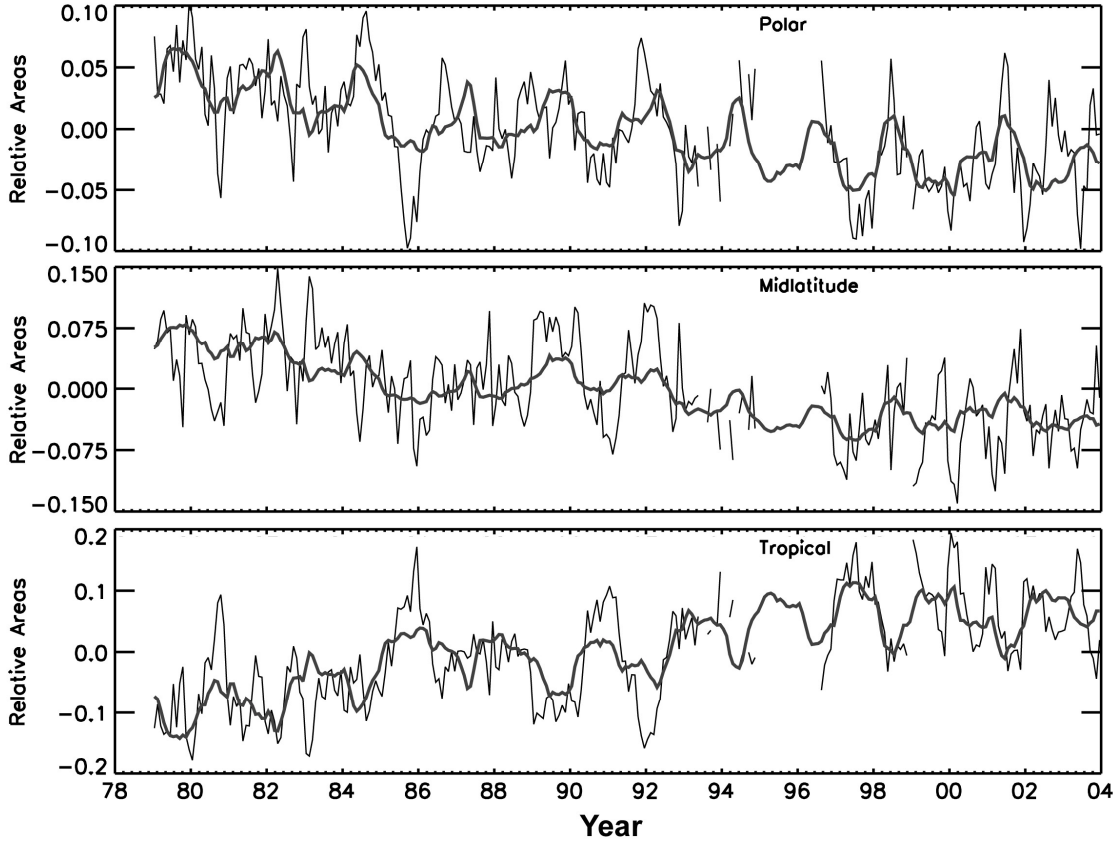

Figure 5.14 Monthly relative area residuals (thin solid line) for the meteorological regimes. The thick curve is the fit obtained from eq. 5.2 including all terms.

5.4 Linear Trends

The preceding analyses (sections 5.2 and 5.3) showed that when the ozone field is divided into meteorological regimes, the total ozone linear trends within the regimes are smaller than the overall trend. Table T5.5 summarizes the results of the regression analysis for both total ozone and relative areas for the period between January 1979 through December 2003. This table shows that the trends for the midlatitude and tropical regimes are almost half of the overall trend. How can it be possible that the trend within each regime is smaller than the overall trend?

In order to have a better understanding of the problem let us consider the mass of ozone, M_a, between 25º-60ºS:

$$M_a = \sum_i \Omega_i a_i = M_t + M_m + M_p + M_v \qquad (5.4)$$

where Ω_i and a_i are the ozone column and area which correspond to the *i-th* pixel on the TOMS data. Clearly M_t, M_m, M_p, and M_v are the masses of ozone within each of the regions of analysis: the three regimes and the polar vortex.

	Regime	**EV**	linear α	QBO β	Mg-II γ
OZONE	Overall	69.40	-0.747	-0.449	378.25
	Polar	45.95	-0.744	-0.187	433.86
	Midlatitude	56.81	-0.332	-0.150	175.84
	Tropical	66.23	-0.353	-0.250	255.37
AREAS	Polar	47.294	-0.00289	-0.00247	0.978
	Midlatitude	39.376	-0.00399	-0.00175	2.216
	Tropical	57.414	0.00660	0.00435	-3.266

Table T5.5 Coefficients from the regression analysis, equation 5.2, applied to the total ozone and the relative area residuals.

The polar vortex is present for only a few months of the year, mainly in fall and spring. Its mass never exceeded 5% of the total ozone mass between 25º and 60ºS for the period of analysis, and, in average, it represented only 2% of the ozone mass in this band. Thus, it seems reasonable to neglect the Antarctic polar vortex from the present study. In order to test this fact, trends for the overall total ozone were computed with and without the vortex area. When all data is used (analysis includes the Antarctic vortex) the trend is -12.40 DU/decade for the 1979-2004 period. On the other hand, when the vortex is excluded, the overall trend is -12.07 DU/decade. These two values differ by less than 3% supporting the hypothesis that the Antarctic region does not make a large contribution to ozone trends within the 25º-60ºS band.

If the variability of the ozone column within a regime is small, as shown by Hudson et al. (2003) for the NH, the ozone mass within each regime, M_j, can be expressed as,

$$M_j = \bar{\Omega}_j A_j \tag{5.5}$$

with $\bar{\Omega}_j$ as the mean total ozone and A_j as the area within the *j-th* regime. Therefore, dividing eq. 5.4 by the area between 25-60ºS and substituting into eq. 5.3, the mean total ozone column within that latitude band can be written as,

$$\bar{\Omega}_a = \sum_{j=1}^{3} \bar{\Omega}_j R_j + \frac{A_{Antarctic}}{A_{25-60}} \bar{\Omega}_{Antarctic} \approx \sum_{j=1}^{3} \bar{\Omega}_j R_j \tag{5.6}$$

where the term related to the Antarctic vortex has been neglected for the reasons given above.

Equation 5.6 shows explicitly that ozone trends for the overall data can arise due to temporal changes in a regime's mean ozone column, in its spatial extension, or both.

Recalling that $\bar{\Omega}_{trop} < \bar{\Omega}_{mid} < \bar{\Omega}_{polar}$, the analysis in the previous sections suggests that the negative overall ozone trend between 1979 and 2004 is the result of two factors: 1) negative trends in total ozone within the regimes, and 2) an increase in the relative area of the tropical regime at the expense of the areas of the midlatitude and polar regimes. How robust is this conclusion?

It was mentioned previously that total ozone trends could be "contaminated" by intercalibration issues among the three instruments used to measure the ozone data

a)

1979-2004 (full model)			
	Ozone		*Rel. Area*
	DU/dec	%/dec	*%/dec*
Overall	-7.5 ± 0.7	-2.45 ± 0.25	
Polar	-7.4 ± 1.1	-2.10 ± 0.32	*-15.5 ± 2.6*
Midlatitude	-3.3 ± 0.4	-1.08 ± 0.14	*-9.8 ± 1.8*
Tropical	-3.5 ± 0.4	-1.28 ± 0.15	*16.1 ± 2.1*

b)

1/1979-5/1991 (full model)			
	Ozone		*R. Area*
	DU/dec	%/dec	*%/dec*
Overall	-9.4 ± 2.2	-3.13 ± 0.74	
Polar	-12.4 ± 3.4	-3.61 ± 0.99	*-20.8 ± 7.4*
Midlatitude	-5.4 ± 1.2	-1.79 ± 0.41	*-6.1 ± 5.0*
Tropical	-2.9 ± 1.3	-1.04 ± 0.46	*14.6 ± 6.0*

c)

1/1979-5/1991 (linear term only)			
	Ozone		*Rel. Area*
	DU/dec	%/dec	*%/dec*
Overall	-12.4 ± 2.9	-4.12 ± 0.95	
Polar	-14.6 ± 3.6 (0.54)	-4.23 ± 1.05	*-26.8 ± 8.2* (2.0)
Midlatitude	-6.6 ± 1.4 (0.36)	-2.19 ± 0.46	*-9.2 ± 5.2* (2.0)
Tropical	-4.8 ± 1.7 (0.26)	-1.74 ± 0.62	*20.6 ± 7.0* (1.7)

Table T5.6 Linear trends for two different periods of time, and two statistical models. Errors were computed at 95% confidence interval. The period Jan/79 to May/91 was chosen to compare the results with previous analyses. Numbers in parentheses are errors estimated from the Monte Carlo simulation (see text for details). Ozone is expressed in DU/decade and %/decade, whereas relative areas are only in %/decade. Baselines for these percent numbers are based on climatological values. All calculations are done within the latitudinal band of 25º to 60ºS

between 1979 and 2003. The regime relative areas, on the other hand, should not be affected by systematic biases in total ozone because the boundary values only depend on relative differences of the ozone column between the regimes. One way to avoid these intercalibration problems is to use the longest record available for a single instrument, in this case, the TOMS instrument on board the Nimbus-7 satellite. The period chosen to repeat the analysis was January 1979 to May 1991. The latter date was selected to avoid including data after the eruption of Mount Pinatubo, which introduced a large amount of aerosols into the lower stratosphere (Trepte et al., 1993; McCormick et al., 1992), which in turn contaminated the total ozone retrievals. When eq. 5.2 was applied to the ozone residuals for period mentioned above, the results showed again that the linear trends for the midlatitude and tropical regimes are much smaller than the overall trend (see table T5.6b). This is true even if a model containing only a linear term (no QBO or solar cycle terms) is applied to these residuals (table T5.6c). Therefore, despite the fact that different periods of analysis or statistical models were used to compute trends, the values displayed in Table T5.6 show a consistent pattern. Trends in the overall data and polar regime are comparable within experimental error, whereas both midlatitude and tropical trends are much smaller (approximately half). Given the fact that the relative area of the polar regime accounts, on average, for less than 20% of the area between 25º and 60ºS, the difference between trends in the overall data and the midlatitude and tropical residuals can only be explained if the contribution of each regime is taken into account, as suggested by eq. 5.6. Indeed, this is the case for all situations depicted in table T5.6. A relatively large decrease in the area of the polar regime and, more importantly, a substantial increase in the tropical regime area is observed in all cases. Trends in the

midlatitude relative areas also show a decrease, although small in proportion to the increase of the tropical regime.

In order to test if errors in the ozone boundary determination could affect the results discussed above, a Monte Carlo simulation was performed for the period 1979 through 1992. The total ozone values used to determine the regime boundaries were varied by ±25% of the ozone difference between the two regimes the boundary was related to. For example, the subtropical boundary was varied by 25% of the ozone difference between the mean values of the midlatitude and tropical regimes. The ±25% uncertainty range used for the ozone boundary in this error analysis should be considered an upper limit. In order to illustrate this, let us consider 5 September 1990. The mean ozone values within the tropical and midlatitude regimes for that day were 286 DU, and 337 DU, respectively. Therefore, the ozone subtropical boundary, 310 DU for this case, was varied by ±12.75 DU. Next, three values for each boundary were used to create 9 masks when the vortex was not present, or 27 masks when it was present, for every day of the January 1979 to May 1991 period. In order to compute the ozone and relative area monthly mean values, one of these masks was picked at random for every day of the month. New monthly values were then calculated, and the procedure was repeated until a good statistical distribution was obtained. Finally, linear trends from these monthly ozone distributions were estimated for a large number of runs (about 5000). The standard deviations of these trend distributions were about 1.8% of the mean trend for the polar regime, 2.7% for the midlatitude regime, and 2.6% for the tropical regime. Table T5.6c shows the estimated error of the linear trends at a 95% confidence interval (2σ in this case). These results suggest that the calculated total ozone trends are all statistically

a) Ozone

Season	Overall		Tropical		Midlat		Polar	
	Trend	Uncert.	Trend	Uncert.	Trend	Uncert.	Trend	Uncert.
DJF	-11.25	8.85	-3.08	5.22	-3.45	4.52	-14.97	10.11
MAM	-9.77	5.35	-3.82	3.52	-5.00	3.09	-9.95	6.68
JJA	-13.36	12.33	-5.27	8.62	-6.22	5.89	-7.46	11.67
SON	-13.72	16.31	-6.71	8.74	-9.41	6.84	-23.56	21.73

** All trends and uncertainties in DU/decade*

*** Shaded cells indicate trends that are not statistically significant*

b) Relative Areas

Season	Tropical		Midlat		Polar	
	Trend	Uncert.	Trend	Uncert.	Trend	Uncert.
DJF	29.1	22.5	-18.1	17.7	-45.2	27.7
MAM	22.4	19.1	-11.9	15.8	-34.0	19.8
JJA	23.6	30.8	-2.2	15.1	-40.3	32.7
SON	5.0	31.7	-1.0	14.2	-13.0	51.7

** All trends and uncertainties in %/decade*

*** Shaded cells indicate trends that are not statistically significant*

Table T5.7 Seasonal total ozone and relative area trends for the period of Jan/1979-May/1991. Uncertainties were calculated at a 95% confidence interval. All trends were computed for the 25º-60ºS band.

significant and that they are not very sensitive to errors in the determination of the ozone frontal boundaries. By the same token, the simulation indicates that the relative area trends are also statistically significant. Their standard deviations about the mean trends are 3.6%, 10.7%, and 4.6% for the polar, midlatitude, and tropical regimes, respectively. As in the case of ozone, the estimated errors at the 95% confidence interval are much smaller than the error of the trends estimated directly from the linear regression. This too suggests that the linear trends of the midlatitude, and tropical regimes are in fact almost half of the trends of the overall data, or polar regimes, and at the same time, the area of the tropical regime has increased with time at the expense of the areas of the other two regimes.

Finally, it is interesting to analyze the aforementioned trends by season. Table T5.7 shows total ozone and relative area trends for the period Jan/1979-May/1991, before

the eruption of Mount Pinatubo. Ozone trends are presented there in DU/decade and relative area trends in percent per decade. The uncertainties were computed at 95% confidence interval. Table T5.7a shows that the overall trends are similar, within the given uncertainties, all year round for the period of analysis. However, when the total ozone field is classified by regime, the analysis shows that the largest ozone trends occur in the spring (SON), and the smallest in summer (DJF). The exception is the polar regime, which shows a relatively large trend during summer. This result is not surprising if the presence of a strong polar vortex, where ozone is photochemically destroyed every spring (Solomon, 1999), is taken into consideration. The influence of this ozone depletion is detectable even in December, and is especially noticeable in recent years when the "ozone hole" has reached its maximum size[12]. On the other hand, relative areas show a different behavior (table T5.7b). In this case, the largest (in absolute value) trends occur in summer and the smallest in spring where none of the trends is statistically significant. It should be pointed out that the large trends observed in the polar regime, expressed in percent/decade, are misleading. In average, the polar regime covers an area equivalent to 15% of the 25-60ºS band, whereas the midlatitude and tropical areas account for approximately 45% and 40% of the band. Therefore, in absolute value these large polar relative area trends are equivalent to one-third of the observed changes in the other two regimes.

5.5 Relative Areas and Upper-level Jets

The present analysis shows that the relative area of the tropical regime has increased over the last 25 years at the expense of the midlatitude and polar regimes. Most

[12] http://toms.gsfc.nasa.gov/news/press_release_2003.html

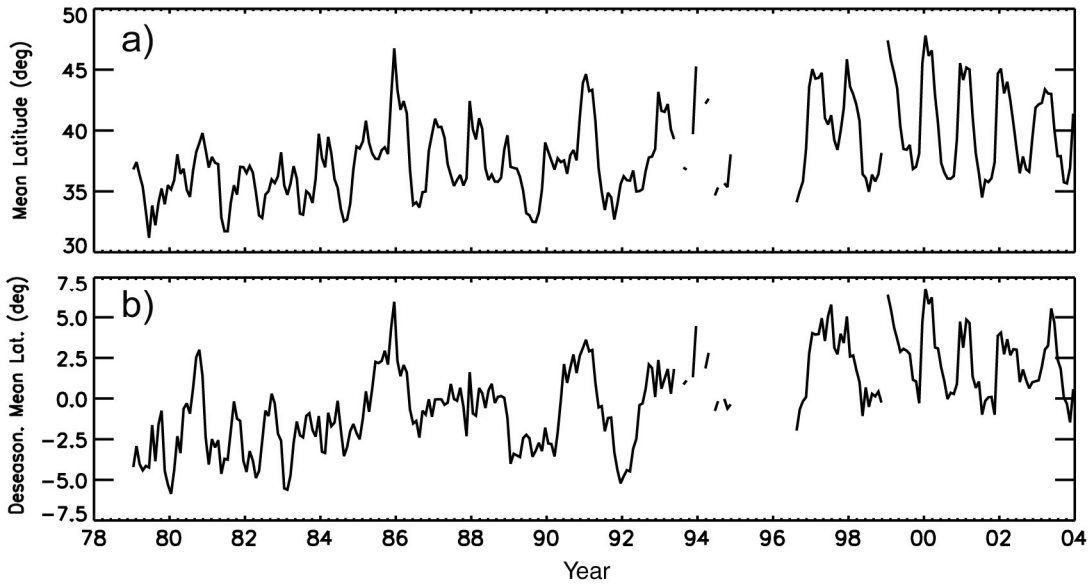

Figure 5.15 a) Monthly mean latitude of the subtropical boundary inferred from the tropical relative areas between 25º-60ºS. b) Same as in a) but the seasonality has been removed.

of these changes occurred between 1979 and 1994. Given the fact that the regimes' boundaries correspond to the location of the upper-level jets, an increase in the relative area of the tropical regime implies a shift of the mean position of the subtropical upper-level jet. The same cannot be said for the midlatitude or polar regimes because their areas are only partially covered in the band 25º-60ºS. In addition, above the upper limit (60ºS), lack of data coverage in the wintertime makes an accurate estimation of their areas difficult.

If the area of the tropical regime between 25-60ºS is equated to an equivalent-latitude of the subtropical boundary, then the monthly mean latitude of the subtropical upper-level jet can be calculated from the ozone record. Figure 5.15a shows the monthly mean latitude of the subtropical jet calculated from the monthly mean tropical relative areas (daily values of these areas are displayed in Figure 5.9). As expected, there is a seasonal dependence with the jet relatively close to the South Pole in summer and further

north in winter. After the seasonal component is removed, a positive trend is even more apparent in the data (figure 5.15b). When a statistical model of the form of eq. 5.2 is applied to the data, a linear trend of 2.1±0.3 degrees/decade is found. The reliability and robustness of this result is intimately related to the reliability and robustness with which the relative areas are determined. Because trends in the latter were statistically significant, the estimated linear trend for the mean position of the tropical jet is also to be statistically significant. In addition, this trend does not seem to be extremely sensitive to errors in the daily determination of the ozone boundaries, as shown by the previous analysis, or to any small long-term drift in the instruments.

6. CONCLUSIONS AND FUTURE WORK

6.1 Conclusions

The preceding sections have shown that the Southern Hemisphere total ozone field can be classified by meteorological regimes in a similar way as the Northern Hemisphere total ozone field (Hudson et al., 2003). The validation, however, is much more difficult in the Southern Hemisphere due to scarcity of ground based measurements. This scarcity also contributes to larger uncertainties in satellite retrievals than in the NH case. In spite of this problem, monthly means of rawinsonde and ozone profiles have shown that the classification is working correctly. That is, mean ozone and tropopause height show very clear distinct values within each regime, as in the case of the Northern Hemisphere (Hudson et al., 2003). Temperature and ozone profiles are also clearly distinct within each regime. Using data for the Northern Hemisphere, a more in-depth analysis of ozone and water vapor showed that these differences are not an artifact induced by any latitude dependence that these elements might have, but on the contrary, they are a manifestation of distinct physical attributes of each regime (Follette et al., 2004). This conclusion is reinforced by the fact that, despite the large latitudinal range covered by every regime, the shape of the temperature profiles within each regime is almost constant, and changes abruptly only when a boundary region is crossed.

In addition, analysis of 200 mb and 300 mb winds from the reanalysis data showed that the regime's boundary regions, obtained from total ozone, outline regions with the highest winds. It should be noted, however, that these high wind regions do not extend continuously across the globe, but they are confined to relatively small regions of the upper troposphere. The total ozone boundaries, on the contrary, not only mark regions

of high winds, but also regions where winds are relatively weak. Nonetheless, regions where winds are weak do in fact correspond to regions where ozone gradients are also weak as suggested by Shapiro et al. (1982).

Temporal behavior of both total ozone and relative area were analyzed for each regime for the period 1979-2004. The statistical analysis showed that the solar flux and QBO have large influence on the regimes' total ozone and their corresponding relative areas. This influence, however, is not the same over all regimes. As a result, the observed anomalies in the overall data are not only influenced by the solar cycle and the QBO, but they are strongly affected by the contribution of each regime as well. These contributions vary in time, and therefore the understanding of their behavior is important in order for long-term trends of ozone to be estimated correctly.

The statistical analysis also revealed that total ozone linear trends within the meteorological regimes are smaller than the linear trend in the overall data. This is true whether the QBO and the solar cycle are taken into consideration in the statistical model, or only a linear term is used for the regression. In order to reconcile this apparent paradox, the contribution of each regime to the overall data should be considered. Trends in relative areas indicate a statistically significant increase of the tropical area for the 25º-60ºS band between 1979 and 2004, although most of this change occurred between 1984 and 1994. The data also shows negative trends for the midlatitude and polar relative areas during the same period. Recalling that total ozone is smaller within the tropical regime than in the midlatitude or polar regime, an increase of its area will produce a negative trend in the overall data, even if there are no negative trends within the regimes. Therefore, the observed difference between the total ozone trends within the

meteorological regimes and the overall data can be accounted for by trends in the regime relative areas.

The results presented here cannot be directly compared with previous studies because none of these have classified ozone by meteorological regime. Overall trends, however, have been studied extensively in the past (Stolarski et al., 1992, WMO, 1999; Staehelin et al., 2001, Fioletov et al., 2002). Using ground based and satellite information, those studies found trends of about -4.5%/decade for the period January/1979 to May/1991 when a model with only a linear trend was applied (WMO, 1995), and about -2.9%/decade when the solar cycle and the QBO were taken into account in the statistical model (WMO, 1999). Fioletov et al. (2002) reported a trend of -2.3±0.9 %/decade between January /1979-December/2000 for a latitudinal band of 35º-60ºS and a statistical model that included the QBO and the solar cycle. Although a different version of TOMS data was used for this analysis, the overall trends reported here (table T5.6) agree well with those computed previously. This essentially indicates that the results do not rely on the retrieval algorithm, and the features displayed by total ozone within the regimes are not an artifact of the data.

The accuracy and robustness of the regime trends calculated in Chapter 5 are clearly tied to the accuracy and precision with which the regime boundaries were determined. These boundaries, calculated independently for each day, were computed with a precision of 5 DU. Sensitivity analysis showed that these values are almost independent, within the experimental error, of the limits of the latitudinal band, or the isentropic surface used to determine the polar vortex. Despite this, a Monte Carlo simulation was carried out to study the sensitivity of the total ozone and relative area

trends to errors in the determination of the boundary values. The analysis demonstrated that even if the errors of the boundary values were larger than those calculated in Chapter 3, the reported trends will still be precise. Therefore, the results presented in Chapter five, notably the positive trend of the tropical relative area between 25º-60ºS, and the smaller ozone trends for each regime than the overall data, are reliable results.

A positive trend in the tropical relative areas implies a shift in the mean position of the ozone subtropical boundary. In fact, it was shown that if the tropical area was equated to a mean latitude, the mean position of the subtropical boundary shifted by 2.1±0.3% /decade in the last 25 years. Because this boundary delineates the location of the upper level jets, a shift in the location of regions of maximum winds in the upper troposphere should be expected. Despite the clear and robust results from total ozone data, no other direct evidence of this shift, at global or regional scale, has been reported for the Southern Hemisphere.

A similar poleward migration of the subtropical boundary has been observed in the Northern Hemisphere (Hudson et al., 2004). In this case, however, there is indirect evidence that backs these findings. McCabe et al. (2001) have found that in the Northern Hemisphere the winter extratropical cyclone frequency has increased at high latitudes and decreased in mid-latitudes between 1959 and 1997. In addition, they found that the intensity of these cyclones has increased in both the high and mid-latitudes. Because it is necessary to have the presence of upper level jets aloft for these extratropical cyclones to occur (Djuric, 1994; Bluestein, 1993), this change in cyclone frequency and intensity at those latitudes suggests a poleward migration of the storm tracks and therefore of the mean position of the upper level jets.

Additionally, Hood et al. (1999) have shown that an increase of anticyclonic, poleward, Rossby wave breaking events that transport low PV, ozone-poor air from the subtropics into higher latitudes have occurred for the period 1979-1998. This behavior seems to be responsible for the increase in the number of days with very low ozone in the extratropical Northern Hemisphere winter (Bronnimann and Hood, 2003). This fact is consistent with poleward migration of the ozone subtropical boundary. Hood et al. (1999) and Bronnimann and Hood (2003) suggested that changes in the atmospheric circulation strongly contributed to the mentioned changes in the Northern Hemisphere. In this sense, changes in the mean position of the subtropical boundary, and by the same token the polar boundary, can be ascribed to changes in the general circulation of the atmosphere.

From the previous discussion, the approximately 5-degree poleward migration of the ozone subtropical boundary observed between 1979 and 2004 could be detected by observing changes in the mean position of the storm tracks and/or increase in the number of intrusions of tropical air into mid-latitude and polar regions. In actual fact, the poleward migration of ozone boundaries is probably the result of contributions from two factors: one being the intrusions of low ozone into higher latitudes, and the other being changes in mean latitude of the storm tracks. Therefore, the reported 5-degree change in the mean position of the subtropical boundary, most likely translates in a smaller shift in the mean position of the upper-level jets, making its detection much more difficult.

Due to the small interannual variability of the boundary values, it could be argued that total ozone trends induced by chemical processes alone, such as those suggested by Solomon (1999), could produce a poleward migration of ozone isopleths without producing changes in the mean position of the upper level jets, or indicating an

increase in the number of poleward tropical air intrusions. In order to see that this is not happening in our case, that is, that the observed trends in relative areas are not an artifact of the data, it should be recalled that the boundary values are computed independently on a daily basis, and that the method makes use of the relative differences in the total ozone data (spatial gradients) in order to define the regime boundaries. Therefore, even if changes in ozone abundance due to chemistry processes does happen, the procedure used to compute the boundaries will still place the boundaries in almost the same spatial location, although this location might be indicated by a different total ozone isopleth. In other words, it should be expected that ozone will still act as a dynamical tracer, even if long-term chemical changes in ozone are occurring. This is true even for the case when slow transport processes in the stratosphere take place, i.e. seasonal changes in the Brewer-Dobson circulation.

A similar argument could be used in the case of temporal drift in the response of the instruments, or the use of more than one instrument in the period of study, which can produce artificial trends in ozone. In the case of TOMS instruments, however, studies of the long-term trends using these instruments (Jaross et al., 2003) showed that when TOMS data is combined without relative adjustments, the trend uncertainty is slightly less than 1%/decade. This small (and presumably slow) change in the retrieved ozone due to instrumental uncertainties is not likely to affect the detection of the regime boundaries. It could, in any case, affect the precision with which total ozone trends within the regimes are estimated, but should not affect trends in the relative areas. Therefore, eq. 5.6 still requires an increase of the tropical relative areas in order to reconcile the observed trends in total ozone, as proved by the analysis.

6.2 Future work

Despite the robustness of the results presented here, there is always more work to be done in order to improve the reliability of the method described here. For example, rawinsonde data for only one year was used to validate the ozone classification. Because the rawinsondes are direct measurements, this data set was the most robust and conclusive test of the ozone classification. For this reason, a more extensive validation would be important. This validation would be especially important for periods where total ozone retrievals could have suffered from interferences due to aerosol loading, as the one produced by the eruption of Mount Pinatubo, or events of strong tropospheric pollution, as those produced by biomass burning.

In addition, the use of independent data sets to validate the results presented here would also be important. The natural choice to do this seems to be the reanalysis data. However, preliminary analysis using MPV or PV on isentropic surfaces showed larger trends in ozone and smaller trends in relative area. The problem in those cases is that either the isentropic surface or the pressure levels to integrate PV were kept constant during the period of analysis. If changes in the upper-troposphere or lower stratosphere were taking place between 1979 and 2004, it would be expected that those assumptions were not necessarily correct. In any case, the fact that the spatial correlation between MPV and total ozone is very high on the daily basis, suggests that more in-depth analysis could be worthwhile in order to gain more insight and validate the conclusions discussed above.

Because temperature and ozone profiles show little variability within each regime, a relatively small number of profiles would be needed in order to compute reliable

climatological profiles within each regime. This is especially important in the Southern Hemisphere where ground based measurements are much more scarce than in the Northern Hemisphere. On the same note, this also could help in getting better intercomparisons between satellite and ground based instruments, and therefore improving the validation of satellite data.

Finally, the regime boundaries, computed from total ozone, can be used as a diagnostic tool for weather analysis given their ability to locate the upper-level jets. Improvements in the reanalysis products and forecast models could be a result of incorporating this information.

APPENDIX A

The Total Ozone Mapping Spectrometer (TOMS) instrument[a]

1. Introduction

Since November 1978 four Total Ozone Mapping Spectrometer (TOMS) instruments have been launched successfully. The first was flown on board the Nimbus-7 satellite and provided data from 1 November 1978 to 5 May 1993. The second was carried by the Russian satellite Meteor-3 and operated between 15 August 1991 and 27 December 1994. A third TOMS instrument was flown on the Japanese satellite ADEOS which was launched on 17 August 1996, and measured the ozone column from 11 September 1996 to 29 June 1997. The last successfully launched TOMS instrument is being flown on the Earth Probe (EP) satellite. This satellite was launched on 2 July 1996, and the instrument began providing ozone data on 25 July 1996. Due to the short duration and time overlap with EP-TOMS, data from ADEOS-TOMS was not used in this thesis.

Almost all of the TOMS instruments had a polar sun-synchronous orbit with a equator crossing time close to the local noon. The exception was Meteor-3-TOMS whose orbit precessed relative to the Earth-Sun line with a period of 212 days. The altitude of the orbit is different for each instrument. The lowest altitude corresponds to EP-TOMS which at the beginning was flying at 495 km, but its orbit was lifted to 739 km in December 1997 in order to improve spatial coverage. The nominal crossing times, as well as inclinations, and altitudes are shown in table TA.1.

[a] Extracted from McPeters et al. (1996), Herman et al. (1996), Krueger et al. (1998), McPeters et al. (1998), and Barthia et al. (2004).

Satellite	Began	Ended	Altitude (km)	Inclination (degrees)	Equator crossing time (Local noon)	Orbital period (min)
Nimbus-7	01-Nov-78	05-May-93	995	104.9	12:00	104
Meteor-3	15-Aug-91	27-Dec-94	1200	82.5		109
ADEOS	11-Sep-96	29-Jun-97	800	98.6	10:30±15	101
Earth Probe	25-Jul-96		739*	98.4	11:15±0:15	100

** Altitude at launch time was 495 km*

Table TA.1 General information of satellites flying TOMS instruments.

The TOMS instruments scan along a line perpendicular to the orbital plane in three-degree steps to collect a total of 35 samples. In a single cycle, the first sample is collected at 51º with respect to the direction of flight on one side of the aircraft, and the last at 51º on the other side of the aircraft. After taking the last sample, the scanning mirror quickly returns to the first position, not making measurements on the retrace, and then another scan begins. Every cycle takes approximately eight seconds. The measurements used for ozone retrieval are made during the sunlit portions of the orbit.

The backscattered solar ultraviolet radiation is collected through a slit that produces an instantaneous field-of-view (IFOV) of 3 x 3 degrees. This IFOV results in a footprint varying approximately from a 50 km x 50 km square at nadir to a 125 km x 280 km diamond at the scan extremes. The projections of the IFOV on the Earth's surface for the two different altitudes of Earth Probe-TOMS are shown in figure A.1. In this particular case, at its final height of 739 km, the projected area is about 42 km x 42 km at nadir and about 210 km x 80 km at the scan extremes. With the higher orbit the spatial resolution of the pixels is smaller, but global coverage is better.

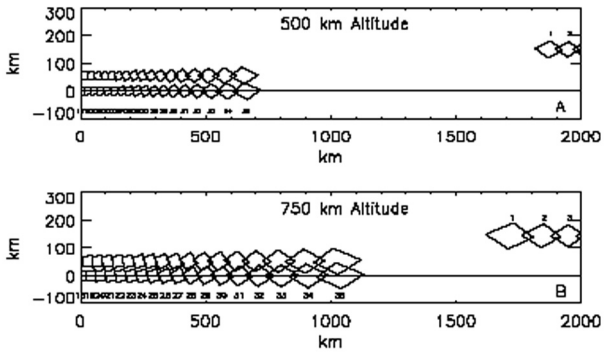

Figure A.1 Spatial footprint for two different satellite altitudes.

The total swath width varies between 2000 and 3000 km depending on the satellite altitude. In the case of Nimbus-7 and Meteor-3, their orbits are at enough altitude to provide equatorial interorbit overlap, producing in this way a continuous mapping of total ozone data. EP-TOMS swaths, on the other hand, do not overlap in the equatorial region leaving areas with no data in the tropics.

2. Instrument

The TOMS instruments use a single, fixed monochromator which resolves the incoming light into six wavelengths (table TA.2). The latest version of the algorithm, version 8, uses only two wavelengths (317.5 and 331.2 nm) to derive total ozone. The other four wavelengths are used for diagnostics and error correction. Version 7, on the other hand, used the shortest four wavelengths to infer ozone, and the longest two (which are not sensitive to ozone absorption) to estimate the effective reflectivity which accounts for the combined influence of the Earth's surface, clouds, and aerosols.

Nimbus-7	Meteor-3	ADEOS	Earth-Probe
312.34	312.35	308.68	308.60
317.35	317.40	312.59	313.50
331.06	331.13	317.61	317.50
339.66	339.73	322.40	322.30
359.88	360.00	331.31	331.20
379.95	380.16	360.11	360.40

Table TA.2 Waveleghts used for different TOMS instruments.

Figure A.2 shows a schematic of the TOMS instruments. The scan and transfer mirrors direct the incoming light into a depolarizer. The exiting light goes then through the objective lens and the entrance slit in order to produce a quasi-parallel beam. A collimating mirror reflects this beam to a fixed grating that spectrally decomposes and reflects back the incoming radiation. The collimating mirror reflects the now monochromatic radiation towards the exit slit array, and finally the optic array directs it into a photomultiplier tube. It is interesting to note that both the entrance and exit slit

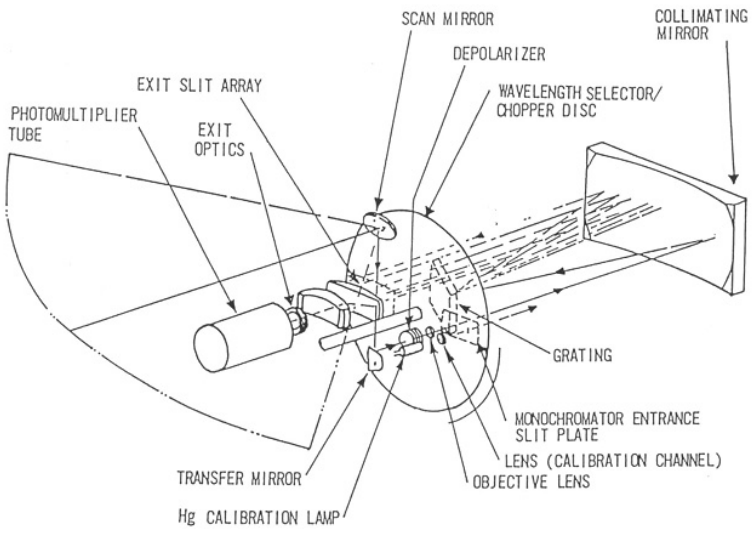

Figure A.2 Schematic of a TOMS instrument (from GSFC, 1992).

arrays are mounted onto a rotating chopperwheel. The slits are located at different distances from its center in order to transmit only the desired wavelength.

An Hg lamp is used for in-flight wavelength calibration. Radiometric calibration, on the other hand, use the Sun as reference. In this case, the scan mirror reflects incident solar irradiance onto a diffuser plate. This device fills the whole IFOV of the spectrometer, and reduces the intensity of the incoming direct solar irradiance by about 96% in order to avoid saturation and damage of the instrument. Degradation of the reflectivity of the only diffuser on the Nimbus7-TOMS , led to improvements in the design of the instrument. EP-TOMS, for example, has three diffuser plates. The rate at which they are exposed to solar irradiance is different allowing calibration by examining the differences in degradation.

3. Algorithm

In order to derive the Earth's total ozone column, the concept of differential absorption is applied to measurements from backscattered ultraviolet (UV) radiation. The

basic idea is to sample regions of the spectral band where ozone is absorbed strongly, and regions where is not. In practice, the TOMS retrieval algorithm makes use of a radiative forward model and an inversion algorithm to calculate the Earth's column ozone from backscattered Earth radiance measurements at the top of the atmosphere (TOA). The forward model estimates the intensity of the backscattered solar UV radiation at the TOA given a set of geometric and atmospheric conditions. The inversion model makes use of these results and the measured radiances to estimate the ozone column.

All versions of the TOMS algorithm make two key assumptions about the nature of the backscattered UV radiation: a) wavelengths greater than 310 nm are primarily a function of total ozone amount, with only a weak dependence on the ozone profile that can be accounted for using a set of standard profiles; b) clouds, aerosols, and surfaces can be treated as Lambertian reflectors whose spectral dependence on backscattered UV radiation can be accounted in a simple radiative transfer model.

Forward model

The base of the TOMS algorithm, called TOMRAD, is an improved version of a radiative transfer model developed in 1964. This code accounts for all orders of scattering in a pseudo-spherical atmosphere, as well as the effects of polarization. Although the code is limited to Rayleigh scattering, and can handle only reflection by Lambertian surfaces, the computed radiances are fairly accurate.

TOMRAD calculates the radiance, *I*, at the top of the atmosphere using the following equation,

$$I = I_0(\theta_0, \theta) + I_1(\theta_0, \theta)\cos\phi + I_2(\theta_0, \theta)\cos 2\phi + \frac{RI_R(\theta_0, \theta)}{1 - RS_b} \qquad \text{(A.1)}$$

where, θ_0 is the solar zenith angle, θ is the satellite zenith angle, ϕ is the relative azimuth angle between the plane containing the sun and local nadir at the viewing location and the plane containing the satellite and local nadir, R is the effective reflectivity of the surface, I_R the incident radiation to that surface, and $(1-RS_b)^{-1}$ accounts for multiple reflections between the surface and the overlying atmosphere. The first three terms on the right-hand side of eq. A.1 represent the purely atmospheric component of the radiance, unaffected by the surface. The last term represents the surface contribution.

In order to compute these radiances, the terrain pressure, cloud top pressure, and climatological temperature and ozone profiles are needed. The terrain pressure is obtained by converting a standard terrain height data base using the US standard temperature profiles. A cloud top height climatology has been produced using the coincident measurements of TOMS and the Temperature Humidity Infrared Radiometer (THIR) both on board Nimbus-7. Using all this information as input, look-up tables of the radiances are computed for 10 solar zenith angles and 6 satellite zenith angles selected to reduce errors due to the interpolation processes.

Inversion algorithm

Total ozone is retrieved by the inversion algorithm following a 3-step procedure:

1) A first guess of the effective reflectivity and total ozone are computed using the 21 standard profile radiance tables and the measured radiance to irradiance ratios at 317.5 nm and 331.2 nm.
2) The first guess is corrected by using seasonally and latitudinally varying ozone and temperature climatologies.

3) The differences between measured and computed radiances for the longest four wavelengths are used to estimate pixels containing large amounts of aerosols, sea glint, volcanic SO_2, or with unusual ozone profiles.

Errors

The ozone values derived from the radiances measured by TOMS have errors produced by several sources: a) instrumental errors that directly affect the radiance measurements; b) errors in the values of input physical quantities obtained from laboratory measurements that affect the model calculations; c) errors in the parameterization of atmospheric properties used as input to the radiative transfer computations; and d) limitations in the representation of the physical processes that occur in the atmosphere.

Errors of type b) and d) are mainly associated with the forward model, for example, spectroscopic constants, while c) type errors are related to the inversion model, for example temperature and ozone profiles. Instrumental errors affect both the forward and the inversion model.

The estimated rms error of the total ozone retrieved from TOMS measurements is thought to be of the order of 2%. These errors, however, are not necessarily randomly distributed over the globe. They increase with solar zenith angle and in presence of heavy aerosol loading.

REFERENCES

Allaart, M. A. F., H. Kelder, L. C. Heijboer, On the relation between ozone and potential vorticity, *Geophys. Res. Lett*., **20**, 811-814, 1993.

Andrews, D. G., J. R. Holton, and C. B. Leovy, *Middle Atmospheric Dynamics*, 489 pp, Academic Press, 1987.

Barry, R.G., and R.J. Chorley, *Atmosphere, Weather & Climate*, 392 pp, Routhledge, 1992.

Beekmann M., G. Ancellet, and G. Mégie, Climatology of tropospheric ozone in southern Europe and its relation to potential vorticity, *J. Geophys. Res.*, **99**, 12841-12853, 1994.

Bethan S., G. Vaughan, and S.J. Reid, A comparison of ozone and thermal tropopause heights and the impact of tropopause definition on quantifying the ozone content on the troposphere, *Quart. J. Roy. Meteor. Soc.,* **122,** 929-944, 1996.

Bluestein, H. B., *Synoptic-Dynamic Meteorology in Midlatitudes:Vol II*, 594 pp, Oxford Univ. Press, 1993.

Brasseur, G., and S. Solomon, *Aeronomy of the Middle Atmosphere*, 441 pp, Reidel Norwell, 1984.

Brewer, A. W., Evidence for a world circulation provided by measurements of helium and water vapour distribution in the stratosphere. *Quart. J. Roy. Meteorol. Soc.*, **75**, 351-363, 1949.

Bronnimann S., and L. Hood, Frequency of low-ozone events over northwestern Europe in 1952-1963 and 1990-2000, *Geophys. Res. Lett*., **30**, doi:10.1029/2003GL018431, 1996.

Chu, W.P., M. P. McCormick, J. Lenoble, C. Brogniez, and P. Pruvost, SAGE II inversion algorithm, *J. Geophys. Res.*, **94**, 8339-8351, 1989.

Dameris, M., D. Nodorp, and R. Sausen, Correlation between tropopause height pressure and TOMS-data for the EASOE-winter 1991/1992, *Contributions to Atmospheric Physics*, **68**, 227-232, 1995.

Danielsen, E. F., Stratospheric-Tropospheric exchange based on radioactivity, Ozone and potential vorticity, *J. Atmos. Sci.*, **25**, 502-518, 1968.

Danielsen, E.F., R. Bleck, J.P. Shedlovsky, A. Wartburg, P. Haagenson, and W. Pollack, Observed distribution of radioactivity, ozone and potential vorticity associated with tropopause folding, *J. Geophys. Res.*, **75**, 2353-2361, 1970.

Danielsen, E. F., Ozone transport, in *Ozone in the free atmosphere*, edited by R.C.Whitten and S.S. Prasad, pp.123-159, Van Nostrand Reinhold Company Inc., 1985.

Danielsen, E. F., Hipskind R. S., Gaines S.E., Sachse G.W., Gregory G. L., and Hill G. F., Three-Dimensional Analysis of Potential Vorticity Associated with Tropopause Folds and Observed Variations of Ozone and Carbon Monoxide, *J. Geophys. Res.*, **92**, 2103-2111, 1987.

Davis, C., S. Low-Nam, M.A. Shapiro, X. Zou, and A.J. Krueger, Retrieval of wind from Total Ozone Mapping Spectrometer (TOMS) data: Examples from FASTEX, *Quart. J. Roy. Meteor. Soc.,* **125,** 3375-3391, 1999.

DeLand, M. T., and R. P. Cebula, The composite Mg II solar activity index for solar cycles 21 and 22, *J. Geophys. Res.*, **98**, 12809-12823, 1993.

Dessler, A., *The Chemistry and Physics of Stratospheric Ozone,* 214 pp, Academic Press, 2000.

Djuric, D., *Weather Analysis*, 304 pp, Prentice Hall, 1994.

Dobson, G. M. B., D. N. Harrison, and J. Lawrence, Measurements of the amount of ozone in the Earth's atmosphere and its relation to other geophysical conditions-Part II, *Proc. Roy. Soc. London,* **A114**, 521-541, 1927.

Dobson, G. M. B., Origin and distribution of the polyatomic molecules in the atmosphere. *Proc. Roy. Soc. London,* **236A,** 187–193, 1956.

Dobson, G. M. B., Forty Year's Research on Atmospheric Ozone at Oxford: a History, *Applied Optics*, **7** 387-405, 1968a.

Dobson, G. M. B., *Exploring the atmosphere*, 188 pp, Clarendon Press, 1968b.

Finlayson-Pitts, B.J., and J.N. Pitts, Jr. , *Atmospheric Chemistry: Fundamentals and Experimental Techniques***,** 969pp, Academic Press, 1999.

Fioletov, V. E., G. E. Bodeker, A. J. Miller, R. D. McPeters, and R. Stolarski, Global and zonal total ozone variations estimated from ground-based and satellite measurements: 1964–2000, *J. Geophys. Res.*, **107**(D22), 4647,doi:10.1029/2001JD001350, 2002.

Follette, M. B., R. D. Hudson, and M. F. Andrade, Classification of HALOE data by meteorological regime, *Proc. Quadrennial Ozone Symposium*, edited by Christos S. Zerefos, 336-337, University of Athens, 2004.

Galliani A., Siani A. M., N. J. Muthama, S. Palmieri, Synptic-scale fluctuations of total ozone in the atmosphere, *Annales Geophysicae*, **14**, 1044-1050, 1996.

GSFC, TOMS-M-1005, *Project Description for Meteor 3/TOMS*, National Aeronautics and Space Administration, Goddard Space Flight Center Greenbelt, Maryland 20771, 1992.

Haynes, P. H., and M. E. McIntyre, On the Conservation and Impermeability Theorems for Potential Vorticity. *J. Atmos. Sci.*, **47**, 2021–2031, 1990.

Heath, D. F., and B. M. Schelesinger, The Mg-280 nm doublet as a monitor of changes in solar ultraviolet irradiance, *J. Geophys. Res*., **91**, 8672-8682, 1997.

Herman, J. R., P.K. Bhartia, A.J. Krueger, McPeters, C.G. Wellemeyer, C.J. Seftor, G. Jaross, R. D., B.Schlesinger, O. Torres, G. Labow, W. Byerly, S.L. Taylor, T. Swissler, R.P. Cebula, and Xiao-Yue Gu, *Meteor-3 Total Ozone Mapping Spectrometer (TOMS) Data Products User's Guide*, NASA, National Aeronautics and Space Administration, Goddard Space Flight Center Greenbelt, Maryland 20771, 1996.

Hoerling, M. P., T.K. Schaack, and A. J. Lenzen, Global objective tropopause analysis, *Mon. Wea. Rev.*, **119**, 1816-1831, 1991.

Hoinka, K. P., H. Claude and U. Kohler, On the correlation between tropopause pressure and ozone above Central Europe, *Geophys. Res. Lett*., **23**, 1753-1756, 1996.

Hoinka, K. P., The tropopause: discovery, definition and demarcation, Meteorol. Zeitschrift., N.F. **6**, 281-303, 1997.

Hollandsworth, S. M., K. P. Bowman, and R. D. McPeters, Observational study of the quasi-biennial oscillation in ozone, *J. Geophys. Res.*, **100**, 7347-7361, 1995.

Holton, J. R., P. H. Haynes, M. E. McIntyre, A. R. Douglass, R. B. Rood, and L. Pfister, Stratosphere-troposphere exchange, *Reviews of Geophysics*, 33, 403-439, 1995.

Hoskins, B. J., M. E. McIntyre, and A. W. Robertson, On the use and significance of isentropic potential vorticity maps. *Quart. J. Roy. Meteor. Soc.,* **111,** 877–946, 1985.

Hoskins, B. J., Towards a PV-θ view of the general circulation, *Tellus*, **43** AB, 27-35, 1991.

Hsu, N. C., R. D.McPeters, C.J. Seftor, and A. Thompson, Effect of an improved cloud climatology on the total ozone mapping spectrometer total ozone retrieval, *J. Geophys. Res*., **102**, 4247-4255, 1997.

Hood L., S. Rossi, and M. Beulen, Trends in lower stratospheric zonal winds, Rossby wave breaking behavior, and column ozone at northern midlatitudes, *J. Geophys. Res*., **104**, 24321-24339, 1999.

Hudson R.D., and A. Frolov, Separation of Total Ozone by Meteorological Regime. *Proc. of the Quadrennial Ozone Symposium,* 1-2, 2000.

Hudson, R D., Frolov, A. D., Andrade, M. F., Follette, M. B., The total ozone field separated into meteorological regimes. Part I: Defining the regimes. *J. Atmos. Sci,* **60**, 1669–1677, 2003.

James, I. N., *Introduction to Circulating Atmospheres*, 422 pp, Cambridge University Press, 1994.

Jaross G., S. L. Taylor, C. G. Wellemeyer, R. P. Cebula, L.-K. Huang, R.S. Stolarski, and R.D. McPeters, An assessment of long-term ozone trend uncertainties using Total Ozone Mapping Spectrometers (TOMS), *Int. J. Remote Sensing*, **24**, 329-338, 2003.

Kalnay, E., M. Kanamitsu, R. Kistler, W. Collins, D. Deaven, L. Gandin, M. Iredell, S. Saha, G. White, J. Woollen, Y. Zhu, A. Leetmaa, R. Reynolds, M. Chelliah, W. Ebisuzaki, W.Higgins, J. Janowiak, K. C. Mo, C. Ropelewski, J. Wang, R. Jenne, and D. Joseph, The NCEP/NCAR 40-year reanalysis project, *Bull. Am. Meteorol. Soc*., **77**, 437-471, 1996.

Karol, I. L., L. P. Klyagina, A. D. Frolov, and A. M. Shalamyanskiy, Fields of ozone and temperature within the boundaries of air masses, *Meteorologiya i Gidrologiya*, **10**, 47-52, 1987.

Karoly, D., D. G. Vincent, and J. M. Schrage, General Circulation, *Meteorology of the Southern Hemisphere*, D. Karoly and D. G. Vincent Eds. AMS, 1998.

Keyser, D. and M. A. Shapiro, A Review of the Structure and Dynamics of Upper-Level Frontal Zones. *Mon. Wea. Rev.*, **114**, 452–499, 1986.

Kistler, R., E. Kalnay, W. Collins, S. Saha, G. White, J. Woollen, M. Chelliah, W. Ebisuzaki, M. Kanamitsu, V. Kousky, H. van den Dool, R. Jenne, and M. Fiorino, The NCEP/NCAR 50-year reanalysis:Monthly means CD-ROM and documentation, *Bull. Am. Meteorol. Soc*., **82**, 247-267, 2001.

Krueger A.J., P.K. Bhartia, R.D. McPeters, J.R. Herman, C.G. Wellemeyer, G. Jaross, C.J. Seftor, O. Torres, G. Labow, W. Byerly, S.L. Taylor, T. Swissler, and R.P. Cebula, *ADEOS Total Ozone Mapping Spectrometer (TOMS) Data Product User's Guide*, NASA, National Aeronautics and Space Administration, Goddard Space Flight Center Greenbelt, Maryland 20771, 1998.

McCabe GJ, Clark, MP, Serreze MC: Trends in Northern Hemisphere Surface Cyclone Frequency and Intensity. *J. Climate*, **12**, 2763-2768, 2001.

McCormack, J. P., and L. L. Hood, Apparent solar cycle variations of upper stratospheric ozone and temperature: Latitude and seasonal dependences, *J. Geophys. Res*., **101**, 20933-20944, 1996.

McCormick, M.P., R.E. Veiga, SAGE II measurements of early Pinatubo aerosols, *Geophys. Res. Lett*., **19**,155-158, 1992.

McIntyre, M. E., On the Antarctic ozone hole. *J. Atmos. Terr. Phys.*, **51**, 29-43, 1989.

McPeters, R. D., P.K. Bhartia, A.J. Krueger, J.R. Herman, B.Schlesinger, C.G. Wellemeyer, C.J. Seftor, G. Jaross, S.L. Taylor, T. Swissler, O. Torres, G. Labow, W. Byerly, and R.P. Cebula, *Nimbus–7 Total Ozone Mapping Spectrometer (TOMS) Data Products User's Guide*, NASA Ref. Publ. 1384, National Aeronautics and Space Administration, , Goddard Space Flight Center Greenbelt, Maryland 20771, 1996.

McPeters, R. D., P.K. Bhartia, A.J. Krueger, J.R. Herman, C.G. Wellemeyer, C.J. Seftor, G. Jaross, O. Torres, G. Labow, W. Byerly, S.L. Taylor, T. Swissler, and R.P. Cebula, *Earth Probe Total Ozone Mapping Spectrometer (TOMS) Data Product User's Guide*, NASA, National Aeronautics and Space Administration, , Goddard Space Flight Center Greenbelt, Maryland 20771, 1998.

Morgan, M.C., and J. Nielsen-Gammon, Using Tropopause Maps to Diagnose Midlatitude Weather Systems, *Mon. Wea. Rev.*, **126**, 2555-2579, 1998.

Nash, E.R., P.A. Newman, J.E. Rosenfield, and M.R. Schoeberl, An objective determination of the polar vortex using Ertel's potential vorticity, *J. Geophys. Res.*, **101**, 9471-9478, 1996.

Newchurch, M. J., X. Liu, J. H. Kim, and P. K. Barthia, On the accuracy of total ozone mapping spectrometer retrievals over tropical cloudy regions, *J. Geophys. Res.*, **106**, 32315-32326, 2001.

Petzoldt, K., B. Naujokat, and K. Neugebohren, Correlation between stratospheric temperature, total ozone, and tropospheric weather systems, *Geophys. Res. Lett.*., **21**, 1203-1206, 1994.

Planet, W.G., D.S. Crosby, J.H. Lienisch, and M.L. Hill, Determination of Total Ozone Amount from TIROS Radiances Measurements, *J. Clim. Appl. Meteorol.*, **23**, 308-316, 1984.

Rao, T. N., S. Kirkwood, J. Arvelius, P. von der Gathen, and R. Kivi, Climatology of UTLS ozone and the ratio of ozone and potential vorticity over northern Europe, *J. Geophys. Res*., **108(D22)**, 4703, doi:10.1029/2003JD003860, 2003.

Reed, R. J., The role of vertical motions in ozone-weather relationships, *J. Meteorol*., **7**, 263–267, 1950.

Reed R. J., A study of a characteristic type of upper-level frontogenesis, *J. Atmos. Sci.*, **12**, 226-237, 1955.

Reed R. J., and E. F. Danielsen, Fronts in the vicinity of the tropopause, *Arch. Meteor. Geophys. Bioklam.*, **A11**, 1-17, 1959.

Reed, R. J., and B. A. Kunkel, The Arctic circulation in summer. *J. Meteor.*, **17**, 489-506, 1960.

Reichler, T., M. Dameris, R. Sausen and D. Nodorp, A global climatology of the tropopause height based on ECMWF-analyses, DLR Oberpfaffenhofen, Institute of atmospheric physics, 57, ISSN 0943-4771, 23 pp, 1996.

Riishøjgaard, L.P. and E. Källén, On the correlation between ozone and potential vorticity for large-scale Rossby waves, *J. Geophys. Res*., **102**, 8793-8804, 1997.

Salby M.L. and P.F. Callaghan, Fluctuations of Total Ozone and Their Relationship to Stratospheric Air Motions, *J. Geophys. Res.*, **98**, 2715-2727, 1993.

Schoeberl, M. R., L. R. Lait, P. A. Newman, and J. E. Rosenfield, The structure of the polar vortex, *J. Geophys. Res.*, **97**, 7859-7882, 1992.

Schoeberl, M. R., and A. J. Krueger, Medium Scale Disturbances in Total Ozone During Southern Hemisphere Summer, *Bull. Amer. Meteor. Soc.*, **64**, 1358-1365, 1983.

Schubert, S. D., and M.J. Munteanu, An Analysis of Tropopause Pressure and Total Ozone Correlations, *Mon. Wea. Rev.*, **116**, 570-582, 1988.

Serreze, M., A. H. Lynch, and M. P. Clark, The Arctic Frontal Zone as seen in the NCEP–NCAR Reanalysis, *J. Climate*, **14**, 1150-1567, 2001.

Shalamyanskiy, A.M., Horizontal Distribution of the Total Ozone Content from Aircraft Data in 1974-1977, *Trudy GGO*, **419**, 126-135, 1980.

Shalamyanskiy, A.M., and A.K. Romanshkina, Distribution and Variation in the Total Ozone Concentration in Various Air Masses, *Atmospheric and Oceanic Physics*, **16**, 931-937, 1980.

Shapiro, M.A., The Role of Turbulent Heat Flux in the Generation of Potential Vorticity in the Vicinity of Upper-Level Jet Stream Systems, *Mon. Wea. Rev.*, **104**, 892-906, 1976.

Shapiro, M.A., Further Evidence of the Mesoscale and Turbulent Structure of Upper Level Jet Stream–Frontal Zone Systems, *Mon. Wea. Rev.*, **106**, 1100–1111, 1978.

Shapiro, M.A., Turbulent Mixing within Tropopause Folds as a Mechanism for the Exchange of Chemical Constituents between the Strtosphere and the Troposphere, *J. Atmos. Sci.*, **37**, 994-1004, 1980.

Shapiro, M. A., A. J. Krueger, and P. J. Kennedy, Nowcasting the position and intensity of jet streams using satellite-borne total ozone mapping spectrometer, *Nowcasting*, K. A. Browning, Ed., Academic Press, 137-145, 1982.

Shapiro, M.A., Dropwindsonde Observations of an Icelandic Low and a Greenland Mountain-Lee Wave, *Mon. Wea. Rev.*, **113**, 680-683, 1985.

Shapiro, M. A., T. Hampel, and A. J. Krueger, The Artic Tropopause Fold, *Mon. Wea. Rev.*, **115**, 444-454, 1987.

Shapiro, M. A., and E. Donall-Grell, In search of synoptic/dynamic conceptualizations of the life cycles of fronts, jet streams, and the tropopause. *Vol. I, Proc. Int. Symp. on the Life Cycles of Extratropical Cyclones*, Bergen, Norway, Geophysical Institute, University of Bergen, Norway, 163–181, 1994.

Shapiro, M., H. Wernli, J. Bao, J, Methven, X. Zou, J. Doyle, T. Holt, E.Donall-Grell, and Paul Neiman, A Planetary-Scale to Mesoscale Perspective of the Life Cycles of Extratropical Cyclones: The Bridge between Theory and Observations, in *The Life Cycles of Extratropical Cyclones*, edited by M. Shapiro and S. Gronås, pp.139-185, American Meteorological Society, 1999.

Solomon S., Stratospheric ozone depletion: A review of concepts and history, *Reviews of Geophysics*, **37**, 275-316, 1999.

Soukharev, B., and L. Hood, Possible solar modulation of the equatorial quasi-biennial oscillation: Additional statistical evidence, *J. Geophys. Res.*, **106**, 14,855–14,868, 2001.

Stratospheric Processes And their Role in Climate (SPARC), Assessment *of Trends in the Vertical Distribution of Ozone*, Report No.1. (WMO Ozone Research and Monitoring Project Report No. 43), Geneva, 1998.

Staehelin, J, N. R. P. Harris, C. Appenzeller, and J. Eberhard, Ozone trends: A review, *Reviews of Geophysics*, **39**, 231-290, 2001.

Steinbrecht, W., H. Claude, and U. Kohler, Correlations between tropopause height and total ozone: Implications for long-term changes, *J. Geophys. Res*., **103**, 19,183-19,192, 1998.

Stolarski R., R. Bojkov, L. Bishop, C. Zerefos, J. Staehelin, and J. Zawodny, Measured Trends in Stratospheric Ozone, *Science* **256**, 342-349, 1992.

Swanson, K. L., Upper-Tropospheric Potential Vorticity Fluctuations and the Dynamical Relevance of the Time Mean, *J. Atmos. Sci.*, **58**, 1815-1826, 2001.

Trepte, C.R., R.E. Viega, M.P. McCormick, The poleward dispersal of Mount Pinatubo volcanic aerosol, *J. Geophys. Res*., **98**, 18563-18573, 1992.

Vaughan, G. and J.D. Price, On the relation between total ozone and meteorology, in Ozone in th Atmosphere, edited by R.D. Bojkov and P. Fabian, pp. 91-94, A. Deepak, Hampton, Va., 1989.

Vaughan, G. and D.A. Begum, Correlation between Total Ozone and Potential Vorticity, *Quart. J. Roy. Meteor. Soc.*, **117,** 1281-1298, 1991.

World Meteorological Organization (WMO), *Atmospheric ozone 1985*, *Rep. 44*, Global Ozone Res. and Monit. Proj., Geneva, 1986.

World Meteorological Organization (WMO), *Scientific Assesment of Ozone Depletion:1998, Rep. 44,* Global Ozone Res. and Monit. Proj., Geneva, 1999.

World Meteorological Organization (WMO), *Definition of the Thermal Tropopause,* Bull. Vol. **6**, 1957.